SRI KRISHNA COLLEGE OF TECHNOLOGY

[An Autonomous Institution |Affiliated to Anna University and Approved by AICTE|Accredited by NAAC – UGC with 'A' Grade]

KOVAIPUDUR, COIMBATORE – 641042,INDIA

info@skct.edu.in|www.skct.edu.in Ph:+91 422 2604567 to 70 |Fax: +91 422 2607152

CRITERIA 3

3.7.1 – Collaborative Activities

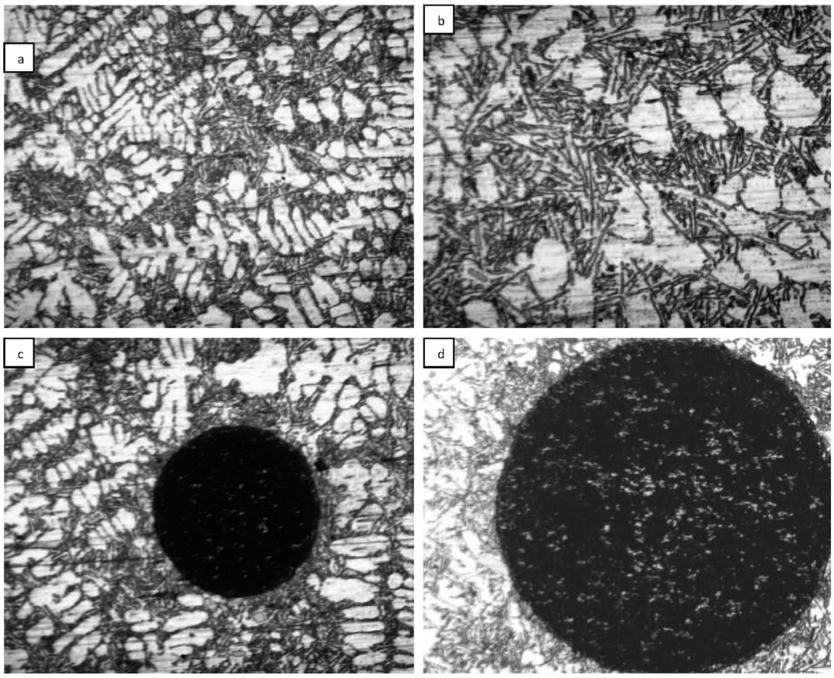

Figure 4: Optical micrographs of LM6 aluminium alloy reinforced with zinc-coated steel-wire mesh: a) LM6 matrix at 50×, b) LM6 matrix at 100×, c) LM6 matrix with a steel wire at 50×, d) LM6 matrix with a steel wire at 100×

3.3 Tensile strength

The tensile-strength values for the LM6 alloy and the composites are given in **Table 3**. The variation in the tensile strength of the composites against the orientation of the zinc-coated steel-wire mesh is shown in **Figure 6**. It is observed that the tensile strength of the composites increases with the increasing angle of orientation. The steel-wire mesh at the orientation of 90° allows the highest tensile strength compared to the 0° and 45° orientations. This is due to the reinforcement of the steel-wire mesh parallel to the loading condition; the matrix transmits the load to the steel-wire mesh, allowing a high tensile strength of 164 MPa. However, the steel-wire mesh at the orientations of 0° and 45° allows a low tensile strength compared to the matrix. This is due to the micropores at the interface of aluminium and the steel wire, which act as crack-nucleating points and reduce the tensile strength of the composites.

Table 3: Mechanical properties of the matrix and the composite with various angles of steel-wire-mesh orientation

Specimen code	Tensile strength (MPa)	% of elongation
LM6	148	23.75
LM6 – ZnFe – 0°	119	14.7
LM6 – ZnFe – 45°	141	15.95
LM6 – ZnFe – 90°	164	17.35

The ductility of the composites was measured based on the percentage of elongation as shown in **Table 3**. It is observed that the ductility of a composite decreases with the incorporation of the steel-wire mesh into the

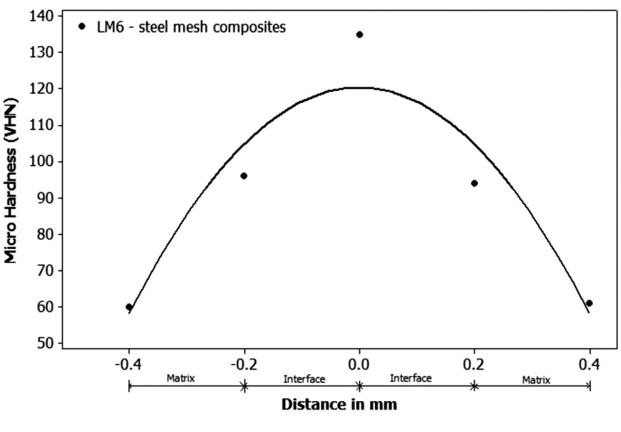

Figure 5: Variation of micro-hardness with the distance between the matrix and steel wire

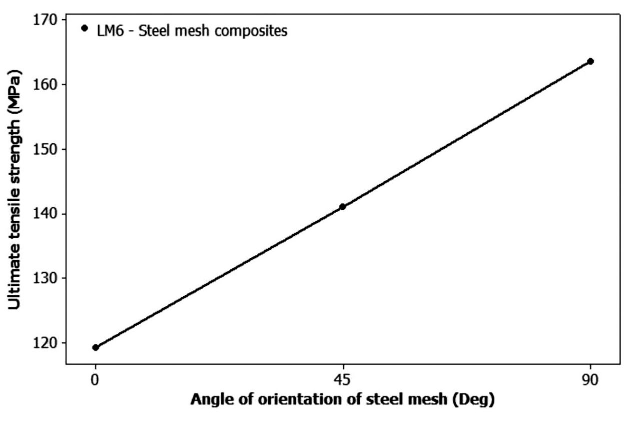

Figure 6: Variation of the tensile strength of the composites due to the angle of orientation

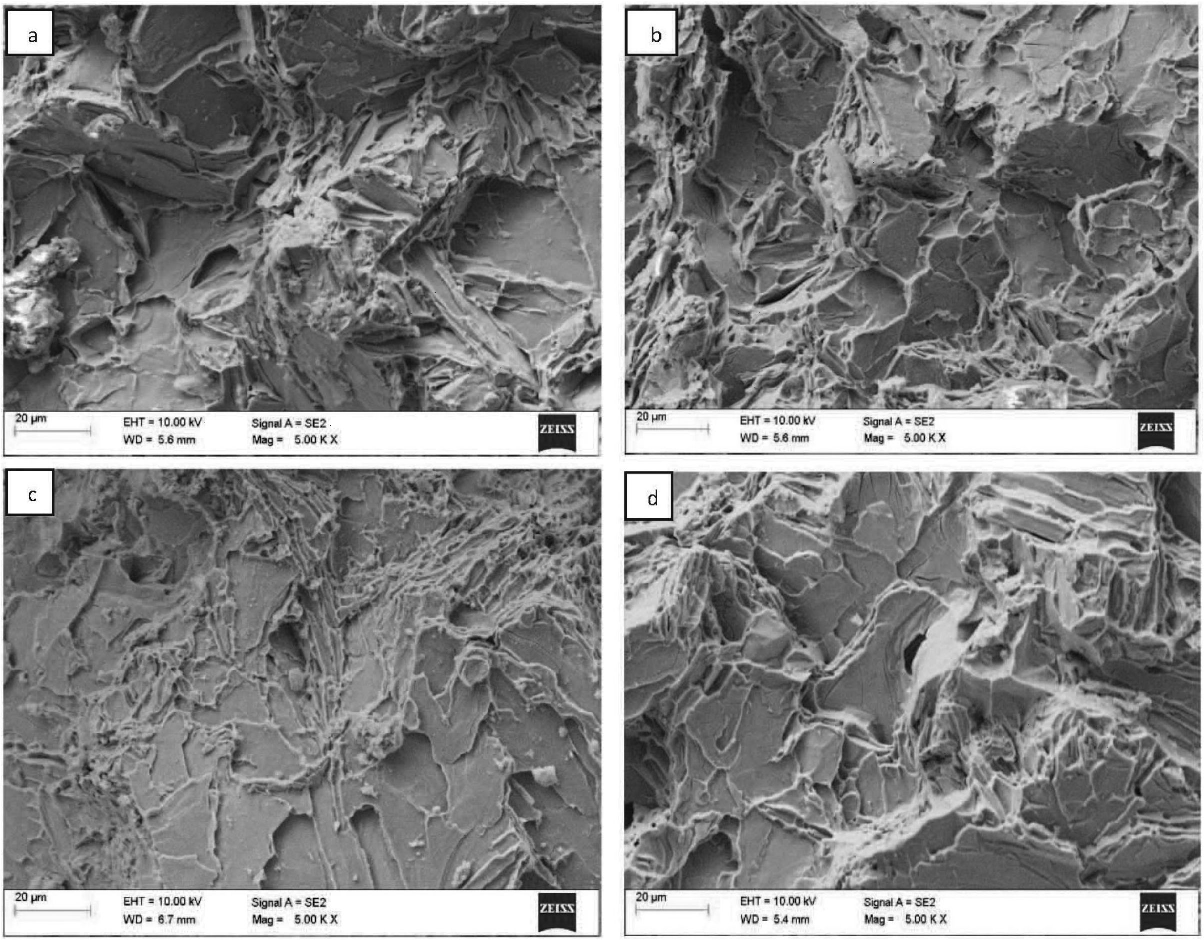

Figure 7: FESEM photographs of the fracture surfaces of different composites: a) LM6 matrix, b) LM6-ZnFe – 0°, c) LM6-ZnFe – 45°, d) LM6-ZnFe – 90°

aluminium alloy. The presence of micropores at the interface of aluminium and steel wire, the crack initiation at the interface and the propagation cause the failure of the composites.

3.4 Fracture surface

Figure 7 shows photographs of the fracture surfaces of the LM6 matrix and composites with orientations of (0, 45 and 90)°. A ductile fracture was observed in the matrix and composites during the tensile test. **Figure 7a** depicts the fracture surface of the LM6 matrix and the fracture occurs due to a dimple formation. **Figures 7b** to **7c** show the fracture surfaces of the zinc-coated steel-wire mesh at the orientations of 0° and 45°, respectively. The fracture mechanism is dominated by the steel wire pull-out due to the presence of the micropores and voids at the interface of steel and aluminium and dimple formation. The fracture surface of the zinc-coated steel-wire mesh at the orientation of 90° is shown in **Figure 7d**. Fracture is dominated by the steel wire pull-out, resulting from a broken steel wire rather than a dimple formation. R. Baron et al.[8] and R. B. Bhagat[9] and D. Mandal et al.[11] worked with stainless-steel wire/steel preform/steel fibres reinforced in an aluminium matrix by squeeze casting and stir casting and observed that a crack was initiated at the interface of the reinforcement and the matrix causing a fracture of the composite upon propagation.

4 CONCLUSIONS

Zinc-coated steel-wire mesh was reinforced at different orientations of (0, 45 and 90)° in the LM6 aluminium alloy by squeeze casting. The microstructures of the composites were analysed and the mechanical properties, viz., the hardness, tensile strength, ductility were investigated. From the above investigation, the following conclusions are made:

- The microstructures of the composites showed good interface bonding between aluminium and steel wire due to zinc coating of the steel wires.
- The hardness of the composites increased with the increasing distance from the matrix to the steel wire. The maximum hardness values of 135 VHN and 96 VHN were observed for the steel wire and the interface.

- The tensile strength of the composites increased with the orientation of the reinforcement. The maximum tensile strength of 164 MPa was observed for the steel-wire mesh at the angle of 90° orientation. The ductility of the composites decreased with the incorporation of steel-wire mesh into the aluminium alloy.
- The fracture surfaces of the composites caused steel-wire pull-outs and broken wires; and a dimple formation was observed in the matrix.
- This developed composite may be considered as a potential candidate to be used as a structural member in automobile, aerospace and marine applications because of its advantageous hardness and tensile strength.

5 REFERENCES

[1] S. D. Saravanan, M. S. Kumar, Effect of mechanical properties on rice husk ash reinforced aluminum alloy (AlSi10Mg) matrix composites, Procedia Engineering, 64 (**2013**), 1505–1513, doi:10.1016/j.proeng.2013.09.232

[2] M. K. Akbari, O. Mirzaee, H. R. Baharvandi, Fabrication and study on mechanical properties and fracture behavior of nanometric Al2O3 particle-reinforced A356 composites focusing on the parameters of vortex method, Materials & Design, 46 (**2013**), 199–205, doi:10.1016/j.matdes.2012.10.008

[3] J. D. R. Selvam, D. S. Robinson Smart, I. Dinaharan, Microstructure and some mechanical properties of fly ash particulate reinforced AA6061 aluminum alloy composites prepared by compocasting, Materials & Design, 49 (**2013**), 28–34, doi:10.1016/j.matdes.2013.01.053

[4] S. A. Sajjadi, H. R. Ezatpour, M. T. Parizi, Comparison of microstructure and mechanical properties of A356 aluminum alloy/Al2O3 composites fabricated by stir and compo-casting processes, Materials & Design, 34 (**2012**), 106–111, doi:10.1016/j.matdes.2011.07.037

[5] A. Mazahery, M. O. Shabani, Mechanical properties of squeeze-cast A356 composites reinforced with B4C particulates, Journal of Materials Engineering and Performance, 21 (**2012**) 2, 247–252, doi:10.1007/s11665-011-9867-6

[6] A. Mazahery, M. O. Shabani, Characterization of cast A356 alloy reinforced with nano SiC composites, Transactions of Nonferrous Metals Society of China, 22 (**2012**) 2, 275–280, doi:10.1016/S1003-6326(11)61171-0

[7] S. Sulaiman, M. Sayuti, R. Samin, Mechanical properties of the as-cast quartz particulate reinforced LM6 alloy matrix composites, Journal of Materials Processing Technology, 201 (**2007**) 1–3, 731–735, doi:10.1016/j.jmatprotec.2007.11.221

[8] S. V. Prasad, R. Asthana, Aluminum metal-matrix composites for automotive applications: Tribological considerations, Tribology Letters, 17 (**2004**) 3, 445–453, doi:10.1023/B:TRIL.0000044492.91991.f3

[9] Z. Ahmad, Mechanical behavior and fabrication characteristics of aluminum metal matrix composite alloys, Journal of Reinforced Plastics and Composites, 20 (**2001**) 11, 921–944, doi:10.1177/073168401772678896

[10] P. Sharma, K. Paliwal, R. Kumar, S. Sharma, A study on wear behaviour of Al/6101/graphite composites, Journal of Asian Ceramic Societies, 5 (**2017**) 1, 42–48, doi:10.1016/j.jascer.2016.12.007

[11] V. R. Rao, N. Ramanaiah, M. M. M. Sarcar, Dry sliding wear behavior of TiC – AA7075 metal matrix composites, International Journal of Applied Science and Engineering, 14 (**2016**) 1, 27–37

[12] L. Francis Xavier, P. Suresh, Wear behavior of aluminium metal matrix composite prepared from industrial waste, The Scientific World Journal, 2016 (**2016**), 1-8, doi: 10.1155/2016/6538345

[13] G. Karthikeyan, G. R. Jinu, Dry sliding wear behaviour of stir cast LM 25 / ZrO2 metal matrix composites, Transactions of Femina, 39, (**2015**) 4, 89–98

[14] G. B. V. Kumar, R. Pramod, Influence of WC particulate reinforcement on the mechanical properties and sliding wear of Al6061 alloys, Applied Mechanics and Materials, 813-814 (**2015**), 67–73, doi:10.4028/www.scientific.net/AMM.813-814.67

[15] A. Canakci, F. Arslan, Abrasive wear behaviour of B4C particle reinforced Al2024 MMCs, The International Journal of Advanced Manufacturing Technology, 63 (**2012**) 5–8, 785–795, doi:10.1007/s00170-012-3931-8

[16] G. B. V. Kumar, N. Selvaraj, Mechanical and dry sliding wear behavior of Al7075 alloy-reinforced with SiC particles, Journal of Composite Materials, 46 (**2012**) 10, 1201–09, doi:10.1177/0021998311414948

[17] J. B. Rao, D. V. Rao, K. S. Prasad, N. R. M. R. Bhargava, Dry sliding wear behaviour of fly ash particles reinforced AA 2024 composites, Materials Science-Poland, 30 (**2012**) 3, 204–211, doi:10.2478/s13536-012-0026-z

[18] S. Seshan, A. Guruprasad, M. Prabha, A. Sudhakar, Fibre-reinforced metal matrix composites – a review, Journal of Indian Institute of Science, 76 (**1996**), 1–14

[19] H. B. M. Rajan, S. Ramabalan, I. Dinaharan, S. J. Vijay, Synthesis and characterization of in situ formed titanium diboride particulate reinforced AA7075 aluminum alloy cast composites, Materials and Design, 44 (**2013**), 438–445, doi:10.1016/j.matdes.2012.08.008

[20] R. Soundararajan, A. Ramesh, S. Sivasankaran, M. Vignesh, Modeling and analysis of mechanical properties of aluminium alloy (A413) reinforced with boron carbide (B4C) processed through squeeze casting process using artificial neural network model and statistical technique, Materials Today Proceedings, 4 (**2017**) 2, 2008–2030, doi:10.1016/j.matpr.2017.02.047

[21] R. Soundararajan, A. Ramesh, N. Mohanraj, N. Parthasarathi, An investigation of material removal rate and surface roughness of squeeze casted A413 alloy on WEDM by multi response optimization using RSM, Journal of Alloys and Compounds, 685 (**2016**), 533–545, doi:10.1016/j.jallcom.2016.05.292

[22] R. Soundararajan, A. Ramesh, S. Sivasankaran, A. Sathishkumar, Modeling and analysis of mechanical properties of aluminium alloy (A413) processed through squeeze casting route using artificial neural network model and statistical technique, Advances in Materials Science and Engineering, 2015 (**2015**), 1–16, doi:10.1155/2015/714762

[23] P. Senthil, K. S. Amirthagadeswaran, Optimization of squeeze casting parameters for non symmetrical AC2A aluminium alloy castings through Taguchi method, Journal of Mechanical Science and Technology, 26, (**2012**) 4, 1141–1147, doi:10.1007/s12206-012-0215-z

[24] Q. Zhang, M. Masoumi, H. Hu, Influence of applied pressure on tensile behaviour and microstructure of squeeze cast Mg alloy AM50 with Ca addition, Journal of Materials Engineering and Performance, 21 (**2012**) 1, 38–46, doi:10.1007/s11665-010-9810-2

[25] S. Koksal, F. Ficici, R. Kayikci, O. Savas, Experimental optimization of dry sliding wear behavior of in situ AlB2/Al composite based on Taguchi's method, Materials & Design, 42 (**2012**), 124–130, doi:10.1016/j.matdes.2012.05.048

[26] C. S. Goh, K. S. Soh, P. H. Oon, B. W. Chua, Effect of squeeze casting parameters on the mechanical properties of AZ91-Ca Mg alloys, Materials & Design, 31 (**2010**) 1, S50–S53, doi:10.1016/j.matdes.2009.11.039

[27] R. Baron, J. Wert, D. Gerard, F. Wawner, The processing and characterization of sintered metal-reinforced aluminium matrix composites, Journal of Materials Science, 32 (**1997**) 24, 6435–6445

[28] R. B. Bhagat, High pressure squeeze casting of stainless steel wire reinforced aluminium matrix composites, Composites, 19 (**1988**) 5, 393–399, doi:10.1016/0010-4361(88)90127-9

[29] S. Pourhosseini, H. Beygi, S. A. Sajjadi, Effect of metal coating of reinforcements on the microstructure and mechanical properties of Al-Al2O3 nanocomposites, Materials Science and Technology, (**2017**), 1–8, doi:10.1080/02670836.2017.1366708

[30] E. Hajjari, M. Divandari, H. Arabi, Effect of applied pressure and nickel coating on microstructural development in continuous carbon fiber-reinforced aluminum composites fabricated by squeeze casting, Materials and Manufacturing Processes, 26 (**2011**), 599–603, doi:10.1080/10426910903447311

[31] E. J. Guo, H. Yue, W. Fei, L. Wang, Tensile properties of ZnO- and ZnAl2O4- coated aluminum borate whiskers reinforced aluminum composites at elevated temperatures, Journal of Composite Materials, 46 (**2011**) 12, 1475–1481, doi:10.1177/0021998311421041

[32] E. Hajjari, M. Divandari, A. R. Mirhabibi, The effect of applied pressure on fracture surface and tensile properties of nickel coated continuous carbon fiber reinforced aluminum composites fabricated by squeeze casting, Materials & Design, 31 (**2010**) 5, 2381–2386, doi:10.1016/j.matdes.2009.11.067

[33] B. B. Singh, M. Balasubramanian, Processing and properties of copper-coated carbon fibre reinforced aluminium alloy composites, Journal of Materials Processing Technology, 209 (**2009**) 4, 2104–2110, doi:10.1016/j.jmatprotec.2008.05.002

[34] Y.Tang, L. Liu, W. Li, B. Shen, W. Hu, Interface characteristics and mechanical properties of short carbon fibers/Al composites with different coatings, Applied Surface Science, 255 (**2009**) 8, 4393–4400, doi:10.1016/j.apsusc.2008.10.124

[35] C. S. Ramesh, R. Keshavamurthy, B. H. Channabasappa, A. Ahmed, Microstructure and mechanical properties of Ni-P coated Si3N4 reinforced Al6061 composites, Materials Science and Engineering: A, 502 (**2009**) 1–2, 99–106, doi:10.1016/j.msea.2008.10.012

[36] L. Xia, B. Jia, J. Zeng, J. Xu, Wear and mechanical properties of carbon fiber reinforced copper alloy composites, Materials Characterization, 60 (**2009**) 5, 363–369, doi:10.4028/www.scientific.net/KEM.474-476.1605

[37] A. Urena, J. Rams, M. Campo, M. Sanchez, Effect of reinforcement coatings on the dry sliding wear behaviour of aluminium/SiC particles/carbon fibres hybrid composites, Wear 266 (**2009**) 11–12, 1128–1136, doi:10.1016/j.wear.2009.03.016

[38] C. Tekmen, U. Cocen, Squeeze casting of Ni coated SiC particle reinforced Al based composite, Journal of Composite Materials, 42 (**2008**) 13, 1271–1279, doi:10.1177/0021998308092195

[39] D. Mandal, B. K. Dutta, S.C. Panigrahi, Effect of copper and nickel coating on short steel fiber reinforcement on microstructure and mechanical properties of aluminium matrix composites, Materials Science and Engineering: A, 492 (**2008**) 1–2, 346–352. doi:10.1016/j.msea.2008.03.031

[40] V.V. Ganesh, C. K. Lee, M. Gupta, Enhancing the tensile modulus and strength of an aluminum alloy using interconnected reinforcement methodology, Materials Science and Engineering: A, 333 (**2002**) 1–2, 193–198. doi:10.1016/S0921-5093(01)01831-7

Springer Link

Investigation of Mechanical Properties and Dry Sliding Wear Behaviour of Squeeze Cast LM6 Aluminium Alloy Reinforced with Copper Coated Short Steel Fibers

Transactions of the Indian Institute of Metals

April 2018, Volume 71, Issue 4, pp 813–822 | Cite as

- Samson Jerold Samuel Chelladurai (1) Email author (samsonjeroldsamuel@skcet.ac.in)
- Ramesh Arthanari (2)
- Nisaanthakumar Nithyanandam (1)
- Karthikeyan Rajendran (1)
- Kesavaprasad Kothandapani Radhakrishnan (1)

1. Department of Mechanical Engineering, Sri Krishna College of Engineering and Technology, , Coimbatore, India
2. Department of Mechanical Engineering, Sri Krishna College of Technology, , Coimbatore, India

Technical Paper
First Online: 28 December 2017

Abstract

LM6 aluminium alloy with 2.5–10 wt% of copper coated short steel fiber reinforced composites were prepared using squeeze casting process. Microstructure and mechanical properties viz., hardness, tensile strength and ductility were investigated. Dry sliding wear behaviour was tested by considering sliding distance and load. Fracture surface and worn surface were examined using field emission scanning electron microscope (FESEM). Hardness of composites increased with increasing wt% of fiber. Tensile strength of composites increased up to 19% for 5 wt% fiber composites. Further addition of fibers decreased the tensile strength of composites. Ductility of the composites decreased with the addition of fibers into the matrix. Wt% of fibers significantly decreased the weight loss, coefficient of friction and wear rate. Also the cumulative weight loss decreased up to 57% for 10 wt% of composites compared to LM6 aluminium alloy. Fracture surface of composite tensile specimen showed dimple formation and fiber pullout. Worn surface of matrix showed long continuous grooves due to local delamination on the surface. However, worn surface of composites showed fine and smooth grooves due to ploughing rather than local delamination. Copper coated steel fiber reinforcement in LM6 aluminium alloy exhibited better mechanical properties and wear resistance compared to matrix.

Keywords

LM6 aluminium alloy Steel fiber Squeeze casting Microstructure Tensile strength Wear resistance

References

1. Chou T W, Kelly A, and Okura A, *Composites* **16** (1985) 187. https://doi.org/10.1016/0010-4361(85)90603-2 (https://doi.org/10.1016/0010-4361(85)90603-2).
CrossRef (https://doi.org/10.1016/0010-4361(85)90603-2)
Google Scholar (http://scholar.google.com/scholar_lookup?&author=TW.%20Chou&author=A.%20Kelly&author=A.%20Okura&journal=Composites&volume=16&pages=187&publication_year=1985&doi=10.1016%2F0010-4361%2885%2990603-2)

2. Dwivedi S P, Sharma S, and Mishra R K, *J Braz Soc Mech Sci Eng* **37** (2014) 57. https://doi.org/10.1007/s40430-014-0138-y (https://doi.org/10.1007/s40430-014-0138-y).
CrossRef (https://doi.org/10.1007/s40430-014-0138-y)
Google Scholar (http://scholar.google.com/scholar_lookup?&author=SP.%20Dwivedi&author=S.%20Sharma&author=RK.%20Mishra&journal=J%20Braz%20Soc%20Mech%20Sci%20Eng&volume=37&pages=57&publication_year=2014&doi=10.1007%2Fs40430-014-0138-y)

3. Hosking F M, Portillo F F, Wunderlin R, and Mehrabian R, *J Mater Sci* **17** (1982) 477. https://doi.org/10.1007/bf00591483 (https://doi.org/10.1007/bf00591483).
CrossRef (https://doi.org/10.1007/BF00591483)
Google Scholar (http://scholar.google.com/scholar_lookup?&author=FM.%20Hosking&author=FF.%20Portillo&author=R.%20Wunderlin&author=R.%20Mehrabian&journal=J%20Mater%20Sci&volume=17&pages=477&publication_year=1982&doi=10.1007%2FBF00591483)

4. Mandal D, Dutta B K, and Panigrahi S C, *J Mater Sci* **41** (2006) 4764. https://doi.org/10.1007/s10853-006-0036-5 (https://doi.org/10.1007/s10853-006-0036-5).
CrossRef (https://doi.org/10.1007/s10853-006-0036-5)
Google Scholar (http://scholar.google.com/scholar_lookup?&author=D.%20Mandal&author=BK.%20Dutta&author=SC.%20Panigrahi&journal=J%20Mater%20Sci&volume=41&pages=4764&publication_year=2006&doi=10.1007%2Fs10853-006-0036-5)

5. Manna A, Mahapatra P B, and Bains H S, *J Compos Mater* **44** (2010) 3069. https://doi.org/10.1177/0021998310366362 (https://doi.org/10.1177/0021998310366362).
CrossRef (https://doi.org/10.1177/0021998310366362)

Google Scholar (http://scholar.google.com/scholar_lookup?&author=A.%20Manna&author=PB.%20Mahapatra&author=HS.%20Bains&journal=J%20Compos%20Mater&volume=44&pages=3069&publication_year=2010&doi=10.1177%2F0021998310366362)

6. Miller W, Zhuang L, Bottema J, Wittebrood A, De Smet P, Haszler A, and Vieregge A, *Mater Sci Eng A* **280** (2000) 37. https://doi.org/10.1016/s0921-5093(99)00653-x (https://doi.org/10.1016/s0921-5093(99)00653-x). CrossRef (https://doi.org/10.1016/S0921-5093(99)00653-X) Google Scholar (http://scholar.google.com/scholar_lookup?&author=W.%20Miller&author=L.%20Zhuang&author=J.%20Bottema&author=A.%20Wittebrood&author=P.%20Smet&author=A.%20Haszler&author=A.%20Vieregge&journal=Mater%20Sci%20Eng%20A&volume=280&pages=37&publication_year=2000&doi=10.1016%2FS0921-5093%2899%2900653-X)

7. Surappa M K, and Rohatgi P K, *J Mater Sci* **16** (1981) 983. https://doi.org/10.1007/bf00542743 (https://doi.org/10.1007/bf00542743). CrossRef (https://doi.org/10.1007/BF00542743) Google Scholar (http://scholar.google.com/scholar_lookup?&author=MK.%20Surappa&author=PK.%20Rohatgi&journal=J%20Mater%20Sci&volume=16&pages=983&publication_year=1981&doi=10.1007%2FBF00542743)

8. Zhu X, Zhao Y, Wang H, Wang Z G, Wu M, Pei C H, Chen C, and Jiang Q C, *J Mater Eng Perform* (2016). https://doi.org/10.1007/s11665-016-2308-9 (https://doi.org/10.1007/s11665-016-2308-9). Google Scholar (http://scholar.google.com/scholar_lookup?&author=X.%20Zhu&author=Y.%20Zhao&author=H.%20Wang&author=ZG.%20Wang&author=M.%20Wu&author=CH.%20Pei&author=C.%20Chen&author=QC.%20Jiang&journal=J%20Mater%20Eng%20Perform&publication_year=2016&doi=10.1007%2Fs11665-016-2308-9)

9. Asano K, *Mater Manuf Process* **30** (2015) 1312. https://doi.org/10.1080/10426914.2015.1019101 (https://doi.org/10.1080/10426914.2015.1019101). CrossRef (https://doi.org/10.1080/10426914.2015.1019101) Google Scholar (http://scholar.google.com/scholar_lookup?&author=K.%20Asano&journal=Mater%20Manuf%20Process&volume=30&pages=1312&publication_year=2015&doi=10.1080%2F10426914.2015.1019101)

10. Bhagat R B, Amateau M F, Conway J C, Paulick J M, Chisholm J M, Parnell J M, and Seidensticker D G, *J Compos Mater* **23** (1989) 961. https://doi.org/10.1177/002199838902300906 (https://doi.org/10.1177/002199838902300906). CrossRef (https://doi.org/10.1177/002199838902300906) Google Scholar (http://scholar.google.com/scholar_lookup?&author=RB.%20Bhagat&author=MF.%20Amateau&author=JC.%20Conway&author=JM.%20Paulick&author=JM.%20Chisholm&author=JM.%20Parnell&author=DG.%20Seidensticker&journal=J%20Compos%20Mater&volume=23&pages=961&publication_year=1989&doi=10.1177%2F002199838902300906)

11. Ghomashchi M R, and Vikhrov A, *J Mater Process Technol* **101** (2000) 1. https://doi.org/10.1016/s0924-0136(99)00291-5 (https://doi.org/10.1016/s0924-0136(99)00291-5). CrossRef (https://doi.org/10.1016/S0924-0136(99)00291-5) Google Scholar (http://scholar.google.com/scholar_lookup?&author=MR.%20Ghomashchi&author=A.%20Vikhrov&journal=J%20Mater%

20Process%20Technol&volume=101&pages=1&publication_year=2000&doi=10.1016%2FS0924-0136%2899%2900291-5)

12. Gurusamy P, Prabu S B, and Paskaramoorthy R, *Mater Manuf Process* **30** (2015) 367. https://doi.org/10.1080/10426914.2014.973587 (https://doi.org/10.1080/10426914.2014.973587).
CrossRef (https://doi.org/10.1080/10426914.2014.973587)
Google Scholar (http://scholar.google.com/scholar_lookup?&author=P.%20Gurusamy&author=SB.%20Prabu&author=R.%20Paskaramoorthy&journal=Mater%20Manuf%20Process&volume=30&pages=367&publication_year=2015&doi=10.1080%2F10426914.2014.973587)
13. Lu Y, Li J, Yang J, and Li X, *Mater Manuf Process* **31** (2016) 1306. https://doi.org/10.1080/10426914.2015.1070417 (https://doi.org/10.1080/10426914.2015.1070417).
CrossRef (https://doi.org/10.1080/10426914.2015.1070417)
Google Scholar (http://scholar.google.com/scholar_lookup?&author=Y.%20Lu&author=J.%20Li&author=J.%20Yang&author=X.%20Li&journal=Mater%20Manuf%20Process&volume=31&pages=1306&publication_year=2016&doi=10.1080%2F10426914.2015.1070417)
14. Rajagopal S, Leader G, and Tech- M, *J Appl Metalwork* **1** (1981) 3.
CrossRef (https://doi.org/10.1007/BF02834341)
Google Scholar (http://scholar.google.com/scholar_lookup?&author=S.%20Rajagopal&author=G.%20Leader&author=M.%20Tech-&journal=J%20Appl%20Metalwork&volume=1&pages=3&publication_year=1981)
15. Soundararajan R, Ramesh A, Mohanraj N, and Parthasarathi N, *J Alloys Compd* **685** (2016) 533. https://doi.org/10.1016/j.jallcom.2016.05.292 (https://doi.org/10.1016/j.jallcom.2016.05.292).
CrossRef (https://doi.org/10.1016/j.jallcom.2016.05.292)
Google Scholar (http://scholar.google.com/scholar_lookup?&author=R.%20Soundararajan&author=A.%20Ramesh&author=N.%20Mohanraj&author=N.%20Parthasarathi&journal=J%20Alloys%20Compd&volume=685&pages=533&publication_year=2016&doi=10.1016%2Fj.jallcom.2016.05.292)
16. Vijayaram T R, Sulaiman S, Hamouda A M S, and Ahmad M H M, *J Mater Process Technol* **178** (2006) 34. https://doi.org/10.1016/j.jmatprotec.2005.09.026 (https://doi.org/10.1016/j.jmatprotec.2005.09.026).
CrossRef (https://doi.org/10.1016/j.jmatprotec.2005.09.026)
Google Scholar (http://scholar.google.com/scholar_lookup?&author=TR.%20Vijayaram&author=S.%20Sulaiman&author=AMS.%20Hamouda&author=MHM.%20Ahmad&journal=J%20Mater%20Process%20Technol&volume=178&pages=34&publication_year=2006&doi=10.1016%2Fj.jmatprotec.2005.09.026)
17. Vijian P, and Arunachalam V P, *Int J Adv Manuf Technol* **33** (2006) 1122. https://doi.org/10.1007/s00170-006-0550-2 (https://doi.org/10.1007/s00170-006-0550-2).
CrossRef (https://doi.org/10.1007/s00170-006-0550-2)
Google Scholar (http://scholar.google.com/scholar_lookup?&author=P.%20Vijian&author=VP.%20Arunachalam&journal=Int%20J%20Adv%20Manuf%20Technol&volume=33&pages=1122&publication_year=2006&doi=10.1007%2Fs00170-006-0550-2)

18. Bhagat R B, *Composites* **19** (1988) 393. https://doi.org/10.1016/0010-4361(88)90127-9 (https://doi.org/10.1016/0010-4361(88)90127-9).
CrossRef (https://doi.org/10.1016/0010-4361(88)90127-9)
Google Scholar (http://scholar.google.com/scholar_lookup?&author=RB.%20Bhagat&journal=Composites&volume=19&pages=393&publication_year=1988&doi=10.1016%2F0010-4361%2888%2990127-9)

19. Baron R, Wert J, Gerard D, and Wawner F, *J Mater Sci* **32** (1997) 6435.
CrossRef (https://doi.org/10.1023/A%3A1018686505563)
Google Scholar (http://scholar.google.com/scholar_lookup?&author=R.%20Baron&author=J.%20Wert&author=D.%20Gerard&author=F.%20Wawner&journal=J%20Mater%20Sci&volume=32&pages=6435&publication_year=1997)

20. Suzuki T, Umehara H, Hayashi R, and Watanabc S, *J Mater Res* **8** (1993) 2492.
https://doi.org/10.1557/JMR.1993.2492 (https://doi.org/10.1557/JMR.1993.2492)
CrossRef (https://doi.org/10.1557/JMR.1993.2492)
Google Scholar (http://scholar.google.com/scholar_lookup?&author=T.%20Suzuki&author=H.%20Umehara&author=R.%20Hayashi&author=S.%20Watanabc&journal=J%20Mater%20Res&volume=8&pages=2492&publication_year=1993&doi=10.1557%2FJMR.1993.2492)

21. Wang Y Q, and Zhou B L, *Compos Part A Appl Sci Manuf* **27** (1996) 1139.
https://doi.org/10.1016/1359-835x(96)00072-3 (https://doi.org/10.1016/1359-835x(96)00072-3).
CrossRef (https://doi.org/10.1016/1359-835X(96)00072-3)
Google Scholar (http://scholar.google.com/scholar_lookup?&author=YQ.%20Wang&author=BL.%20Zhou&journal=Compos%20Part%20A%20Appl%20Sci%20Manuf&volume=27&pages=1139&publication_year=1996&doi=10.1016%2F1359-835X%2896%2900072-3)

22. Mandal D, Dutta B K, and Panigrahi S C, *Mater Sci Eng A* **492** (2008) 346.
https://doi.org/10.1016/j.msea.2008.03.031 (https://doi.org/10.1016/j.msea.2008.03.031).
CrossRef (https://doi.org/10.1016/j.msea.2008.03.031)
Google Scholar (http://scholar.google.com/scholar_lookup?&author=D.%20Mandal&author=BK.%20Dutta&author=SC.%20Panigrahi&journal=Mater%20Sci%20Eng%20A&volume=492&pages=346&publication_year=2008&doi=10.1016%2Fj.msea.2008.03.031)

23. Deuis R L, Subramanian C, and Yellupb J M, *Compos Sci Technol* **57** (1997) 415. https://doi.org/10.1016/s0266-3538(96)00167-4 (https://doi.org/10.1016/s0266-3538(96)00167-4).
CrossRef (https://doi.org/10.1016/S0266-3538(96)00167-4)
Google Scholar (http://scholar.google.com/scholar_lookup?&author=RL.%20Deuis&author=C.%20Subramanian&author=JM.%20Yellupb&journal=Compos%20Sci%20Technol&volume=57&pages=415&publication_year=1997&doi=10.1016%2FS0266-3538%2896%2900167-4)

24. Alpas A T, and Zhang J, *Wear* **155** (1992) 83. https://doi.org/10.1016/0043-1648(92)90111-k (https://doi.org/10.1016/0043-1648(92)90111-k).
CrossRef (https://doi.org/10.1016/0043-1648(92)90111-K)
Google Scholar (http://scholar.google.com/scholar_lookup?&author=AT.%20Alpas&author=J.%20Zhang&journal=Wear&volume=155&pages=83&publication_year=1992&doi=10.1016%2F0043-1648%2892%2990111-K)

25. Iwai Y, Honda T, Miyajima T, Iwasaki Y, Surappa M K, and Xu J F, *Compos Sci Technol* **60** (2000) 1781. https://doi.org/10.1016/s0266-3538(00)00068-3 (https://doi.org/10.1016/s0266-3538(00)00068-3).
CrossRef (https://doi.org/10.1016/S0266-3538(00)00068-3)
Google Scholar (http://scholar.google.com/scholar_lookup?&author=Y.%20Iwai&author=T.%20Honda&author=T.%20Miyajima&author=Y.%20Iwasaki&author=MK.%20Surappa&author=JF.%20Xu&journal=Compos%20Sci%20Technol&volume=60&pages=1781&publication_year=2000&doi=10.1016%2FS0266-3538%2800%2900068-3)

26. Kumar B A, Murugan N, and Dinaharan I, *Trans Nonferr Met Soc China* **24** (2014) 2785. https://doi.org/10.1016/s1003-6326(14)63410-5 (https://doi.org/10.1016/s1003-6326(14)63410-5).
CrossRef (https://doi.org/10.1016/S1003-6326(14)63410-5)
Google Scholar (http://scholar.google.com/scholar_lookup?&author=BA.%20Kumar&author=N.%20Murugan&author=I.%20Dinaharan&journal=Trans%20Nonferr%20Met%20Soc%20China&volume=24&pages=2785&publication_year=2014&doi=10.1016%2FS1003-6326%2814%2963410-5)

27. Monikandan V V, Joseph M A, and Rajendrakumar P K, *J Mater Eng Perform* (2016). https://doi.org/10.1007/s11665-016-2276-0 (https://doi.org/10.1007/s11665-016-2276-0).
Google Scholar (http://scholar.google.com/scholar_lookup?&author=VV.%20Monikandan&author=MA.%20Joseph&author=PK.%20Rajendrakumar&journal=J%20Mater%20Eng%20Perform&publication_year=2016&doi=10.1007%2Fs11665-016-2276-0)

28. Poovazhagan L, Kalaichelvan K, and Sornakumar T, *Mater Manuf Process* **6914** (2015) 1. https://doi.org/10.1080/10426914.2015.1026354 (https://doi.org/10.1080/10426914.2015.1026354).
Google Scholar (http://scholar.google.com/scholar_lookup?&author=L.%20Poovazhagan&author=K.%20Kalaichelvan&author=T.%20Sornakumar&journal=Mater%20Manuf%20Process&volume=6914&pages=1-11&publication_year=2015&doi=10.1080%2F10426914.2015.1026354)

29. Radhika N, and Raghu R, *Tribol Lett* **59** (2015) 2. https://doi.org/10.1007/s11249-015-0516-3 (https://doi.org/10.1007/s11249-015-0516-3).
CrossRef (https://doi.org/10.1007/s11249-015-0516-3)
Google Scholar (http://scholar.google.com/scholar_lookup?&author=N.%20Radhika&author=R.%20Raghu&journal=Tribol%20Lett&volume=59&pages=2&publication_year=2015&doi=10.1007%2Fs11249-015-0516-3)

30. Sathiskumar R, Dinaharan I, Murugan N, and Vijay S J, *Trans Nonferr Met Soc China (English Ed)* **25** (2015) 95. https://doi.org/10.1016/s1003-6326(15)63583-x (https://doi.org/10.1016/s1003-6326(15)63583-x).

31. Soorya Prakash K, Kanagaraj A, and Gopal P M, *Trans Nonferr Met Soc China (English Ed)* **25** (2015) 893. https://doi.org/10.1016/s1003-6326(15)64036-5 (https://doi.org/10.1016/s1003-6326(15)64036-5).

32. Suresh K R, Niranjan H B, Jebaraj P M, and Chowdiah M P, *Wear* **255** (2003) 638. https://doi.org/10.1016/s0043-1648(03)00292-8 (https://doi.org/10.1016/s0043-1648(03)00292-8).
CrossRef (https://doi.org/10.1016/S0043-1648(03)00292-8)
Google Scholar (http://scholar.google.com/scholar_lookup?&author=KR.%20Suresh&author=HB.%20Niranjan&author=PM.%20Jebaraj&

author=MP.%20Chowdiah&journal=Wear&volume=255&pages=638&publication_year=2003&doi=10.1016%2FS0043-1648%2803%2900292-8)

33. Yuvaraj N, and Aravindan S, *Integr Med Res* (2015) 1. https://doi.org/10.1016/j.jmrt.2015.02.006 (https://doi.org/10.1016/j.jmrt.2015.02.006).

34. Mandal D, Dutta B K, and Panigrahi S C, *J Mater Sci*, **42** (2007) 2417. https://doi.org/10.1007/s10853-006-1271-5 (https://doi.org/10.1007/s10853-006-1271-5).
CrossRef (https://doi.org/10.1007/s10853-006-1271-5)
Google Scholar (http://scholar.google.com/scholar_lookup?&author=D.%20Mandal&author=BK.%20Dutta&author=SC.%20Panigrahi&journal=J%20Mater%20Sci&volume=42&pages=2417&publication_year=2007&doi=10.1007%2Fs10853-006-1271-5)

35. Akbulut H, Durman M, and Yilmaz F, *Wear* **215** (1998) 170. https://doi.org/10.1016/s0043-1648(97)00237-8 (https://doi.org/10.1016/s0043-1648(97)00237-8).
CrossRef (https://doi.org/10.1016/S0043-1648(97)00237-8)
Google Scholar (http://scholar.google.com/scholar_lookup?&author=H.%20Akbulut&author=M.%20Durman&author=F.%20Yilmaz&journal=Wear&volume=215&pages=170&publication_year=1998&doi=10.1016%2FS0043-1648%2897%2900237-8)

36. Mandal D, Dutta B K, and Panigrahi S C, *J Mater Process Technol* **198** (2008) 195. https://doi.org/10.1016/j.jmatprotec.2007.06.074 (https://doi.org/10.1016/j.jmatprotec.2007.06.074).
CrossRef (https://doi.org/10.1016/j.jmatprotec.2007.06.074)
Google Scholar (http://scholar.google.com/scholar_lookup?&author=D.%20Mandal&author=BK.%20Dutta&author=SC.%20Panigrahi&journal=J%20Mater%20Process%20Technol&volume=198&pages=195-201&publication_year=2008&doi=10.1016%2Fj.jmatprotec.2007.06.074)

Copyright information

About this article

Cite this article as:

Chelladurai, S.J.S., Arthanari, R., Nithyanandam, N. et al. Trans Indian Inst Met (2018) 71: 813. https://doi.org/10.1007/s12666-017-1258-8

- Received 04 February 2017
- Accepted 04 October 2017
- First Online 28 December 2017
- DOI https://doi.org/10.1007/s12666-017-1258-8
- Publisher Name Springer India
- Print ISSN 0972-2815
- Online ISSN 0975-1645

- About this journal
- Reprints and Permissions

Personalised recommendations

1. Tensile and Wear Behaviour of Aluminium Alloy LM6 Reinforced with Magnesium and Copper
   Rubesh, Prabhu G.... Sahu, Mona
   Journal of Computational and Theoretical Nanoscience (2019)

2. Investigation on Mechanical Properties and Wear Behaviour of Squeeze Cast LM13 Aluminium Alloy Reinforced with Copper Coated Steel Wires
   Chelladurai, Samson Jerold Samuel... Veerakumar, Gajendhiran
   Zeitschrift für Physikalische Chemie (2018)

3. Effect of stir cast process parameters on wear behaviour of copper coated short steel fibers reinforced LM13 aluminium alloy composites
   Chelladurai, Samson Jerold Samuel... Arthanari, Ramesh
   Materials Research Express (2018)

Dry sliding wear characterization of squeeze cast LM13/FeCu composite using response surface methodology

Article *in* China foundry · November 2017

DOI: 10.1007/s41230-017-7101-3

Samson Jerold Samuel C
Sri Krishna College of Engineering and Technology

Arthanari Ramesh
Sri Krishna College of Technology

https://doi.org/10.1007/s41230-017-7101-3

Overseas Foundry CHINA FOUNDRY
Vol.14 No.6 November 2017

Dry sliding wear characterization of squeeze cast LM13/FeCu composite using response surface methodology

***Samson Jerold Samuel Chelladurai[1], Ramesh Arthanari[2], Arunprasad Narippalayam Thangaraj[1], and Harishankar Sekar[1]**

1. Department of Mechanical Engineering, Sri Krishna College of Engineering and Technology, Coimbatore 641008, India

2. Department of Mechanical Engineering, Sri Krishna College of Technology, Coimbatore 641042, India

Abstract: Dry sliding wear is one of the predominant factors to be considered while selecting material for automotive and aerospace applications. Researchers have been exploring novel aluminium matrix composites (AMC), which offer minimum wear rate for various tribological applications. In this present work, an attempt has been made to reinforce LM13 aluminium alloy with copper coated steel fibers (10wt.%) using squeeze casting process and to perform dry sliding wear test using pin-on-disc tribometer. Microstructure of cast samples was examined using image analysis system to investigate the dispersion of reinforcement in matrix. Dry sliding wear test was performed by considering factors such as load (10–50 N), sliding velocity (1–5 $m \cdot s^{-1}$) and sliding distance (500–2,500 m). Wear test was performed according to the experimental design at room temperature. Three factors and five levels central composite design were used to design the experiments using response surface methodology. Based on the results of the experiments, a regression model was developed to predict the wear rate of composites and checked for its adequacy using significance tests, analyses of variance and confirmation tests. Worn surface of samples was investigated using field emission scanning electron microscope and reported with its mechanisms. Microstructure of cast samples revealed uniform dispersion of reinforcement throughout the matrix. Response surface plots revealed that wear rate of composites increases with increasing load up to 50 N with the velocity 1–5 $m \cdot s^{-1}$ and a sliding distance up to 2,500 m. However wear rate decreasesd with increasing velocity at lower loads (up to 20 N) and increased after reaching transition velocity of 2 $m \cdot s^{-1}$. Dry sliding wear process parameters were optimised for obtaining minimum wear rate and they were found to be a load of 18.46 N, velocity of 4.11 $m \cdot s^{-1}$, sliding distance of 923 m. Worn surface of samples revealed a mild wear at lower loads (up to 30 N), and severe wear was observed at high loads (40–50 N) due to higher level of deformation on the surface.

Key words: aluminium alloy; casting; response surface methodology; microstructure; wear

CLC numbers: TG146.21/249.2 **Document code:** A **Article ID:** 1672-6421(2017)06-525-09

Aluminium alloys have been used in automotive, space and aeronautical industries because of its light weight, high specific strength and stability at high temperatures[1,2]. However, these alloys exhibit poor tribological properties. Previous studies showed that wear resistance of aluminium alloys can be improved by reinforcing with hard particles such as SiC, Al_2O_3, B_4C, TiB_2, AlN, ZrB_2, rock dust and Fe[3–10].

***Samson Jerold Samuel Chelladurai**

Male, born in 1987, Assistant Professor. His research interests mainly focus on the preparation and characterization of metal matrix composites.

E-mail: samsonjeroldsamuel@skcet.ac.in

Received: 2017-07-15; Accepted: 2017-09-20

Aluminium matrix composites have been prepared by powder metallurgy, diffusion bonding, spray co-deposition, in-situ solidification and casting methods. Among all manufacturing processes, casting route has been widely accepted as a simple, viable and most economical method to produce composites[11]. Squeeze casting is the combination of gravity die casting and closed die forging, which produces near net shaped components with minimal post processing operations, minimum porosity, excellent surface finish, low operating cost, zero defects and have superior mechanical and tribological properties over the conventional castings due to fast heat transfer rate. In this process, a premeasured quantity of molten metal is poured into the preheated die and pressure is applied until the solidification process is completed [12–14].

Suresh et al. [15] investigated the mechanical and wear properties of Al-Si-Mg/beryl composites fabricated by squeeze casting and gravity casting process. It was found that squeeze cast composites could offer better tensile strength and hardness than gravity casting process, and addition of beryl particles in matrix increased the wear rate as compared to gravity cast composite.

Senthil and Amirthagadeswaran [16] studied the influence of squeeze casting process parameters on tensile strength and hardness of AC2A aluminium alloy. L27 orthogonal array was used to design the experiments. The results showed that squeeze pressure, die preheating temperature and compression holding time were significant process parameters. Squeeze pressure was the predominant contributing factor for the improvement of mechanical properties of castings.

Many researchers have attempted the reinforcement of steel wires/preform in aluminium alloys by various manufacturing processes. Bhagat [17] experimented the reinforcement of stainless steel wires in aluminium alloy using squeeze casting process, and found that tensile strength and hardness of composites increase with increasing fiber volume fraction. Several iron-aluminide intermetallic compounds such as Fe_3Al, FeAl, Fe_2Al_5, $FeAl_2$, $FeAl_3$ and Fe_2Al_7 were observed at fiber/matrix interface. Weak interface bonding between fiber and matrix caused fiber pull-out while the composite was subjected to tension.

Mandal et al. [7] investigated the wear behaviour of copper and nickel coated steel fibers reinforced in aluminium by stir casting process. It was observed that addition of steel fibers reduced the wear rate considerably at all applied loads. Copper coating on steel fibers improved the wettablity and high stirring speed during the processing resulted in uniform dispersion of reinforcement in matrix. Coating on fibers eliminated the formation of iron-aluminide intermetallic compounds and copper coated steel fibers reinforced composites offered better wear resistance than uncoated and nickel coated reinforced composites. However from the literatures, it is found that scanty research works have been carried out on the wear behaviour of copper coated steel fibers/aluminium alloy composites. In this present work, LM13 aluminium alloy was selected as matrix because of its wide range of applications like pistons in automotive industries. Copper coated steel fibers were selected as reinforcement. Three factors (load, velocity and sliding distance), five levels central composite design were selected to design the experiments using response surface methodology (RSM). A regression model has been developed to predict the wear rate of composites within the levels and checked its adequacy using significance tests, analyses of variance and confirmation tests. The main aim of this research work is to develop a regression equation to predict the wear rate of LM13/FeCu composites and analyse the influence of load (L), velocity (V) and sliding distance (D) on wear rate.

1 Materials and experimental methods

1.1 Selection of materials and composite fabrication

Commercially available steel fibers of 133 μm diameter with chemical composition as listed in Table 1, were copper coated using electroless plating technique and deoxidized in hydrogen atmosphere for 2 h at a temperature of 800 ºC [3]. Copper coated steel fibers were chopped into minimum length (500 – 1,500 μm) and the coating thickness was measured as 27 μm. LM13 aluminium alloy was selected as matrix because of its tribological applications in automotive pistons. Density of copper coated steel fiber (3.01 $g\cdot cm^{-3}$) and aluminium alloy (2.69 $g\cdot cm^{-3}$) were measured using Archimedes (water displacement) principle [18]. Bottom pouring type of squeeze casting machine with a maximum capacity of 40 tonnes as shown in Fig.1 was used to prepare composites. Die and punch were made up of H11 die steel and EN8 alloy steel, respectively. 1.2 kg of LM13 aluminium alloy with chemical composition as listed in Table 2 was melted, degassed using hexachloroethane tablets and the temperature was raised to 750 ºC. 10wt. % of copper coated steel fibers were preheated to 200 ºC using muffle furnace and added to the melt in a continuous stream while stirring was continued. The melt was stirred using stainless steel stirrer at a constant speed of 750 rpm to form vortex. Die was preheated to a temperature of 225 ºC using ceramic electric heater and the composite melt was poured using bottom pouring arrangement. Subsequently a squeeze pressure of 125 MPa was applied on the melt until the solidification was complete. Cylindrical castings of 50 mm diameter with 130 mm height were prepared using this process.

Table 1: Chemical composition of steel fiber (wt.%)

C	Si	Mn	Ni	Cr	S	Fe
0.10	0.36	18.29	0.33	3.20	0.003	Bal.

Table 2: Chemical composition of LM13 aluminium alloy (wt.%)

Si	Fe	Cu	Mn	Mg	Ni	Pb	Ti	Al
10.8	0.51	1.3	0.12	0.86	0.72	0.01	0.05	Bal

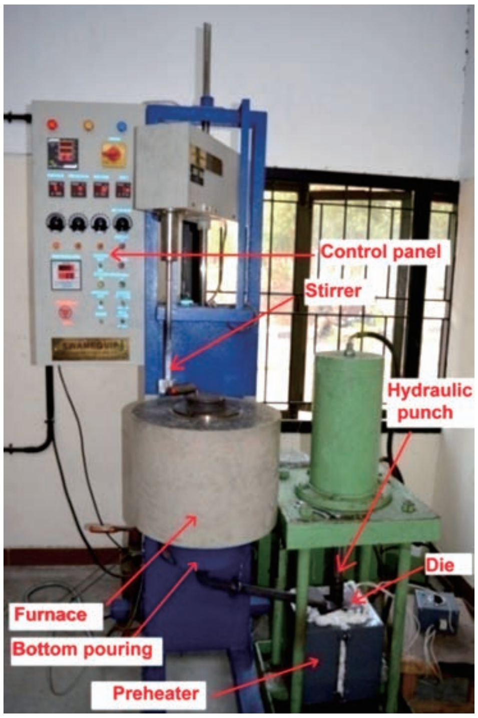

Fig. 1: Squeeze casting setup

1.2 Microstructure and hardness examination

The microstructure observation was performed for cast samples to study the dispersion of reinforcement in matrix. Linisher polisher (Model VLWS97307, U.P. National Manufacturers Ltd., India) was used to polish the samples at the earlier stages, followed by different grades of emery sheets to obtain good surface finish. Subsequently, disc polisher (Model 7800, B.S. Pyromatic India Ltd., India) was used to obtain the scratch free surface. Keller reagent was used to etch the specimen and the samples were examined using image analysis system. Samples of 20 × 20 × 10 mm^3 were prepared to investigate the hardness of composites. Hardness was measured using a semi automatic micro hardness tester (Model MVK-H11, Mitutoyo make, Japan) by applying a load of 0.02 kg for a dwell time of 15 s. Hardness test was repeated for six times and the average value of hardness was presented.

Chemical analysis of sample was performed using scanning electron microscope (Model S-3000H, Hitachi High-Technologies Corporation) with energy dispersive X- ray spectroscopy (EDS).

1.3 Design of experiments using response surface methodology

Three parameters viz., load (10–50 N), velocity (1–5 m·s^{-1}) and sliding distance (500–2,500 m) were considered. Design expert version 10 was used to design the experiments. Central composite design was selected and it generated 20 experimental runs for three factors and five levels. Dry sliding wear test process parameters and their levels are shown in Table 3. The objective function of optimisation is to minimise the wear rate of composites. Wear rate was calculated using cumulative volume loss and sliding distance. Also a second order polynomial regression equation as shown in Eq. (1) was developed to predict the response by correlating the input parameters:

$$w = b_0+\sum b_1 x_i+\sum b_2 x_i^2+\sum b_3 x_i x_j \tag{1}$$

where, w is wear rate (response), b_0, b_1, b_2 and b_3 are coefficients. The second term (x_i) denotes linear effect; third term (x_i^2) represents second order effect and fourth term ($x_i x_j$) represents interaction effect.

Table 3: Experimental process parameters and their levels

Parameters	Levels				
Load (N)	10	18	30	42	50
Velocity (m·s^{-1})	1	1.8	3	4.2	5
Sliding distance (m)	500	905	1500	2095	2500

1.4 Dry sliding wear testing

Samples of 10 mm diameter with 40 mm height were prepared as per ASTM G99 standard [4] to test the wear rate of composites. Dry sliding wear test was performed as per experimental design using pin-on-disc wear testing apparatus (Model TR-20LE-M108 and Ducom make, India) at room temperature. Pin-on-disc apparatus consists of a hardened steel disc with hardness of 64 HRc and the samples were rotated against the disc, producing sliding wear. Load was applied through a lever arrangement which makes the contact between the specimen and the disc.

Initially the samples were cleaned with acetone and the disc was polished using emery sheet to obtain a clean surface. Based on the experimental design, samples were tested and the weight of the pin was measured using electronic weighing balance with an accuracy of 0.001 mg. Wear rate was calculated using the following formula:

$$w = m/\rho D \tag{2}$$

where, w is wear rate of specimen (mm^3·m^{-1}), m is mass loss (g). ρ is density (g·mm^{-3}) and D is sliding distance (m).

Mass loss was calculated by measuring the weight of the pin before and after wear test. Density of pin was calculated using Archimedes principle and wear rate was calculated based on the mass loss, density and sliding distance for each experiment.

According to Archards law [4], wear rate is given as follows:

$$w = bLD \quad (3)$$

where, w is wear rate of specimen ($mm^3 \cdot m^{-1}$), b is wear coefficient, L is load applied in normal direction (N), and D is sliding distance (m).

Worn surfaces of samples were examined and characterized using field emission scanning electron microscope (FESEM).

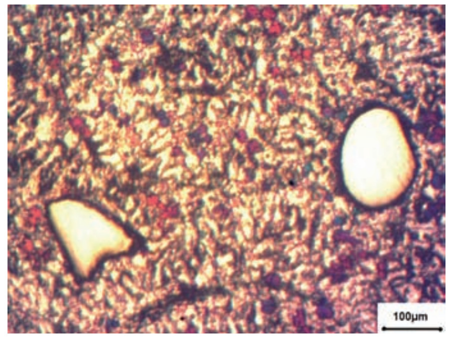

Fig. 2: Optical microstructure of LM13/FeCu composite

2 Results and discussion

2.1 Microstructure

Figure 2 shows the microstructure of FeCu/LM13 composite examined using image analyser. It can be seen that copper coated steel fibers are uniformly dispersed in matrix. During the composite preparation, composite melt stirred at a high speed of 750 rpm produced vortex, and the fibers were uniformly distributed throughout the matrix. Better interface bonding between steel fibers and aluminium alloy was observed due to the presence of copper coating on fibers. A constant pressure was applied during the solidification which minimized the porosity resulting in fine grain structure. Radhika, et al [8] also reported a similar result of uniform dispersion which were achieved using a high stirring speed in the stirring casting process.

Micrograph of FeCu/LM13 composite as shown in Fig. 3 reveals the reinforcement of copper coated steel fibers in LM13 aluminium alloy with various elements distribution in matrix and reinforcement. Figure 4 shows EDS spectrum of FeCu/LM13 composite which reveals the presence of major constitutions in matrix such as Al and Si and reinforcement (Fe). Also intermetallic compound (Fe,Cu) is observed at the interface of aluminium and steel fibers. This may be attributed to the effect of copper coating on reinforcement which prevents the formation of Fe/Al compounds at the interface of matrix and reinforcement.

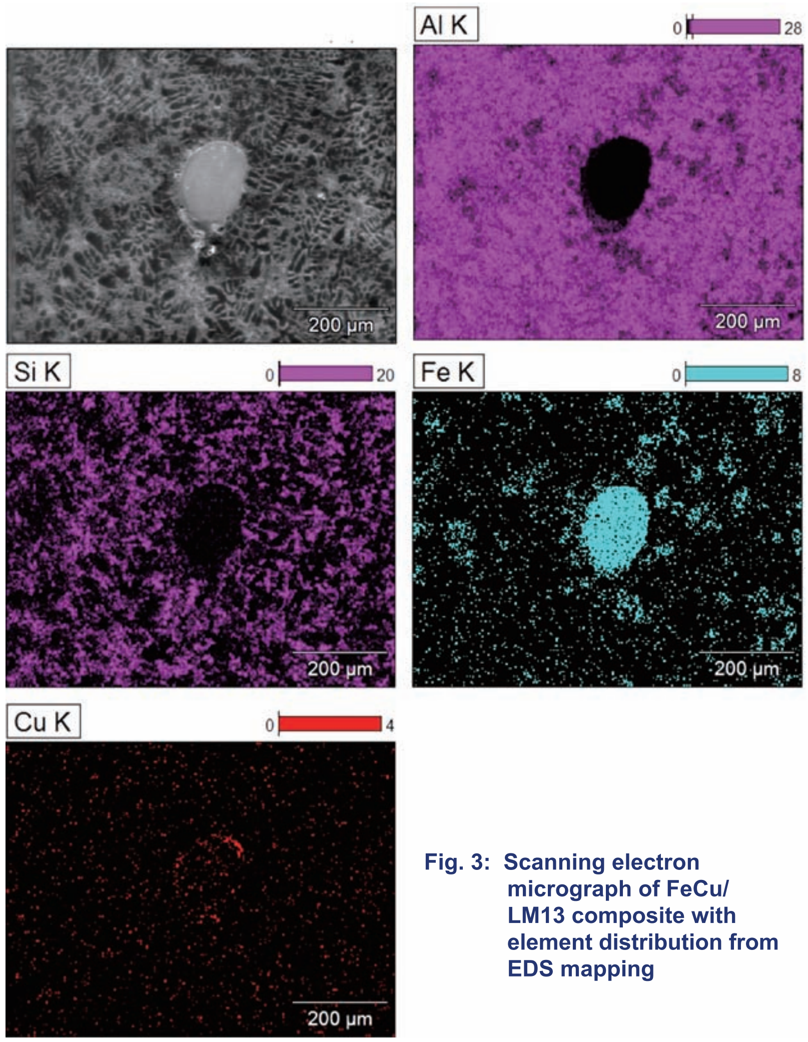

Fig. 3: Scanning electron micrograph of FeCu/LM13 composite with element distribution from EDS mapping

2.2 Characterization of dry sliding wear

Design of experiments developed using RSM for three parameters (load, velocity and sliding distance) and five levels are shown in Table 4. Six trials were performed for each experiment and average wear rate of composite was presented. During the wear test, it was observed that weight loss of pin decreased due to the reinforcement of copper coated steel fibers in LM13 aluminium alloy.

R^2 and adjusted R^2 values are found as 98.75

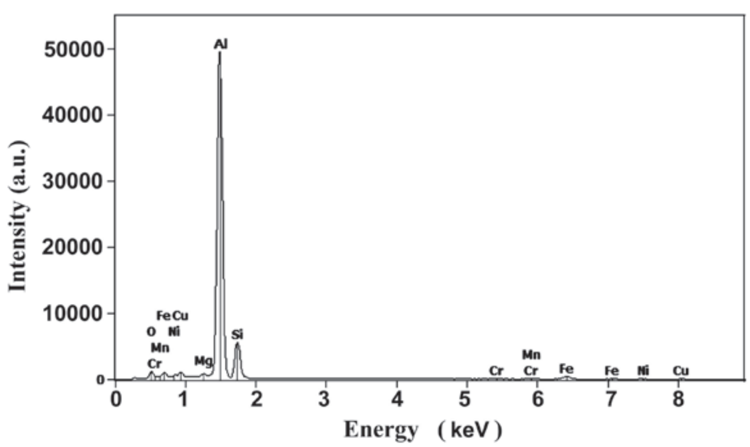

Fig. 4: Spectrum of FeCu/LM13 composite EDS

Table 4: Experimental design matrix and results of wear rate

Test run	Load (N)	Velocity (m·s^{-1})	Sliding distance (m)	Wear rate (mm^3·m^{-1})
1	30	3	500	0.00282
2	10	3	1,500	0.00238
3	42	4.2	2,095	0.00354
4	18	4.2	905	0.00234
5	42	4.2	905	0.00328
6	30	1	1,500	0.00275
7	30	5	1,500	0.00298
8	30	3	1,500	0.00287
9	30	3	1,500	0.00285
10	30	3	1,500	0.00285
11	18	1.8	905	0.00274
12	50	3	1,500	0.00340
13	30	3	1,500	0.00292
14	18	1.8	2,095	0.00274
15	42	1.8	2,095	0.00294
16	42	1.8	905	0.00284
17	30	3	1,500	0.00292
18	18	4.2	2,095	0.00259
19	30	3	1,500	0.00280
20	30	3	2,500	0.00297

and 97.63%, respectively. These values are very closer to each other and the parameters were tested for the significance at 95% confidence level. Significant parameters are considered in regression model and insignificant parameters are removed without affecting the accuracy. The results showed that load, velocity, sliding distance, interaction of load and velocity, interaction of velocity and sliding distance have more significant effects on wear rate. In addition, the interaction of load and sliding distance, second order terms of load, velocity and sliding distance have the p value greater than 0.10, which are not significant. A regression equation is obtained for predicting the wear rate and is given as:

$$w = b_0 + b_1L + b_2V + b_3D + b_4LV + b_5VD \qquad (4)$$

where, w is wear rate of specimen (mm^3·m^{-1}), b_0, b_1, b_2, b_3, b_4 and b_5 are regression coefficients, L is load applied in normal direction (N), V is sliding velocity (m·s^{-1}) and D is sliding distance (m). The coefficients of regression equation are listed in Table 5.

This developed model can predict the wear rate of composites with respect to input parameters, viz., load, velocity and sliding distance. To check the accuracy of the regression model, confirmation tests were performed and new sets of input parameters were selected which differed from the earlier experimental design developed using central composite design. Wear rate was calculated for the new sets of dry sliding wear parameters which were compared with predicted wear rate

Table 5: Coefficients of regression equation for wear rate of FeCu/LM13 composites

	Regression coefficients					
	b0	b1	b2	b3	b4	b5
Value	0.00362	0.000017	0.00054	0.00000025	0.000014	0.00000012

Table 6: Comparison of wear rate using regression analysis and experimental results

Test run	Load (N)	Velocity (m·s^{-1})	Sliding distance (m)	Actual wear rate (mm^3·m^{-1})	Predicted wear rate (mm^3·m^{-1})	Error (%)
1	5	1.5	800	0.00287	0.002779	3.27
2	15	3.5	1,600	0.00243	0.002487	-2.29
3	25	4.5	2,400	0.00321	0.003041	5.56

and the results are shown in Table 6. The percentage of error was calculated using experimental and predicted wear rates and the error percentage was within ± 6, which confirms that the developed model can predict the wear rate with greater accuracy. Several researchers used central composite design and developed the regression model to predict the response[20–23]. The relationship between predicted and actual wear rates is shown in Fig. 5. It can be seen that there is a good agreement between predicted and actual wear rates, and the values are scattered on both sides and the slope is close to unity.

Analysis of variance (ANOVA) for wear rate is shown in Table 7. The significance of each term in regression model is checked at 95% confidence level and 5% significance level. The load, velocity, sliding distance, interaction of load and velocity, interaction of velocity and sliding distance have significance in wear rate (p value < 0.05). Also the lack of fit has F value of 0.82, which is lesser than the standard F value of 5.05 (95% confidence level), hence the developed model is adequate with greater accuracy and it can be used to predict the wear rate within these input parameters and their levels.

Figures 6 – 8 show the response surface plot of actual wear rate for all pairs of process parameters. Figure 6 shows the interaction of load and velocity with respect to wear rate. It can be seen that wear rate of composites increases with increasing load at all levels of velocity and sliding distances (Figs. 6 and 7). During the wear test, the load was applied using lever attachment, which made the composite pin closer contact to the rotating steel disc. As load increases from 10 to 50 N,

Table 7: Analysis of variance for wear rate

Source	Sum of Squares	Degree of freedom	Mean square	F value	p - value
Model	0.000001567	9	0.0000001741	87.86	< 0.0001*
Load (N)	0.000001083	1	0.000001083	546.57	< 0.0001*
Velocity ($m \cdot s^{-1}$)	0.000000060	1	0.00000006045	30.50	0.0003*
Sliding distance (m)	0.000000026	1	0.00000002603	13.14	0.0047*
Load (N) x Velocity ($m \cdot s^{-1}$)	0.000000338	1	0.0000003383	170.73	< 0.0001*
Load (N) x sliding distance (m)	0.000000003	1	0.0000000027	1.40	0.2640
Velocity ($m \cdot s^{-1}$) x sliding distance (m)	0.000000055	1	0.00000005538	27.94	0.0004*
Load (N) x load (N)	0.0000000001	1	0.00000000015	0.078	0.7863
Velocity ($m \cdot s^{-1}$) x velocity ($m \cdot s^{-1}$)	0.0000000003	1	0.00000000032	0.16	0.6955
Sliding distance (m) x sliding distance (m)	0.0000000004	1	0.00000000042	0.22	0.6516
Residual	0.0000000198	10	0.00000000198		
Lack of fit	0.0000000089	5	0.00000000178	0.82	0.5859
Pure error	0.0000000109	5	0.00000000218		
Total	0.00000158	19			

R^2 : 0.9875, adjusted R^2: 0.9763; *significant at $p < 0.05$

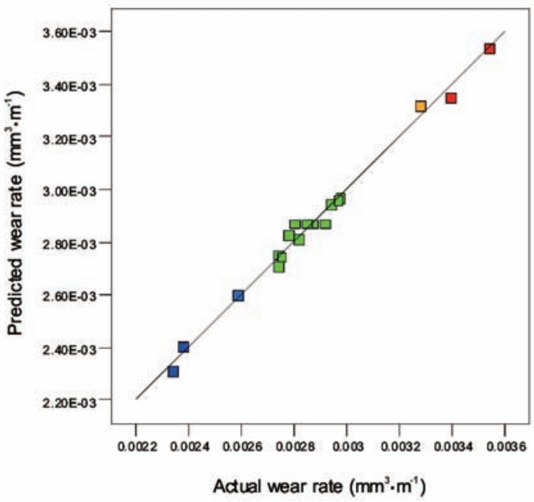

Fig. 5: Scatter diagram for wear rate of FeCu/LM13 composite

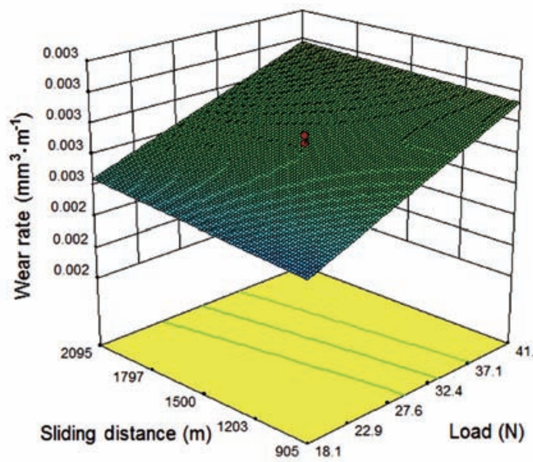

Fig. 7: Response surface plot of wear rate as a function of load and sliding distance for a constant velocity of 3 $m \cdot s^{-1}$

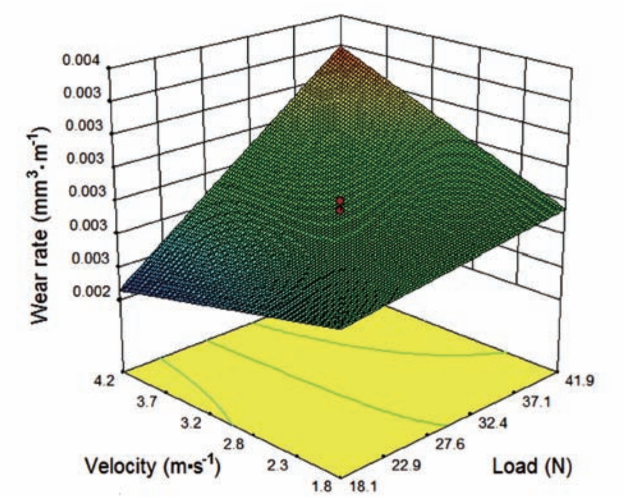

Fig. 6: Response surface plot of wear rate as a function of load and velocity for a constant sliding distance of 1,500 m

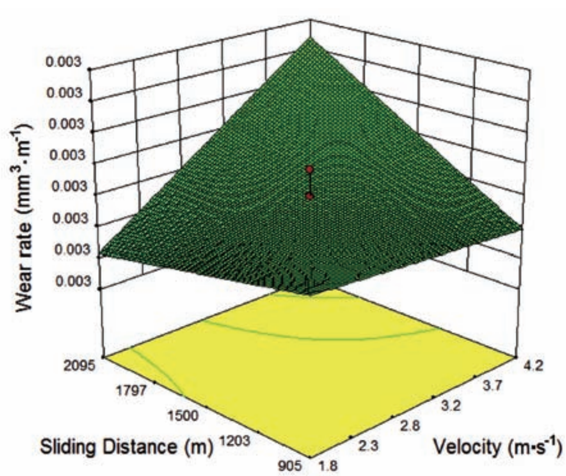

Fig. 8: Response surface plot of wear rate as a function of velocity and sliding distance for a constant load of 30 N

the contact between the pin and disc reduces which in turn increases the temperature at the interface resulting in increased wear rate. The same wear behaviour has been obtained in other studies by our research team [4,24]. The increase in sliding velocity (1.8–4.2 m·s^{-1}) decreases the wear rate of composites at lower loads. Wear rate of composite is found minimum at the earlier stage and reaches the maximum value while increasing load and sliding velocity. At lower velocity, the contact time between pin with disc is more, which increases the amount of material loss resulting in high wear rate. As sliding velocity increases, the temperature at the interface increases which forms a mechanically mixed layer (MML) over the surface of pin. This oxide layer prevents the specimen from adhesive wear, which reduces the wear rate of composite at minimum load. As load increases from 10 to 50 N, the oxide layer breaks down that causes high wear rate at 50 N and velocity of 5 m·s^{-1}. Similar wear mechanism has been observed in other studies [9,25] which reported that wear rate of materials increases with increment in sliding velocity.

The interaction of load and sliding distance with wear rate is depicted in Fig. 7. The wear rate increases with increasing sliding distance at all levels of loads. Figure 8 shows the relationship between velocity and sliding distance with respect to wear rate. It is observed that wear rate increases with increasing velocity and sliding distance. At earlier stage, wear rate of composites decreases slightly with increasing sliding distance. This is due to presence of copper coated steel fibers that protrude at the surface, which establishes contact with the counterface. As sliding distance and velocity increases, the hard asperities at the surface smoothes after run for a certain sliding distance. A few researchers [3,10] also reported the same mechanism that uniform contact between pin surface and disc resulting minimum wear rate of specimen.

2.3 Optimisation of dry sliding parameters

Dry sliding parameters viz., load (10–50 N), velocity (1–5 m·s^{-1}) and sliding distance (500–2,500 m) were considered in this present work and experiments were carried out according to the experimental design using response surface methodology. Wear rate of samples were measured and response surface were plotted which reveals the interaction of load, velocity and sliding distance with wear rate. The main objective of optimisation process was to obtain minimum wear rate for FeCu/LM13 composites. During the experimental work, a minimum wear rate of 0.00234 mm^3·m^{-1} (Table 4) was achieved. Hence the target wear rate of 0.00233 mm^3·m^{-1} was used as input for optimisation process, which is less than the minimum experimental wear rate (0.00234 mm^3·m^{-1}). A load of 18.46 N, velocity of 4.11 m·s^{-1} and a sliding distance of 923 m were obtained as the optimum dry sliding parameters for the wear rate of 0.00233 mm^3·m^{-1} .

2.4. Worn surface analysis

Figure 9 shows the worn surface of LM13 – 10wt% copper coated steel fibers reinforced composites tested at dry sliding condition. Worn surface of composites is shown in Fig. 9(a-c). It can be seen from Fig. 9(a) that there are shallow grooves at some regions in addition to fine grooves at lower load (10 N). The wear rate is lower at lower load, since the reinforcement particles act as load bearing elements which avoid the contact between pin and disc. These elements would bear the load and prevent the transfer of load to the LM13 aluminium alloy, resulting in minimum wear rate. Figure 9(b) shows that the worn surface of composite tested at 30 N have continuous grooves parallel to the sliding direction. While increasing load from 10 to 30 N, the contact between pin and disc reduces which results in more amount of material removal from the pin. This removed material slide along the surface of specimen while friction counterface rotates continuously, resulting in continuous grooves on the surface of pin. The worn surface of composite tested at 50 N as shown in Fig. 9(c), reveals local delamination on the surface in addition to continuous grooves. This is due to the generation of high temperature at the interface. As load increases from 30 to 50 N, more amount of heat is generated due to friction which results in deformation of material and in removal of more materials. Wear mechanism changes from mild adhesion wear to severe delamination when load increases from 10 to 50 N. These results are verified with wear trends as observed from the surface plots (Figs. 6 and 7) that wear rate increased linearly with increasing load from 10 to 50 N. The same phenomenon has been observed in a previous study [10].

In general, wear rate of composites increases with increasing load, but the severity of wear is delayed at all loading conditions. This is due to the surface hardness of composites, as the composite has the surface hardness of 251 VHN which resists the amount of deformation at all loading conditions. Hardness of composites increases by reinforcing hard copper coated steel fibers in LM13 aluminium alloy, which reduces the wear rate at all loads. The lower wear rate can also relate to the materials and process parameters. LM13 aluminium alloy has high silicon content of 10.9%, which imparts higher hardness and results in wear resistance to matrix. Also the preheating of reinforcement, stirring at high speed, bottom pouring of composite, and application of squeeze pressure result in uniform dispersion of steel fibers in LM13 aluminium alloy and minimize the porosity in composites. Further, magnesium and silicon content in aluminium alloy promote the wettablity, and copper coating on reinforcement offers better interface bonding between reinforcement and matrix. This good interface bonding and uniform dispersion of reinforcement in matrix result in lower wear rate at all testing conditions.

Figures 9(d) and (e) show the transition of wear mechanism of composite from the sliding velocity of 1 to 3 m·s^{-1}. The worn surface depicted in Fig. 9(d) (V = 1 m·s^{-1}) reveals less amount of material removal than that shown in Fig. 9(e) (V = 3 m·s^{-1}). Increase in sliding velocity causes more frictional heat in the contact area [26]. At lower velocity, low frictional heat is developed in the contact area, low amount of material removal results in minimum wear rate and mild damage on the surface. Figure 9(e) shows that the worn surface of composite tested at

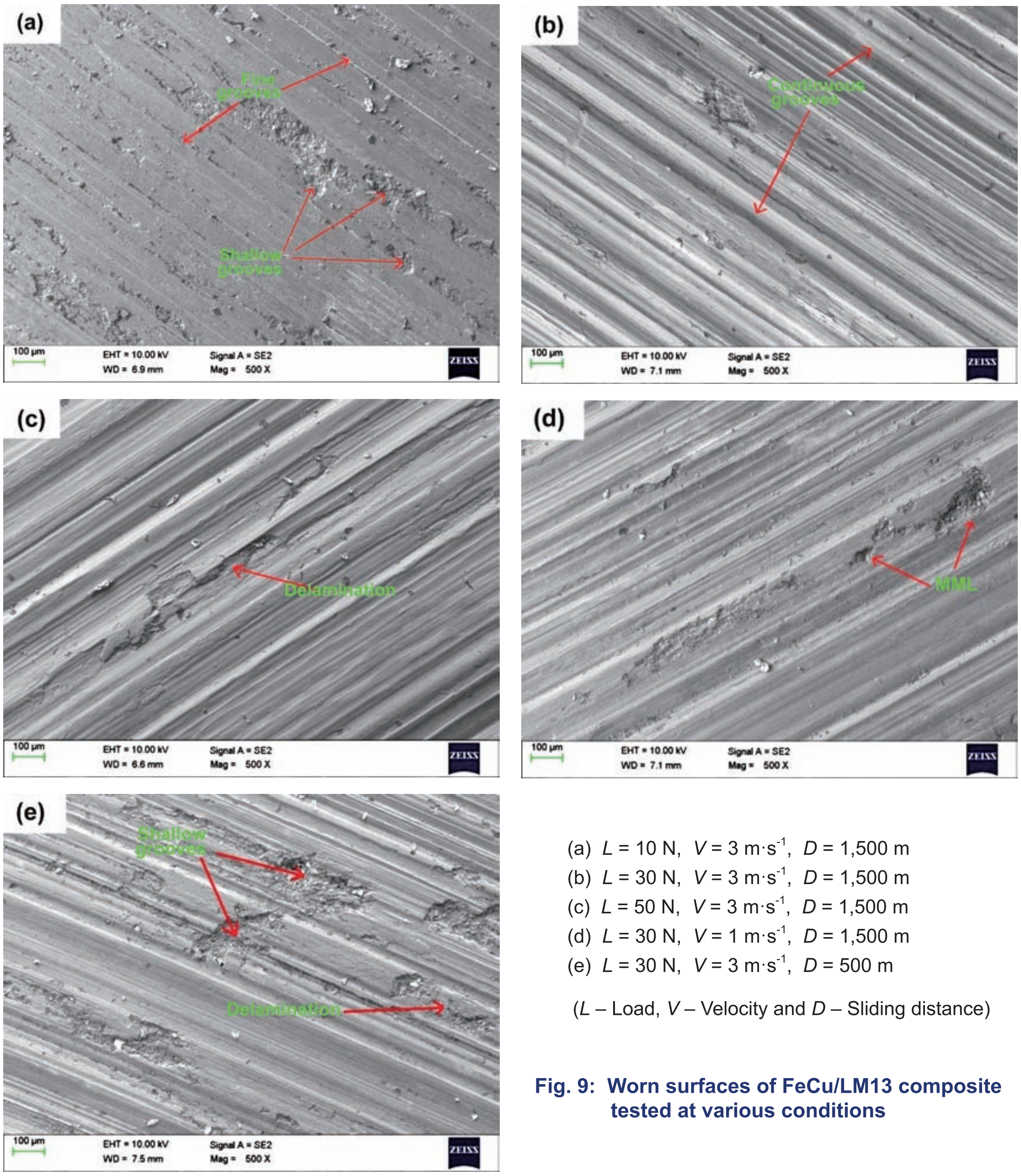

(a) L = 10 N, V = 3 m·s^{-1}, D = 1,500 m
(b) L = 30 N, V = 3 m·s^{-1}, D = 1,500 m
(c) L = 50 N, V = 3 m·s^{-1}, D = 1,500 m
(d) L = 30 N, V = 1 m·s^{-1}, D = 1,500 m
(e) L = 30 N, V = 3 m·s^{-1}, D = 500 m

(L – Load, V – Velocity and D – Sliding distance)

Fig. 9: Worn surfaces of FeCu/LM13 composite tested at various conditions

a velocity of 3 m·s^{-1} have shallow grooves and delamination on the surface. It may be attributed to the high frictional heat developed in the contact area due to high velocity. The results are verified with wear trends as observed from the response surface plots (Fig. 8) that wear rate of composites increases with an increase in the sliding velocity. The same mechanism was observed in previous studies [10,27] that increase in velocity cause severe damage on the surface of pin.

Figure 10 shows the worn surface of composite tested at optimum conditions [L = 18.46 N, V= 4.11 m·s^{-1}, D = 923 m]. The accuracy of developed regression model is checked by investigating the worn surface tested at optimum process parameters. Fine scratches are observed at some regions on the surface resulting in minimum wear rate. This ensures the accuracy of developed regression model which predicts the wear rate within the ranges of load, velocity and sliding distance.

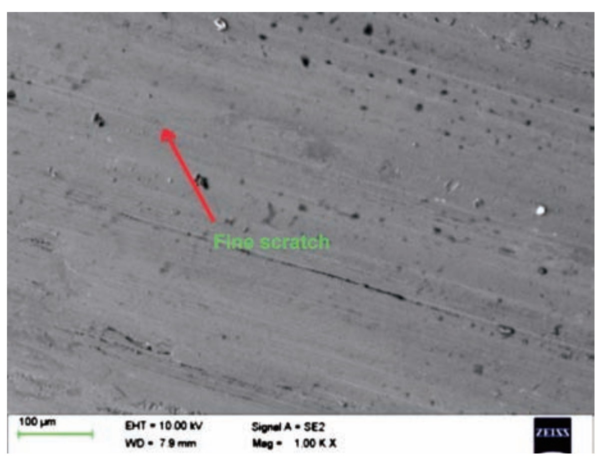

Fig. 10: Worn surface of FeCu/LM13 composite tested at optimum conditions: L = 18.46 N, V = 4.11 m·s^{-1}, D = 923 m (L – Load, V – Velocity and D – Sliding distance)

3 Conclusions

(1) A regression model is developed to predict the wear rate of composite and the error percentage is within ± 6.

(2) Response surface plots reveal that wear rate of composites increases with increasing load up to 50 N with the velocity 1–5 $m \cdot s^{-1}$ and a sliding distance up to 2,500 m. However wear rate decreases with increasing velocity at lower loads (up to 20 N) and increases after reaching transition velocity of 2 $m \cdot s^{-1}$.

(3) 18.46 N load, 4.11 $m \cdot s^{-1}$velocity and 923 m sliding distance are obtained as the optimum dry sliding parameters for obtaining minimum wear rate of 0.00233 $mm^3 \cdot m^{-1}$.

(4) Worn surface of composite shows shallow grooves at lower loads (upto 30 N) and severe wear at higher loads (40–50 N) resulting in delamination and the highest wear rate being 0.00354 $mm^3 \cdot m^{-1}$.

References

[1] Miller W, Zhuang L, Bottema J, et al. Recent development in aluminium alloys for the automotive industry. Mater. Sci. Eng. A., 2000, 280: 37–49.

[2] Heinz A, Haszler A, Keidel C, et al. Recent development in aluminium alloys for aerospace applications. Mater. Sci. Eng. A., 2000, 280: 102–107.

[3] Natarajan N, Vijayarangan S, Rajendran I. Wear behaviour of A356/25SiCp aluminium matrix composites sliding against automobile friction material. Wear. 2006, 261: 812–822.

[4] Kumar B A, Murugan N, Dinaharan I. Dry sliding wear behavior of stir cast AA6061-T6/AlNp composite. Trans. Nonferrous Met. Soc. China, 2014, 24: 2785–2795.

[5] Monikandan V V, Joseph M A, Rajendrakumar P K. Dry Sliding Tribological Studies of AA6061-B 4 C-Gr Hybrid Composites. J. Mater. Eng. Perform., 2016, 25 (10) : 4219–4229

[6] Iwai Y, Honda T, Miyajima T, et al. Dry sliding wear behavior of Al 2 O 3 ber reinforced aluminum composites, Compos. Sci. Technol., 2000, 60: 1781–1789.

[7] Mandal D, Dutta B K, Panigrahi S C. Wear and friction behavior of stir cast aluminium-base short steel fiber reinforced composites. Wear, 2004, 257: 654–664.

[8] Radhika N, Raghu R. Dry Sliding Wear Behaviour of Aluminium Al-Si12Cu/TiB_2 Metal Matrix Composite Using Response Surface Methodology. Tribol. Lett., 2015, 59(1): 2–7.

[9] Soorya Prakash K, Kanagaraj A, Gopal P M. Dry sliding wear characterization of Al 6061/rock dust composite. Trans. Nonferrous Met. Soc. China, 2015, 25: 3893–3903.

[10] Dinaharan I Murugan N. Dry sliding wear behavior of AA6061 / ZrB2 in- situ composite. Transactions of Nonferrous Metals Society of China, 2012, 22 (4): 810–818

[11] Seshan S, Guruprasad A, Prabha M, et al. Fibre-reinforced metal matrix composites — a review. Journal of the Indian Institute of Science, 1996, 76 (1) : 1–14

[12] Vijian P, Arunachalam V P. Optimization of squeeze casting process parameters using Taguchi analysis. Int. J. Adv. Manuf. Technol., 2006, 33: 1122–1127.

[13] Soundararajan R, Ramesh A, Mohanraj N, et al. An investigation of material removal rate and surface roughness of squeeze casted A413 alloy on WEDM by multi response optimization using RSM. J. Alloys Compd., 2016, 685: 533–545.

[14] Ghomashchi M R, Vikhrov A. Squeeze casting: An overview. J. Mater. Process. Technol., 2000, 101: 1–9.

[15] Suresh K R, Niranjan H B, Jebaraj P M, et al. Tensile and wear properties of aluminum composites. Wear, 2003, 255: 638–642.

[16] Senthil P, Amirthagadeswaran K S. Optimization of squeeze casting parameters for non symmetrical AC2A aluminium alloy castings through Taguchi method. J. Mech. Sci. Technol., 2012, 26: 1141–1147.

[17] Bhagat R B. High pressure squeeze casting of stainless steel wire reinforced aluminium matrix composites. Composites, 1988, 19: 393–399.

[18] Gupta M, Lai M O, Soo C Y. Effect of type of processing on the microstructural features and mechanical properties of A1–Cu / SiC metal matrix composites. Materials & Design, 1996, 16 (2): 114–122

[19] Pawar P B, Utpat A A. Development of Aluminium Based Silicon Carbide Particulate Metal Matrix Composite for Spur Gear. Procedia Mater. Sci., 2014, 6: 1150–1156.

[20] Rajakumar S, Muralidharan C, Balasubramanian V. Establishing empirical relationships to predict grain size and tensile strength of friction stir welded AA 6061-T6 aluminium alloy joints. Trans. Nonferrous Met. Soc. China, 2010, 20: 1863–1872.

[21] Karthikeyan R, Balasubramanian V. Predictions of the optimized friction stir spot welding process parameters for joining AA2024 aluminum alloy using RSM. International Journal of Advanced Manufacturing, 2010, 51 (1-4): 173–183

[22] Thambidurai M, Muthukumarasamy N, Murugan N, et al. Development of Mathematical Model for Prediction and Optimization of Particle Size in Nanocrystalline CdS Thin Films Prepared by Sol-Gel Spin-Coating Method. Metallurgical & Materials Transactions B, 2010, 41 (6) : 1338–1345

[23] Rajakumar S, Muralidharan C, Balasubramanian V. Predicting tensile strength, hardness and corrosion rate of friction stir welded AA6061-T6 aluminium alloy joints. Mater. Des., 2011, 32: 2878–2890.

[24] Dwivedi D K. Adhesive wear behaviour of cast aluminium-silicon alloys: Overview. Mater. Des., 2010, 31: 2517–2531.

[25] Radhika N, Subramanian R. Effect of reinforcement on wear behaviour of aluminium hybrid composites. Tribology – Materials Surfaces & Interfaces, 2013, 7 (1): 36–41

[26] Rao R N, Das S. Effect of SiC content and sliding speed on the wear behaviour of aluminium matrix composites. Mater. Des., 2011, 32: 1066–1071.

[27] Kumar B, Murugan N, Dinaharan I. Dry sliding wear behavior of stir cast AA6061- T6 / AlNp composite. Transactions of Nonferrous Metals Society of China, 2014 , 24 (9): 2785–2795

Effect of Copper Coating and Reinforcement Orientation on Mechanical Properties of LM6 Aluminium Alloy Composites Reinforced with Steel Mesh by Squeeze Casting

Article *in* Transactions of the Indian Institute of Metals · December 2017

DOI: 10.1007/s12666-017-1235-2

Samson Jerold Samuel C
Sri Krishna College of Engineering and Technology

Arthanari Ramesh
Sri Krishna College of Technology

Kamal Shankar Selvaraj

Trans Indian Inst Met
https://doi.org/10.1007/s12666-017-1235-2

RAPID COMMUNICATION

Effect of Copper Coating and Reinforcement Orientation on Mechanical Properties of LM6 Aluminium Alloy Composites Reinforced with Steel Mesh by Squeeze Casting

Samson Jerold Samuel Chelladurai[1] · Ramesh Arthanari[2] · Kirubaharan Krishnamoorthy[1] · Kamal Shankar Selvaraj[1] · Prabu Govindan[1]

Received: 31 May 2017 / Accepted: 17 November 2017

Abstract Uncoated and copper coated steel wire mesh reinforcing LM6 aluminium alloy composites have been produced using squeeze casting process by varying reinforcement orientation viz., 0°, 45° and 90° respectively. Microstructure of the castings has been examined and mechanical properties such as hardness, tensile strength and ductility have been investigated. Fracture surface of tensile specimens has been analysed using field emission scanning electron microscope. Microstructure of samples reveals that copper coating on steel wires improves the interface bonding between matrix and reinforcement. Average hardness values of 259 and 90 Hv have been observed in steel wire and matrix respectively. Tensile strength of composites increases with increasing angle of reinforcement orientation from 0° to 90°. Tensile strength increases up to 11% by reinforcing copper coated steel wire mesh at 90° orientation as compared to LM6 aluminium alloy. Fracture surface of composites shows pullout of steel wires in uncoated steel wire mesh composites and broken wires in copper coated steel wire mesh composites respectively. Dimples have been observed on the fracture surface of LM6 aluminium alloy. In general, copper coated steel wire mesh composites offer better hardness and tensile strength compared to uncoated steel wire mesh composites and LM6 aluminium alloy. This may be attributed to the copper coating on steel wires which results better interface bonding between matrix and reinforcement.

✉ Samson Jerold Samuel Chelladurai
samsonjeroldsamuel@skcet.ac.in

1 Department of Mechanical Engineering, Sri Krishna College of Engineering and Technology, Coimbatore 641008, India

2 Department of Mechanical Engineering, Sri Krishna College of Technology, Coimbatore 641042, India

Keywords LM6 aluminium alloy · Steel mesh · Microstructure · Hardness · Tensile strength · Ductility

1 Introduction

Aluminium matrix composites have been used as structural member in automobile, aerospace, marine and industrial applications because of its high specific strength, better wear resistance and stability at high temperatures [1–3]. LM6 aluminium alloy has been selected as matrix because of its high silicon content and excellent fluidity property [4, 5]. Reinforcements such as aluminium oxide, silicon carbide, iron, quartz, aluminium boride, boron carbide, rock dust, carbon and beryl in the form of particles, whiskers and fibers improve the mechanical properties such as hardness, tensile strength and wear resistance. However, ductility of the composites decreases with increasing weight percentage of reinforcement [5–15]. Steel wire mesh has been selected as reinforcement because of its low coefficient of thermal expansion, good wear resistance, high elastic modulus and high strength [16].

Aluminium matrix composites have been prepared using various techniques such as powder metallurgy, diffusion bonding, spray co-deposition, in situ solidification and casting methods. Among all processes, casting route has been widely accepted as most economical, simple and viable method for composite fabrication [1]. Various casting process such as vortex method, compo casting and infiltration method have been widely used in industries. In these, squeeze casting is most preferred manufacturing process for commercial applications because of the capability of mass production, easier operational parameters,

Published online: 06 December 2017

Characterization and Optimization of Abrasive Water Jet Machining Parameters of Aluminium /Tungsten Carbide Composites

Article · April 2018

1 author:

Pridhar Thiagarajan
Sri Krishna College of Technology

Measurement 117 (2018) 57–66

Contents lists available at ScienceDirect

Measurement

journal homepage: www.elsevier.com/locate/measurement

Characterization and optimization of Abrasive Water Jet Machining parameters of aluminium/tungsten carbide composites

K. Ravi Kumar[a,*], V.S. Sreebalaji[a], T. Pridhar[b]

[a] Department of Mechanical Engineering, Dr. NGP Institute of Technology, Coimbatore, India
[b] Department of Mechanical Engineering, Sri Krishna College of Technology, Coimbatore, India

ARTICLE INFO

Keywords:
Composites
Aluminium
Tungsten carbide
Desirability
AWJM
Optimization

ABSTRACT

The present study aims to optimize the Abrasive Water Jet Machining parameters while machining aluminium/tungsten carbide composites. Investigations were carried on 2, 4, 6, 8 and 10 wt% tungsten carbide reinforced composite specimens fabricated by stir casting technique. Response surface methodology was employed to explore the influence of abrasive jet parameters and their relations on the responses. Microstructure of the machined surfaces was examined by scanning electron microscope. Material removal rate is greatly influenced by transverse speed followed by % reinforcement and standoff distance respectively, while surface roughness is highly influenced by % tungsten carbide followed by transverse speed and standoff distance. The optimum parameter set in maximizing the material removal rate and minimizing the surface roughness is standoff distance – 4.22 mm, transverse speed – 223.28 mm/min, and percentage WC – 2.10%. The experimental results and multi response optimization obtained provide a technical database for industrial applications.

1. Introduction

Metal Matrix Composites (MMC) comprise an important structural materials due to its particular interest as lightweight materials for industries possessing improved modulus, strength, fatigue and fracture resistance even at elevated temperatures [1]. Abrasive Water Jet Machining (AWJM) removes material from the surface by erosion of fine-grained abrasive particles striking the surface at a high velocity [2]. The kerf width of composites increased with an increase in pressure and standoff distance, while kerf width decreased with increase in feed rate [3,4]. Kowsari et al. [5] observed that the holes made by AJM became highly non uniform at larger depths along the jet alignment direction. Wang [6] investigated AWJM of alumina ceramics and reported that nozzle oscillation causes negative effect on the depth of cut while selecting improper cutting parameters. Haghbin et al. [7] reported that the erosion rate of composites decreased with increase in channel depth. Nouraei et al. [8] reported that the ductile erosion during AWJM plays a major role in reducing the SR and waviness of the channels. Haghbin et al. [9] reported that the erosion rate of high-pressure slurry jet micro-machining was lower due to the smaller width of micro-channels. Caydas and Hascalik [10] observed three distinct regions along the machined wall surface namely initial damage region, a smooth cutting region and a rough cutting region during microstructure evaluation of AWJM. Jafar et al. [11] reported deeper and rougher channels at higher kinetic energy jets while machining borosilicate glass using abrasive slurry jet machining. Kumar and Shukla [12] observed that the depth of cut is higher for larger impact angles and maximum at an angle of 90°. Gupta et al. [13] revealed that at higher water pressure the kerf angle and top kerf width is primarily influenced by the nozzle transverse speed. Sasikumar et al. [14] suggested that minimum Kerf angle and good surface finish of aluminium composites by AWJM can be achieved at higher water jet pressure, low transverse speed and less standoff distance. Ajit and Shailendra et al. [15] found that delamination of composites decreases with increase in abrasive mass flow rate, pressure and decrease in traverse rate, while decrease in stand-off distance decreases the Kerf width of composites. Zarko Cojbasic et al. [16] reported that the SR depends primarily on abrasive flow rate, thickness of the work piece, cutting speed. According to Adnan Akkurt [17] increase in stand-off distance increased the kerf widths of composite due to the growth and breakdown of jet outside the boundary interaction. Ali et al. [18] described that with an increase in feed rate, the contamination of abrasive particles also increases due to the striation formed on the surface. Santhanakumar et al. [19] reported that the machining parameters namely stand-off distance, water pressure, traverse speed and abrasive flow rate have potential influence on the striation angle and striation zone length of $Al/SiC/Al_2O_3$ composites. Selvaraj et al. [20] fabricated Al composites reinforced with AlN, Si_3N_4 and ZrB_2 particles and reported that the erosion wear is

* Corresponding author.
E-mail addresses: ravik_krish@yahoo.com (K. Ravi Kumar), balajivsv71@gmail.com (V.S. Sreebalaji), preeth_t@rediffmail.com (T. Pridhar).

https://doi.org/10.1016/j.measurement.2017.11.059
Received 10 September 2017; Received in revised form 26 November 2017; Accepted 28 November 2017
Available online 29 November 2017
0263-2241/

characterised by plastic deformation, micro cutting of erosion particles in shallow angle and presence of hardened layer. Srivastava et al. [21] studied the abrasive water jet turning of $Al/B_4C/Al_2O_3$ and reported that traverse speed is one among the important parameter influencing MRR and SR of AWJ turning. Kumaran et al. [22] presented that lower traverse speed and standoff distance combined with increased pressure exhibited a better surface on the carbon fiber reinforced plastics. Viganoa et al. [23] reported that the waviness of Kerf is influenced by the random position of struts in the workpiece. Yuvaraj et al. [24] reported that a jet impingement angle decreases the fragmentation of the particles and assist the particles to move deeply into the work during AWJM of D_2 steel. Ahmed et al. [25] found that the radius of curvature of AWJM groove influences the particle impact angle along the groove surface. Kowsari et al. [26] observed edge rounding along the surface of machined holes because of the cavitation formed due to the flow of abrasive slurry at high speed. Divyansh and Puneet [27] observed that the deformation behavior of composites along the machining path of AWJM process gets softened due to the localised heat and changes the deformation behavior of the work piece.

Taguchi method was employed by Reddy et al. [28] to optimize the AJM machining parameters of Inconel alloy. Rajkamal and Dinesh [29] employed optimization techniques like fire fly algorithm, biogeography, simulated annealing, particle swarm optimization, black hole, artificial bee colony and genetic algorithm to optimize the AWJM parameters of AA631-T6. Grey-fuzzy logic-based hybrid optimization technique was applied by Dewangan et al. [30] to find the optimal settings of EDM parameters of tool steel. Rabania et al. [31] employed iterative learning control based on-linear partial differential equations approach to predict the abrasive milling parameters. Derringer and Suich [32] depicted a desirability based multiple response method to optimize multiple objective problems. Abrasive wear of aluminium/fly ash composite was optimized using desirability based optimization technique by Ravikumar et al. [33].

From the above study, it has been witnessed that only little research works have concentrated on AWJM of metal matrix composites. Some research works have been carried out to study the influence of WAJM parameters on composites. It is also very necessary to obtain an optimal parametric combination of material removal and surface integrity of AWJM process and also the mechanism behind machining. In this paper a medium strength alloy commonly known as structural aluminium alloy (Al 6082) is used as a matrix and tungsten carbide as reinforcement. An attempt was made to study the effect of AWJM parameters on Material Removal Rate (MRR) and Surface Roughness (SR) of aluminium composites. Desirability based multi objective optimization technique was used to optimize the AWJM parameters.

2. Materials and measurements

2.1. Preparation of composite specimen

The composition of Aluminium alloy (Al6082) shown in Table 1 is reinforced with 2, 4, 6, 8 & 10% of tungsten carbide is fabricated by stir casting technique (Fig. 1). Aluminium alloy (Al6082) in the form of rod form was melted at 800 °C in electric resistance furnace and degassed using solid dry hexachloroethane compound. In order to remove the moisture content and gasses in the particulates preheating of WC was carried at 750 °C for an hour. The stirrer was lowered into the crucible and the stirrer was maintained at a constant speed of 500 rpm. Preheated tungsten carbide particles were then added and mixed with the

Table 1
Composition of Aluminium 6082 alloy.

Weight%	Al	Si	Fe	Cu	Mn	Cr	Mg	Zn	Ti	Others
6082	Bal	1.12	0.19	0.02	0.87	0.15	0.92	0.17	0.086	0.075

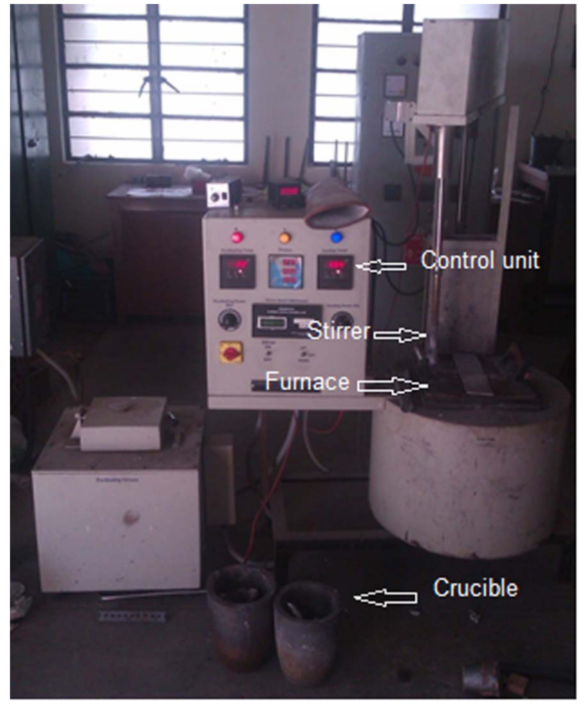

Fig. 1. Stir casting setup.

melt. Magnesium in 1% by weight was added to improve the wettability of the composites. Stirring was continued for 5–7 min to achieve uniform mixing of reinforcement in the matrix. The molten composite mix was poured in the mould to achieve a composite specimen of size of 120 mm × 120 mm × 12 mm and allowed to solidify at room temperature. The cast samples were then machined for a size of 100 mm × 100 mm × 10 mm.

2.2. Measurement of MRR and SR

Experiments were conducted using KMT WATERJET STREAMLINE make with capacity of 60,000 PSI/100 HP with a nozzle diameter of 1.1 mm (Fig. 2). In this study experiments were carried out at a constant pressure of 3600 psi using abrasive silicon sand having particle size of 80 meshes. The specimen was cut into 10 mm diameter for a through depth of 10 mm (Fig. 3). Three input process parameters namely the Standoff distance, Transverse speed and percentage tungsten carbide were considered in AWJM of aluminium composite specimens.

Material removal rate was calculated by using Eq. (1). Loss in weight of the specimen before and after machining is measured using an electronic weighing machine having accuracy 0.0001 g. Density of

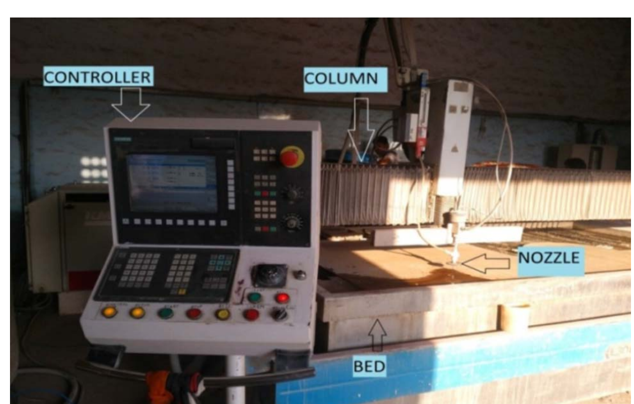

Fig. 2. AWJM machine.

Fig. 3. AWJM Machined specimens.

the sample is obtained using Archimedes principle and machining time was observed using a stop watch. Surface roughness is measured by Mitutoyo make SJ-201P type surface tester. In order to minimize the measurement error three set of reading for each sample were observed and the average value is taken for MRR and SR.

$$\text{MRR} = \text{Loss in weight of work piece/(density of specimen} \times \text{machining time)} \tag{1}$$

3. Response surface methodology

Response surface methodology (RSM) is employed to describe the liaison between AWJM parameters and their responses. A second order polynomial response to study the influence of AWJM can be developed as given by Eq. (2).

$$y = a_o + \sum_{i=1}^{n} a_i x_i + \sum_{i=1}^{n} a_{ii} x_i^2 + \sum_{i<j}^{n} a_{ij} x_i x_j + \varepsilon \tag{2}$$

where y is the response or yield, x_i and x_j are the input variables, x_i^2 and $x_i x_j$ are the quadratic and interaction terms of input variables respectively. The unknown regression coefficients are indicated by *ai, aii* and *aij*. Design Expert-16 was employed for selecting and developing the appropriate response surface models. From the wide ranges of factors available, it is limited to use three factors and five levels of process parameters as shown in Table 2. A central composite design with three control factors at half fraction, with 20 experiment sets were used to optimize the AWJM conditions (Table 3).

Analysis of Variance (ANOVA) is a technique for testing the adequacy of the mathematical models developed by RSM. Mathematical models for the response variables namely MRR and SR are given in Eqs. (3) and (4) respectively. The F-value of the developed model for MRR and SR (Table 4) are 60.69 and 30.40 respectively. The F-values of the developed model exceeds the F-value of standard tabulated F-values for MRR and SR (2.913 and 2.915 respectively) for a desired level of confidence (say 95%). Hence the model can be considered to be adequate within the confidence limit. It can be observed from Table 4, that the two quadratic models of MRR and SR are statistically significant. P-values less than 0.05 indicate that the AWJM parameters are statistically significant on MRR and SR. The square of co-efficient of

Table 2
Process parameter and their levels.

Process parameters & levels	−2	−1	0	1	2
Standoff distance (mm)	2	3	4	5	6
Transverse speed (mm /min)	170	190	210	230	250
% Reinforcement	2	4	6	8	10

Table 3
Experimental results of MRR and SR.

Sl.No.	Stand off distance (mm)	Transverse speed (mm/min)	% WC (wt%)	MRR (mm^3/min)	Surface roughness (Ra)
1	3	190	4	0.947	3.365
2	2	210	6	1.022	4.691
3	5	230	10	1.003	5.292
4	4	210	6	1.005	4.211
5	3	230	4	1.076	4.698
6	5	190	4	0.912	3.164
7	6	210	6	0.896	3.479
8	4	210	2	1.019	3.212
9	4	210	6	1.005	4.215
10	4	210	10	0.891	6.150
11	3	190	8	0.924	4.938
12	4	210	6	1.004	4.215
13	4	210	6	1.005	4.213
14	4	250	6	1.070	5.174
15	5	230	4	1.085	3.129
16	4	210	6	1.005	4.216
17	3	230	8	1.025	5.124
18	4	170	6	0.831	3.680
19	5	190	8	0.844	4.246
20	4	210	6	1.005	4.212

Table 4
ANOVA for response surface reduced quadratic model.

Material removal rate					
Source	Sum of squares	df	Mean square	F value	p-value Prob > F
Model	0.099	7	0.014	60.69	< 0.0001 significant
Residual	2.802E-3	12	2.335E-4		
Lack of Fit	2.802E-3	7	4.003E-4		Insignificant
Pure Error	0.000	5	0.000		
Cor Total	0.10	19			
Std. Dev.	0.015	R-Squared	0.9725		
Mean	0.98	Adj R-Squared	0.9565		
C.V. %	1.56	Pred R-Squared	0.8679		
PRESS	0.013	Adeq Precision	26.873		
Surface roughness					
Source	Sum of squares	df	Mean square	F value	p-value Prob > F
Model	11.56	6	1.93	30.40	< 0.0001 significant
Residual	0.82	13	0.063		
Lack of Fit	0.82	8	0.10		Insignificant
Pure Error	0.000	5	0.000		
Cor Total	12.38	19			
Std. Dev.	0.25	R-Squared	0.9626		
Mean	4.31	Adj R-Squared	0.9454		
C.V. %	5.81	Pred R-Squared	0.8084		
PRESS	4.19	Adeq Precision	27.011		

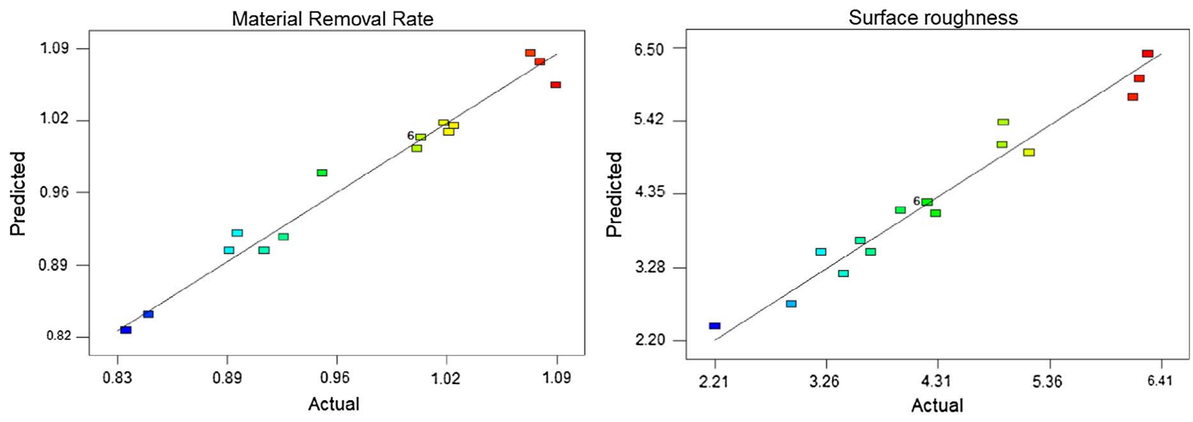

(a) (b)

Fig. 4. Comparison between predicted and experimental values.

correlation (r^2) values of 0.9725 and 0.9626 for MRR and SR respectively indicate closeness between the experimental and the predicted values. From Fig. 4 it can be observed that RSM values results are closer to the experimental values representing that the model is accurate.

$$\begin{aligned} \text{MRR (mm}^3\text{/min)} = {} & 1.00712-(0.0235*\text{SOD}) + (0.0649 * \text{TS}) \\ & -(0.0298 * \text{WC}) + (0.0126 * \text{SOD} * \text{TS}) \\ & -(0.0106 * \text{SOD}^2)-(0.0128 * \text{TS}^2)-(0.0116 * \text{WC}^2) \end{aligned} \tag{3}$$

$$\begin{aligned} \text{SR } (\mu\text{m}) = {} & 4.19385-(0.2947 * \text{SOD}) + (0.3442 * \text{TS}) + (0.6951 * \text{WC}) \\ & -(0.0637 * \text{SOD} * \text{TS}) + (0.1555 * \text{SOD} * \text{WC}) \\ & + (0.1073 * \text{W}\cdot\text{C}^2) \end{aligned} \tag{4}$$

4. Results and discussion

4.1. Influence of parameters on material removal rate

Influence of AWJM parameters on MRR are shown in Fig. 5. Eq. (3) shows that the material removal rate is mainly influenced by transverse speed (0.0649) followed by % WC (0.0298) and standoff distance (0.0235) respectively. Also MRR is significantly influenced by interaction between standoff distance – transverse speed and squares of transverse speed, % tungsten carbide and standoff distance. It can be observed from Fig. 5(a) that an increase in transverse speed from 170 mm/min to 250 mm/min increases the MRR. Increase in percentage tungsten carbide from 2% to 10%, tends to decrease the MRR. Decrease in MRR at higher percentage of WC may be due to the increase in hardness of composites. An increase in MRR at higher transverse speed increases the intermolecular forces and energy leading to shear the surface and erode more material from the work piece at a quicker rate at room temperature. Fig. 5(b) shows that an increase in standoff distance from 2 mm to 6 mm decreases the MRR of aluminium composites at constant pressure. This may be due to the spreading of water jet in air increasing the jet diameter at higher standoff distance, thereby reducing the concentration and impact energy of the jet striking the composites. Reddy et al. [28] reported that MRR increases with three major parameters namely, transverse speed, abrasive flow rate, and standoff distance which coincide with the results obtained in this study. According to Haghbin et al. [7] an increase in standoff distance accelerates the breakup of water jet into droplets leading to the decrease in erosion rate of AWJM.

Abrasive Water Jet Machining is the process of material removal by erosion due to the impingement of hard abrasive particles present in the high velocity water jet. Ductile erosion in composites takes place in two forms namely the deformation wear at large impact angle and cutting

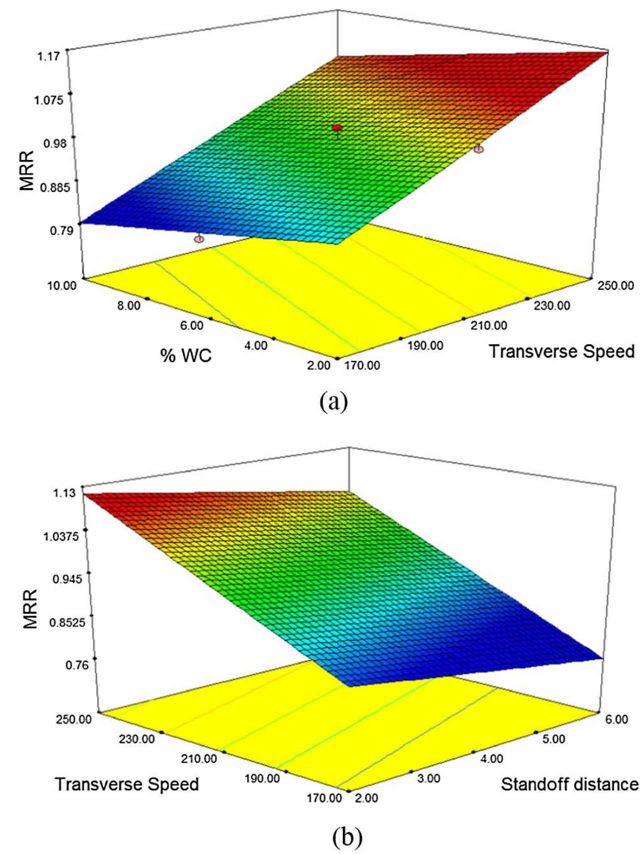

(a) (b)

Fig. 5. Effect of Response parameters on MRR.

wear at low angle of impact [24]. Material removal in ductile material takes place by cutting wear, plastic deformation, deformation wear and plastic strain. In brittle materials radial cracking takes place due to elastic–plastic deformation, critical plastic strain theory, radial cracking and indentation rupture. Maximum erosion of work piece material takes place at large impact angles for brittle materials and low impact angles for ductile materials [25]. Erosion of the work piece material depends on the shape, size, concentration, strength, impact angle and hardness of the abrasive particles [2,26]. Higher level of abrasive flow rate increases the kinetic energy of the water jet due to the penetration of more number of reinforcement particles into the cutting zone and increasing the MRR [19]. Higher kinetic increases the erosion rates and leads to the formation of lateral cracks and removes the material in the form of larger size chips, thereby increasing the MRR [11]. Increase in

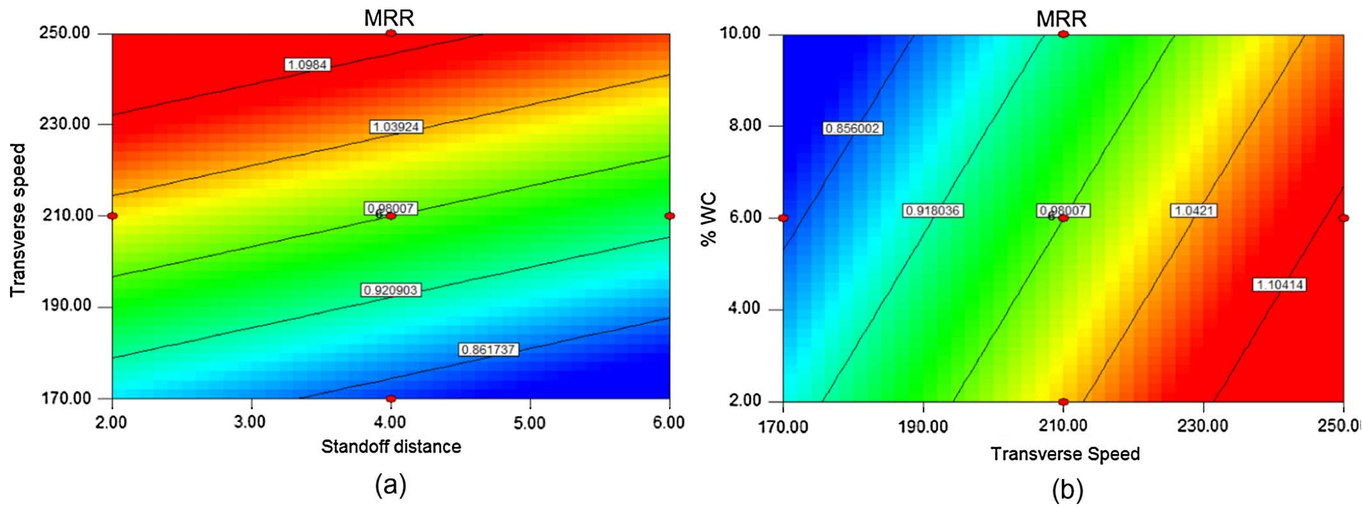

Fig. 6. Contour plot – influence of parameters on MRR.

the standoff distance decreases the depth of cut and deteriorates the machining performance along the lower kerf region due to the scattering of the concentrated jet [7]. Effect of parameters on MRR can be observed with the help of contour plot (Fig. 6). Maximum MRR due to the interaction between parameters is indicated by red region in the contour plot followed by green and blue regions indicating nominal and lower MRR respectively.

4.2. Influence of parameters on surface roughness

From equation.4 it can be observed that surface roughness is mostly influenced by percentage tungsten carbide (0.6951) followed by transverse speed (0.3442) and standoff distance (0.294). SR is significantly influenced by interaction between standoff distance-transverse speed, standoff distance- percentage tungsten carbide and square of % tungsten carbide and standoff distance. However the interaction between % WC-transverse speed, squares of standoff distance and transverse speed is having insignificant influence on surface roughness. The surface roughness of the composites increases with increase in percentage tungsten carbide and transverse speed, while SR decreases with increase in standoff distance (Fig. 7). Increase in percentage of WC from 2% to 10% normally increases the hardness of the composites thereby increasing the resistance to erosion and friction. An increase in presence of WC leads to brittle erosion and increase in surface roughness. Expansion and breakdown of the jet takes place outside the nozzle as the jet is discharged through the nozzle.

This expansion in jet increases with increase in standoff distance from 2 mm to 6 mm thereby reducing the kinetic energy jet and intensity of machining causing a reduction in surface roughness. Increase in transverse speed from 170 mm/min to 250 mm/min increases the surface roughness of composites. This can be correlated to other researchers work that the surface roughness inductile materials is influenced by particle velocity, which depends on the flushing pressure for AWJM [7]. Haj Mohammad Jafar et al. [11] described that particles of higher kinetic energy produces larger chips and rough surface. Minor cavities formed along the surface of the composites due to pull out of reinforcement particles from the composites increases the surface roughness [14]. Surface roughness increases due to the inconsistent distribution of abrasive particles in the water jet during AWJM and also due to the presence of the entrained air in the tangential area of the water jet [9]. Increase in jet pressure decreases the surface roughness due to the striations formed along the surface of the work piece material [10]. Larger size of abrasive grains increases the material removal rate of AWJM, while smaller grain size increases the surface finish [17]. Contour plot shown in Fig. 8 indicates the effect of parameters on SR. In

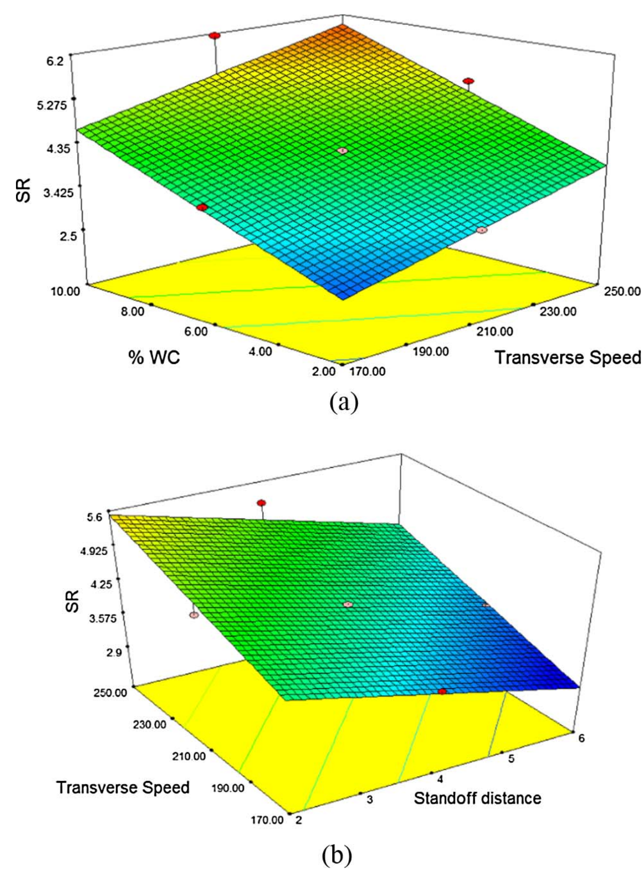

Fig. 7. Effect of Response parameters on SR.

the contour plot the red region indicates the maximum interaction between parameters, the greed region indicates the intermediate values and the blue indicates the lower values of surface roughness.

4.3. Micrograph of machined surface

The scanning electron microscope structure of the machined composite surface is shown in Fig. 9. It can be observed from Fig. 9a that there exists rough surfaces along the top surface and as the depth goes on increasing smooth surface can be observed at the bottom. The uneven top surface created by AWJM was due to the higher impact of the WC particles at the top surface and hence the MRR will be higher. As

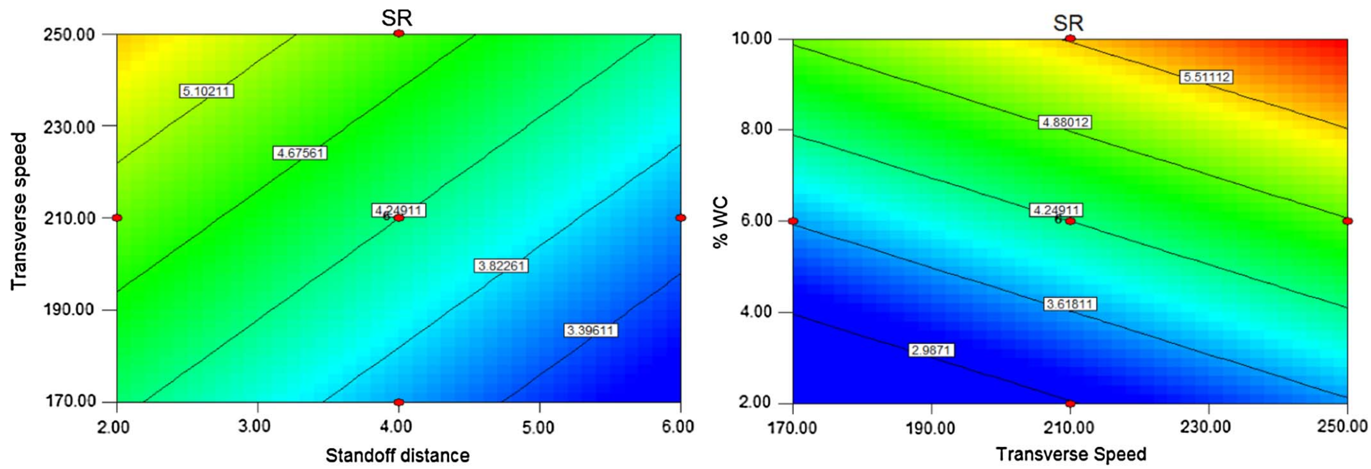

(a) (b)

Fig. 8. Contour plot – influence of parameters onSR.

the depth increases there is a loss of kinetic energy that decreases the depth of penetration at the bottom surface leading to the formation smooth surface. This coincides with Fig. 5b that SR decreases with increase in SOD. The surface waviness varies from Fig. 9a to d which is influenced by variation in cutting conditions. The size of the cutting tracks varies from 9a to 9d due to the variation in process parameters. Ploughing of composites as shown in Fig. 9b indicating the abrasion mechanism of AWJM due to plastic deformation. As the percentage of tungsten carbide increases to 10% as shown in Fig. 9b, the presence of cracks is evidenced due to the brittle nature of the composite. This can be related to Fig. 5 that an increase in WC decreases the MRR. Protrusion of tungsten carbide is also observed along the surface (Fig. 9c) due to the impact of the jet along the surface leading to chipping of reinforcement from the matrix. Also it can be viewed from Fig. 9c that in addition to ploughing of the abrasive jet the chipped tungsten carbide also hits the surface and penetrating through the work piece influencing the MRR and SR of composites. Fig. 9(a) shows the presence of pits in the form of voids at some locations formed due to the high

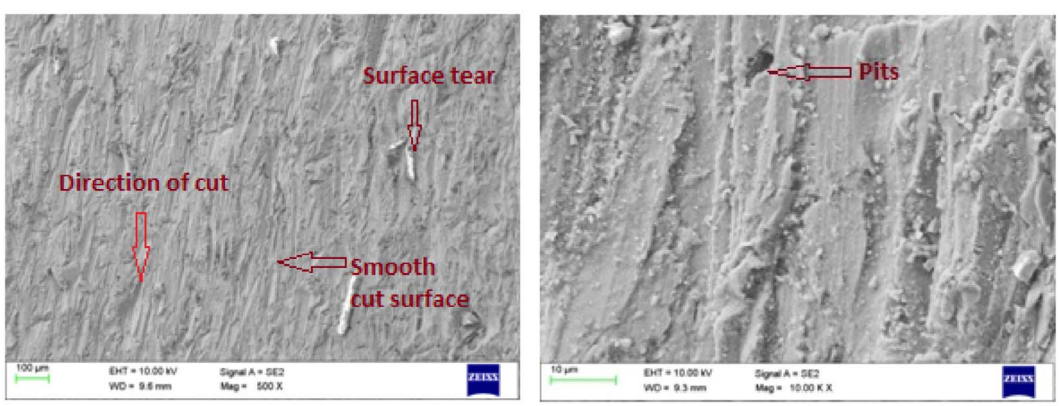

(a) SOD -4 mm, mm, TS – 210 mm/min, % WC- 6, MRR- 1.005 mm^3/min, SR-4.21μm

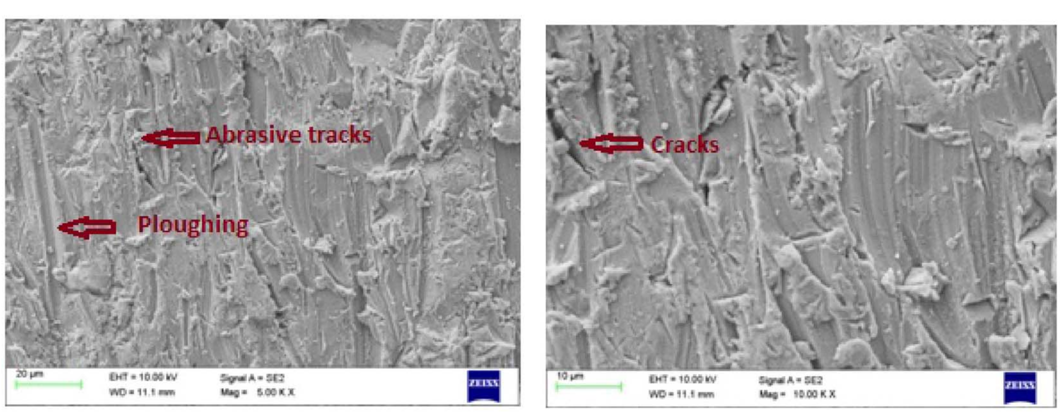

(b) SOD -5 mm, mm, TS – 190 mm/min, % WC- 10, MRR- 0.912 mm^3/min, SR-4.29μm

Fig. 9. SEM micrograph of the machined surface.

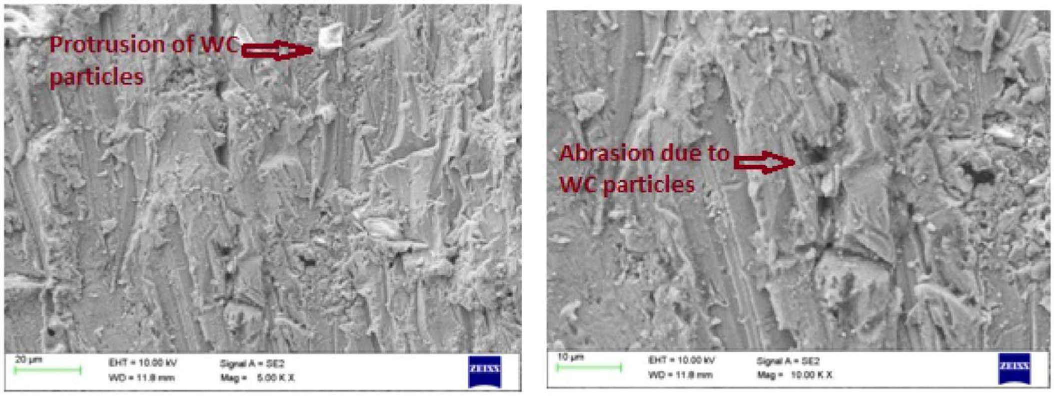

(c) SOD -3 mm, mm, TS – 230 mm/min, % WC- 8, MRR- 1.025 mm^3/min, SR- 3.96µm

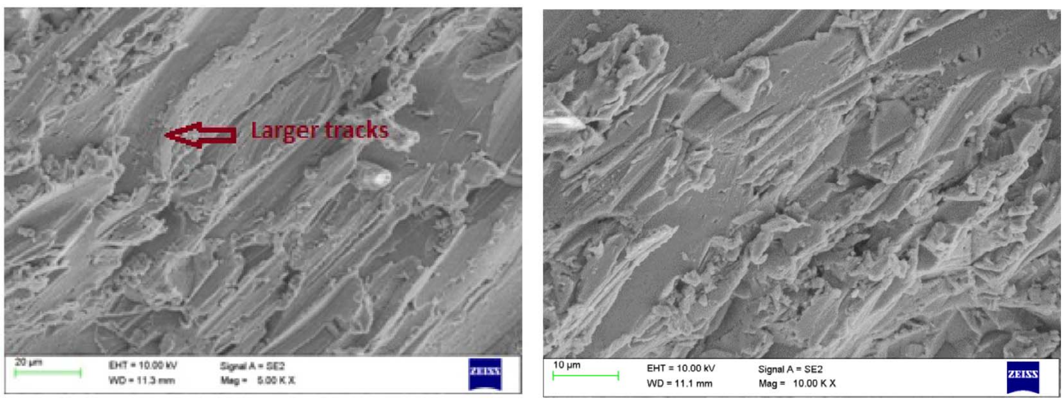

(d) SOD -5 mm, mm, TS – 230 mm/min, % WC- 4, MRR- 1.085 mm^3/min, SR-4.92µm

Fig. 9. (*continued*)

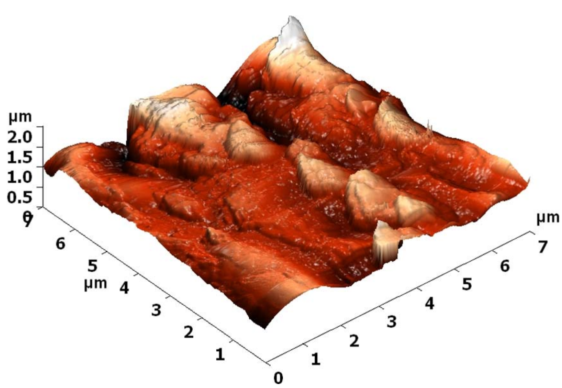

Fig. 10. AFM micrograph of the machined composite sample.

impact between the abrasive and reinforcement particles. Atomic Force Microscopy (AFM) sample of the composite (Fig. 10) shows the presence of non-uniform crater heights of the machined surface, confirming the results observed by SEM.

4.4. Confirmation experiments

In order to authenticate the results obtained by RSM a new set of experiments were performed to carry out the conformity test. Different transitional values for standoff distance (5.5 mm) and transverse speed (200 mm/min) are assigned and the responses were recorded in Table 5. The average deviation of the RSM results from that of the actual values are 5.84% and 6.23% for MRR and SR respectively indicating the accuracy of the developed model.

Table 5
Confirmation of AWJM test results.

Sl. No.	Process parameters in coded form			Actual		Regression		% Error	
	SOD	TS	WC	MRR	SR	MRR	SR	MRR	SR
1	5.5	230	10	0.966	5.986	0.966	6.286	5.80	4.77
2	6	200	8	0.845	5.145	0.845	4.826	7.96	6.60
3	5.5	200	4	0.836	3.279	0.967	3.055	3.77	7.32
Average								5.84	6.23

5. Multi objective optimization

Desirability based Multi Response Optimization utilizes an objective function D(X), called the desirability function. The desirability function is used to convert a response value into a scale-free value (d_i). This technique first coverts each response Y_i into a desirability function (d_i) varying in the range $0 \leqslant d_i \leqslant 1$. The response Y_i is the goal or target and d_i is the desirability of each response value ranging from of 0 to 1, where d = 0, for a completely undesirable response, and d = 1, for a fully desired response [24]. To determine a best combination of n responses, the objective function D is given by Eq. (4).

$$D = (d_1 X d_2 X ......d_n)^{1/n} = (\prod_{i=1}^{n} d_i)^{1/n} \tag{5}$$

The simultaneous optimization process is to find the levels of factors that determine the maximum overall desirability. Design Expert Software was employed for evaluating the desirability value and for multi objective optimization. The responses namely the MRR and SR

Table 6
Responses for desirability and range of parameters.

Sl. No.	Process parameter	Goal	Lower limit	Upper limit	Lower weight	Upper weight	Importance	Optimum values
1	Stand Off Distance (mm)	In range	2	6	1	1	3	4.22
2	Transverse Speed (mm/min)	In range	170	250	1	1	3	223.28
3	% WC	In range	2	10	1	1	3	2.10
4	MRR (mm^3/min)	Maximize	0.831	1.085	1	1	3	1.071
5	SR (μm)	Minimize	3.129	6.15	1	1	3	3.128

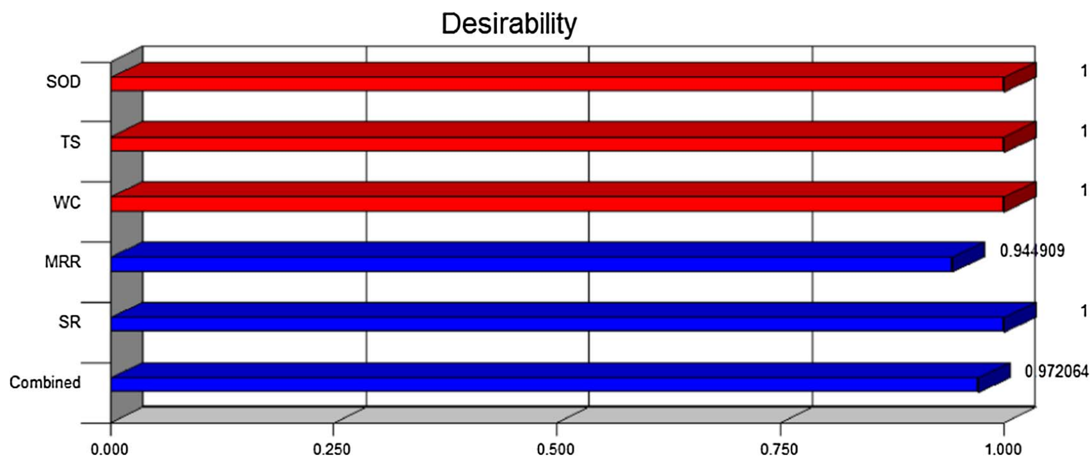

Fig. 11. Bar graph of desirability.

Fig. 12. Ramp graph of desirability.

were optimized simultaneously using a set of 20 process parameters derived by Response Surface Method (RSM). The prime objective of the optimization is to assess the set of input process parameters by maximizing the MRR and minimizing the SR. The range, goals and the optimum values of input parameters namely standoff distance, transverse speed, percentage WC, and the output characteristics are presented in Table 6. The process parameters and responses were assigned equal importance and weights in order to have equal emphasis to the parameters and the goals. The optimal set of conditions with higher desirability function is shown in Table 6.The bar graph and ramp function graph, balancing all responses of desirability are shown in Figs. 11 and 12 respectively. The output desirability varies from 0 to 1depending upon the closeness of the response. The overall desirability value of 0.972 indicates the closeness of the target value. The optimum set of parameters for maximizing the MRR (1.071 mm^3/min) and minimizing the SR (3.128 μm) is standoff distance-4.22 mm, transverse speed-223.28 mm/min, and percentage WC-2.10%. The interaction of of transverse speed and standoff distance at optimum percentage tungsten carbide (2.10%) for maximum desirability is shown in Fig. 13. The red region indicates the area of maximum desirability for the optimum parameters.

6. Conclusions

In the present work the effect of AWJM parameters on Al/WC composites was carried out at different standoff distance, transverse distance and percentage tungsten carbide. Based on the work the following conclusions can be drawn:

- Response surface methodology with a central composite design having three control factors at half fraction, with 20 experiment sets were used to optimize the experimental conditions.

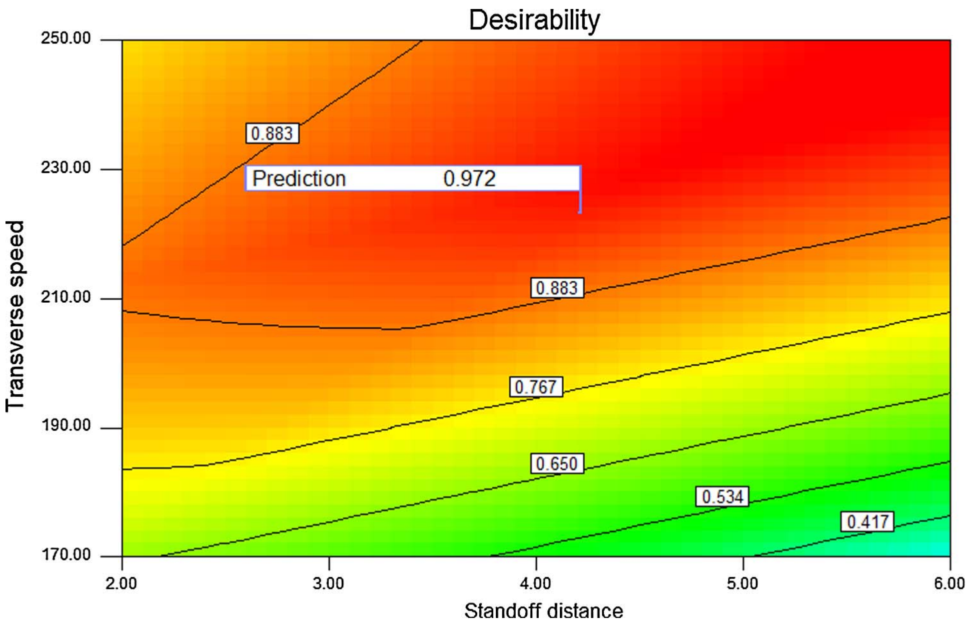

Fig. 13. Interaction of Transverse speed and Standoff distance at %WC = 2.10 for maximum desirability.

- ANOVA method is employed to check the adequacy of the model developed by RSM. The developed model has good adequacy at 95% level of confidence.
- MRR is very much influenced by transverse speed followed by % tungsten carbide and standoff distance respectively.
- Surface roughness was highly influenced by % tungsten carbide followed by transverse speed and standoff distance.
- SEM shows rough surface along the top and as the depth goes on increasing the surface becomes smoother at the bottom.
- Ploughing, cracks, protrusion of the tungsten carbide, and voids are witnessed along the surface of the composites.
- Multi Response Optimization based on desirability is used to evaluate the set of input process parameters by maximizing the MRR and minimizing the SR.
- The optimum parameter set in maximizing the MRR and minimizing the SR is standoff distance-4.22 mm, transverse speed-223.28 mm/min, and percentage WC-2.10%.

Acknowledgements

The authors are very much thankful to Management of Dr. N.G.P. Institute of Technology, Coimbatore for their kind support in carrying out the research.

References

[1] Krishnan Ravi Kumar, Kothavady Mylsamy Mohanasundaram, Ramanathan Subramanian, Balasubramaniam Anandavel, Influence of fly ash particles on tensile and impact behaviour of aluminium (Al/3Cu/8.5Si) metal matrix composites, Sci. Eng. Compos. Mater. 21 (2) (2014) 181–189.
[2] N. Ramachandran, N. Ramakrishnan, A review of abrasive jet machining, J. Mater. Process. Technol. 39 (1993) 21–31.
[3] M. Kantha Babu, O.V. Krishnaiah Chetty, A study on recycling of abrasives in abrasive water jet machining, Wear 254 (2003) 763–773.
[4] Deepak Doreswamy, Basavanna Shivamurthy, Devineni Anjaiah, N. Yagnesh Sharma, An investigation of abrasive water jet machining on graphite/glass/epoxy composite, Int. J. Manuf. Eng. 2015 (2015) 1–11.
[5] K. Kowsari, H. Nouraei, D.F. James, J.K. Spelt, M. Papini, Abrasive slurry jet micro-machining of holes in brittle and ductile materials, J. Mater. Process. Technol. 214 (2014) 1909–1920.
[6] J. Wang, Predictive depth of jet penetration models for abrasive waterjet cutting of alumina ceramics, Int. J. Mech. Sci. 49 (3) (2007) 306–316.
[7] Naser Haghbin, Farbod Ahmadzadeh, K. Jan, Spelt, Marcello Papini, Effect of entrained air in abrasive water jet micro-machining: reduction of channel width and waviness using slurry entrainment, Wear 344–345 (2015) 99–109.
[8] H. Nouraei, A. Wodoslawsk, M. Papini, J.K. Spelt, Characteristics of abrasive slurry jet micro-machining: a comparison with abrasive air jet micro-machining, J. Mater. Process. Technol. 213 (2013) 1711–1724.
[9] Naser Haghbin, JanK. Spelt, Marcello Papini, Abrasive water jet micro-machining of channels in metals: comparison between machining in air and submerged in water, Int. J. Mach. Tools Manuf. 88 (2015) 108–117.
[10] Ulas Caydas, Ahmet Hascalik, A study on surface roughness in abrasive water jet machining process using artificial neural networks and regression analysis method, J. Mater. Process. Technol. 202 (2008) 574–582.
[11] R. Haj Mohammad Jafar, H. Nouraei, M. Emamifar, M. Papini, J.K. Spelt, Erosion modeling in abrasive slurry jet micro-machining of brittle materials, J. Manuf. Process. 17 (2015) 127–140.
[12] Naresh Kumara, Mukul Shukla, Finite element analysis of multi-particle impact on erosion in abrasive water jet machining of titanium alloy, J. Comput. Appl. Math. 236 (2012) 4600–4610.
[13] P.M. Vishal Gupta, Pandey, Mohinder Pal Garg, Rajesh Khanna, N.K. Batra, Minimization of kerf taper angle and kerf width using Taguchi's method in abrasive water jet machining of marble, Procedia. Mater. Sci. 6 (2014) 140–149.
[14] K.S.K. Sasikumar, K.P. Arulshri, K. Ponappa, M. Uthayakumar, A study on kerf characteristics of hybrid aluminium 7075 metal matrix composites machined using abrasive water jet machining technology. Proc. IMechE Part B: J. Eng. Manuf. (2016) 1–15, http://dx.doi.org/10.1177/0954405416654085.
[15] Ajit Dhanawade, Shailendra Kumar, Experimental study of delamination and kerf geometry of carbon epoxy composite machined by abrasive water jet, J. Compos. Mater. 51 (24) (2017) 3373–3390.
[16] Zarko Cojbasic, Dalibor Petkovic, Shahaboddin Shamshirband, Chong Wen Tong, Sudheer Chc, Predrag Jankovic, Nedeljko Ducic, Jelena Barali, Surface roughness prediction by extreme learning machine constructed with abrasive water jet, Precis. Eng. 43 (2016) 86–92.
[17] Adnan Akkurt, The effect of cutting process on surface microstructure and hardness of pure and Al 6061 aluminium alloy, Eng. Sci. Technol., Int. J. 18 (2015) 303–308.
[18] Afifah Mohd Ali, Ahsan Ali Khan, Mohammad Yeakub Ali, Effect of process parameters on abrasive contamination during water abrasive jet machining of mild steel, Adv. Mat. Res. 264–265 (2011) 1015–1020.
[19] M. Santhanakumar, R. Adalarasan, M. Rajmohan, Parameter design for cut surface characteristics in abrasive water jet cutting of Al/SiC/Al_2O_3 composite using grey theory based RSM, J. Mech. Sci. Technol. 30 (1) (2016) 371–379.
[20] Senthil Kumaran Selvaraj, Mathan Kumar Nagarajan, Lakshmi Annamalai Kumaraswamidhas, An investigation of abrasive and erosion behaviour of AA 2618 reinforced with Si_3N_4, AlN and ZrB_2 in situ composites by using optimization techniques Arch, Civ. Mech. Eng. 1 (7) (2017) 43–54.
[21] Ashish Kumar Srivastava, Akash Nag, Amit Rai Dixit, Sandeep Tiwari, Jiri Scucka, Michel Zelenak, Sergej Hloch, Peter Hlavacek, Surface integrity in tangential turning of hybrid MMC A359/B_4C/Al_2O_3 by abrasive water jet, J. Manuf. Process. 28 (1) (2017) 11–20.
[22] S. Thirumalai Kumaran, Tae Jo Ko, M. Uthayakumar, Md. Mofizul Islam, Prediction of surface roughness in abrasive water jet machining of CFRP composites using regression analysis, J. Alloys. Compd. (2017), http://dx.doi.org/10.1016/j.jallcom.2017.07.108.
[23] Yuvaraj Natarajan, Pradeep Kumar Murugasen, Investigation of process parameters influence in AWJ cutting of D2 steel, Mater. Manuf. Processes. 32 (2) (2017) 151–161.
[24] Dewan Hasan Ahmed, Jamal Naser, Deam, Rowan Thomas, Particles impact characteristics on cutting surface during the abrasive water jet machining: numerical study, J. Mater. Process. Technol. 232 (2016) 116–130.
[25] K. Kowsari, M.H. Amini, M. Papini, J.K. Spelt, The effects of fluid vapor pressure and viscosity on the shapes of abrasive slurry jet micro-machined holes and

channels, Int. J. Mach. Tools Manuf. 110 (2016) 80–91.
[26] Divyansh Patel, Puneet Tandon, Experimental investigations of thermally enhanced abrasive water jet machining of hard-to-machine metals, CIRP J. Manuf. Sci. Eng. 10 (2015) 92–101.
[27] F. Viganòa, C. Cristiani, M. Annoni, Ceramic sponge Abrasive Waterjet (AWJ) precision cutting through a temporary filling procedure, J. Manuf. Process. 28 (2017) 41–49.
[28] D. Sidda Reddy, A. Seshu Kumar, M. Sreenivasa Rao, Parametric optimization of abrasive water jet machining of Inconel 800H using Taguchi methodology, Univ. J. Mech. Eng. 2 (5) (2014) 158–162.
[29] Rajkamal Shukla, Dinesh Singh, Experimentation investigation of abrasive water jet machining parameters using Taguchi and Evolutionary optimization techniques, Swarm Evol. Comput. 32 (2017) 167–183.
[30] Shailesh Dewangan, Soumya Gangopadhyay, Chandan Kumar Biswas, Multi-response optimization of surface integrity characteristics of EDM process using grey-fuzzy logic-based hybrid approach, JESTECH 18 (2015) 361–368.
[31] J. Rabania, Madariaga, C. Bouvierc, D. Axinte, An approach for using iterative learning for controlling the jet penetration depth in abrasive water jet milling, J. Manuf. Process. 22 (2016) 99–107.
[32] G. Derringer, R. Suich, Simultaneous optimization of several response variables, J. Qual. Technol. 12 (4) (1980) 214–219.
[33] K. Ravi Kumar, V.S. Sreebalaji, Desirability based multi objective optimization of abrasive wear and frictional behaviour of aluminium (Al/3.25Cu/8.5Si)/fly ash composites, Tribol. Mater. Surf Interfaces 9 (3) (2015) 128–136.

Production and characterization of mechanical and microstructural behaviour of friction stir welded Al6063 composites reinforced with Gr/B4C/SiC particles

Article *in* Journal of Ceramic Processing Research · January 2018

Boopathi Chinnakannan
Bannari Amman Institute of Technology

Pridhar Thiagarajan
Sri Krishna College of Technology

Journal of Ceramic Processing Research. Vol. 19, No. 1, pp. 69~74 (2018)

J O U R N A L O F
Ceramic Processing Research

Production and characterization of mechanical and microstructural behaviour of friction stir welded Al6063 composites reinforced with Gr/B_4C/SiC particles

Suresh Babu B[a,*], Chandramohan G[b], Boopathi C[a], Pridhar T[a] and Srinivasan R[a]
[a]*Sri Krishna College of Technology, Coimbatore 641042, Tamilnadu, India*
[b]*PSG Institute of Technology and Applied Research, Coimbatore 641062, Tamilnadu, India*

The present study elucidates the influence of reinforcement particles in friction stir welded aluminium (Al 6063) matrix composites on mechanical properties of the metal matrix composition. Initially composites were successfully fabricated with different weight percentage and combination of reinforcements (graphite (gr), B_4C and SiC) through stir casting technique. All sets of composite specimen were welded through solid state joining process of friction stir welding technique, the parameters such as tool rotational speed (800, 1000 and 1200 rpm), welding speed (20 and 40 mm/min) and axial loading (10 and 20 kN) are taken for characterization of fabricated composites. The effects of friction stir welding parameters were examined by mechanical and microstructural characterizations. The composites microstructure and dispersion of particle reinforcements were analysed through optical microscope and also the mechanical properties of yield strength, ultimate strength and elongation were analysed using universal testing machine. The optimized friction stir weld parameters were identified for 20% weight fraction reinforced hybrid composites.

Key word: Hybrid composites, Particles, Microscope, Hardness, Friction stir welding.

Introduction

The composites are desirable materials for variety of engineering applications due to its simple processing techniques, high strength to weight ratio and good corrosion resistance. The aluminium alloys are promising materials for different kind of applications like automobile, aerospace and marine. In general the reinforcements and processing techniques are highly influencing the physical and mechanical properties of metal matrix composites in all aspects. Stir casting technique was effectively employed to fabricate various products of metal matrix composites [1]. In addition to that the solid state techniques of friction stir welding (FSW) process plays a vital role on the surface of metal matrix composites (MMC). In FSW process the distortion and residual stress are much lower comparative to other welding techniques. There is no need of filler material in the case of FSW process. The mechanical properties are affected by welding defects in general, from this point of view the FSW process enables materials to be joined without any defects like blowholes and shrinkages. The sound parametric analyses were carried out on FSW process to improve physical, chemical and mechanical properties [2-4]. Apart from aluminium alloys, MMCs exhibit better mechanical properties. In this current scenario many research articles clearly depicts the influence of particle reinforcement of aluminium alloys on improved mechanical properties. Influence of friction stirred and TiB2 reinforced aluminium composites on mechanical, wear and metallurgical properties were evidently studied, it is concluded that FSW process gives better grain structure on composites [5-7]. Al 7075 reinforced with B_4C composites were produced through casting process, hardness of value increased 10% of B_4C particle weight percentage and also increasing the volume percentage of B_4C increasing wear rate as comparatively base matrix [8]. The mechanical and tribological properties of composites such as strength, hardness and ductility were improved based on the proper dispersion of particle inside the composites. Also many of particle reinforced MMCs research articles have been reviewed recently to find the influence of particles sizes on mechanical properties of composites [9-12]. In continuation with that adding of two particles in composites gives clear interfacial bonding between matrix and reinforcements. The binding ability is very important to improve physical and mechanical properties. More number of experiments have been performed in order to understand the effects of various particles on aluminium alloys. The reinforcing particles are silicon carbide, silicon nitride, boron carbide, graphite and aluminium oxide. The hybrid composites reinforced with graphite and boron carbide greatly influences the tensile properties and also the hardness of composite decreased with increasing on graphite particles. Similarly in other studies hybrid SiC+B_4C

*Corresponding author:
Tel : +91-422-2604567
Fax: +91-422-2607152
E-mail: babusrptc@yahoo.co.in

reinforced composites have physical and mechanical properties were analysed [13-14]. Reinforcing hybrid ceramic particles on aluminium based MMCs has developed better mechanical, physical and tribological properties than unreinforced MMCs. An attempt was made to study the mechanical and wear behaviour of SiC+B_4C reinforced aluminium composites [15]. Also the presence of graphite (Gr) with hybrid composites decreases the coefficient of friction [16]. Moreover in this study an attempt has been made to analyse the influence of hybrid reinforcements on mechanical properties of aluminium alloys. The present study elucidates the influence of friction stir welded Al 6063 matrix composites reinforced with hybrid ceramic particles on mechanical properties. The composites were fabricated with different weight percentage and combination of reinforcements (Gr, B_4C and SiC) through stir casting technique to analyze physical and mechanical properties.

Materials and Methods

Materials

The composites comprise of Al 6063 as a matrix material and graphite, boron carbide, silicon carbides act as hybrid particle reinforcements. The chemical composition of Al 6063 shown in Table 1. The role of particle reinforcements in MMCs is very important to depict the mechanical and physical properties of composites. In this study the graphite, boron carbide, silicon carbides are used in powder form in the range of particle size 32 to 40 microns. Table 2 represents the chemical composition of boron carbide reinforcements.

Production method of composites

The hybrid composites initially were fabricated through stir casting process, optimized stirrer speed was maintained for all 36 specimens. The bottom pouring stir casting machine was used to done fabrications of composites. To pre-heat particle reinforcements the muffle furnace was used, the particles were preheated about 350 °C. The perfect vacuum arrangement was done by various tight screws for effective casting of composites. In order to get improved mechanical and physical properties dispersion particle plays a crucial role, the mechanical stirring process is a key element to effectively disperse

Table 1. Chemical composition of Al6063.

Si	Fe	Cu	Mn	Mg	Zn	Ti	Cr	Al
0.6	0.35	0.1	0.1	0.9	0.1	0.1	0.1	Balance

Table 2. Chemical composition of boron carbide.

B_4C	B_2O_3	Total B	Free B	Total C	Free C	Si	Al	Fe
96	0.5	76	0.24	19.5	1.27	0.15	0.05	0.2

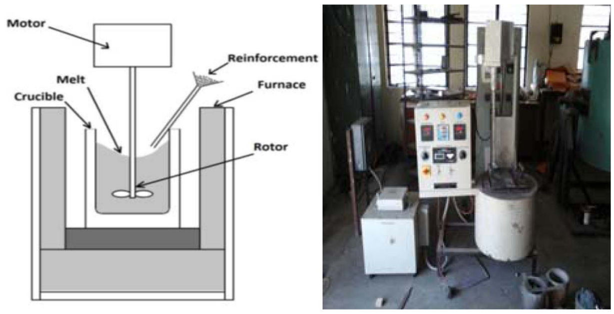

Fig. 1. Stir casting techniques.

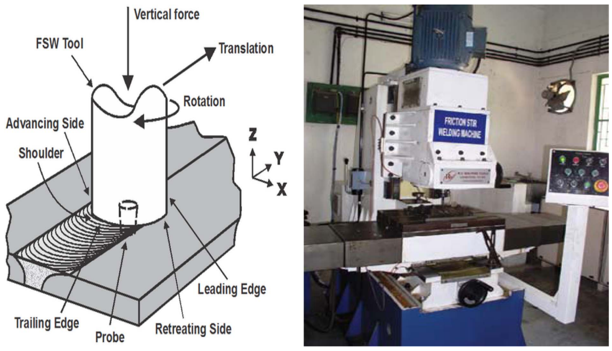

Fig. 2. Friction stir welding techniques.

Fig. 3. Universal testing machine arrangements.

hybrid particle inside the composites. Fig. 1. clearly depicts the stir casting process and its various elements.

Friction stir welding (FSW) techniques is an evolving solid state metal joining process to join two metals without melt and recast, also it is an ideal processing techniques to produce low cost high performance joints. The main intention of this study is to characterize the different parameters of FSW process, such as tool rotational speed, axial load and welding speed. The stir casted hybrid aluminium composites were dimensioned in to two halves, using FSW techniques the dimensioned hybrid composites were welded for all combinations of particle reinforced composites. In this, the different parameters and its magnitudes such as tool rotational speed (800, 1000, 1200 rpm), welding speed (20, 40 mm/min) and axial load (10, 20 kN) were maintained in different levels. Fig. 2. shows the working of FSW process and its elements.

Microstructure analysis

The optical microscope technique was used to capture required microstructure from surface of composites. The particle dispersion in hybrid composites plays a vital role to improve properties of composites in all aspects, the particle dispersion of fabricated hybrid composites for set 1 (SiC+B4C), set 2 (SiC+Gr) and set 3(Gr+B4C) were captured. The SEM micrograph evidently exposes the effective performance of stir casting and friction stir techniques through particle dispersion inside hybrid composites.

Characterisation

In this work the tensile test was carried out using Universal Testing Machine, in that the yield, ultimate and elongation values are taken in to account for all 36 samples of hybrid composites. In general the tensile test values are used to predict the ability of materials to sustain maximum static load, also the specimens were prepared as per ASTM E8-08 standard. Room temperature uniaxial tensile test was performed at a constant cross-head speed of 1 mm/sec for flat hybrid composite specimens. The specimens were loaded hydraulically. Fig. 3. shows the arrangement of specimens at universal testing machine and the load at which the specimen has reached the yield point and break point were values noted.

The physical property of hardness value is much important behaviour for composite specimen, the employability of composites based on the hardness value. The hybrid composites hardness test was performed using Rockwell hardness tester. Multiple hardness test were performed to evaluate accurate harness value. The specimens were directly loaded on polished surfaces about 10 sec. The effect of FSW process parameters are studied for various magnitudes.

Results and Discussion

Effect of FSW parameters and hybrid particle on hardness behaviour of composites

Table 3. Rockwell hardness properties of hybrid composites.

S.No	T R S (rpm)	W S (mm/min)	A L (kN)	Hardness (RHN)		
				Al+B4C +SiC	A+B4C +Gr	Al+SiC +Gr
1	800	20	10	50	40	33
2	800	40	20	52	42	34
3	800	20	10	53	43	32
4	800	40	20	51	41	30
5	1000	20	10	54	45	32
6	1000	40	20	55	45	34
7	1000	20	10	53	46	36
8	1000	40	20	53	44	35
9	1200	20	10	56	43	33
10	1200	40	20	54	42	32
11	1200	20	10	55	40	34
12	1200	40	20	56	43	35

The stir casted hybrid composites hardness properties were increased in general adding 20% volume fraction of hybrid composites. Dispersion of particle inside the composites plays a major role especially in hybrid composites, initially in casting process the particle agglomeration takes place while adding hybrid particle fully after melting of matrix materials. This shows ineffectiveness in stirring, improper particle dispersion and slag formation while casting of hybrid composites. Many trail experiments were conducted to know the particle dispersion inside composites, to overcome this both Al6063 and hybrid particles were added gradually to ensure proper distribution of particles. From the preliminary observations in stir casting process, it is evident from Table 3 that Rockwell hardness properties were increased adding 20% volume fraction of hybrid particle reinforcements. Also Figs. 4(a-b) depict the tensile and hardness value for all sets of hybrid composites.

In part of FSW process the Rockwell hardness value differs for different magnitudes of FSW parameters such as tool rotational speed, welding speed and axial load. From preliminary observations, it is observed that the hardness value has increases about to adding of

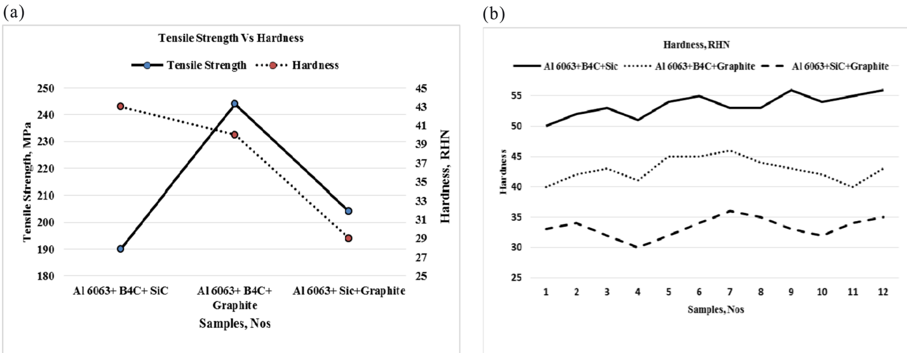

Fig. 4. (a) Tensile and hardness properties of hybrid composites, (b) Hardness of a specimen.

particle reinforcements, this is because coarse grain structures of stir casted composites, it has been observed from microstructure analysis. In part of secondary observation, FSW process parameter leads to decrease in hardness value and improved grain structure. This is due to optimized magnitudes of tool rotation speed, welding speed and axial loads. From Fig. 4(b), it is observed that the tool rotation speed 1000 rpm, welding speed 20 mm/min and axial load 10 kN were optimized process parameters to develop fine grain structures inside the hybrid composites. Also the optimized process parameter tends to arrange the hard hybrid particles in a proper way to achieve fine grain structure and too the molecular interaction between Al6063 matrix and particle reinforcement were improve drastically. Fig. 4(b) evidently exposes the influence of FSW parameters on hybrid composites.

Effect of FSW parameters and hybrid particle on tensile behaviour of composites

The core objective of this research work is to predict the mechanical properties. The tensile strength, it's derivatives of ultimate, yield and elongations of the composites were calculated experimentally using universal testing machine. The effects of FSW process parameters on tensile properties of hybrid composites were clearly observed in this study. Tensile behaviour was calculated for all three sets of composites respectively set 1 (Al 6063 (80 wt%)+SiC(10 wt%)+B_4C (10 wt%)), set 2 (Al 6063 (80 wt%+SiC(10 wt%)+Gr (10 wt%)) and set 3 (Al 6063 (80 wt%)+Gr(10 wt%)+B_4C (10 wt%)). The effect of tool rotational speed, welding speed and axial loads discussed on the following segments.

The hybrid composites were fabricated as per ASTM standard E8-08, the dimensions of ASTM E8-08 shown in Fig. 5. All the fabricated joints were analysed to

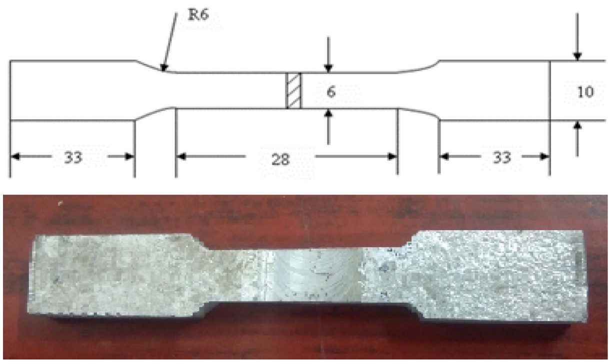

Fig. 5. Tensile specimen of hybrid composite.

ensure the influence of the tool rotational speed on tensile behaviour.

Tool rotation speed is taken as the most significant process variable since it tends to influence the welding performance, the tool rotational speed magnitudes are 800, 1000 and 1200 rpm taken in to account for this study. As the tool rotation speed increases, the welding region increases results strong joints takes place, also the strong joints based on the axial load and welding speed given to the spindle. The most important requirements of FSW process is axial load, which tends to create friction between tool and specimen. The friction due to axial load ultimately produces heat to reform the particle distribution on welding joints and also which improves fine grain structures. Totally 36 specimens were fabricated by varying the axial forces in to two magnitudes 10 kN and 20 kN. In this study the weld joint fabricated using 10 kN axial load exhibits better tensile behaviour compared with the axial load of 20 kN. In addition to this, the welding speed taken in to account to express overall influence

Table 4. Tensile behaviour of FSW processed hybrid composites

S.No.	T R S (rpm)	W S (mm /min)	A L (kN)	Tensile Properties of Hybrid Composites								
				Al6063+B4C+SiC			Al6063+B4C+Gr			Al6063+SiC+Gr		
				Y S (MPa)	U S (Mpa)	E (mm)	Y S (MPa)	U S (Mpa)	E (mm)	Y S (MPa)	U S (Mpa)	E (mm)
1	800	20	10	175.5	180.7	3.34	210.6	216.9	3.14	203.1	209.2	3.61
2	800	40	20	179.8	185.1	2.88	217.6	224.1	3.15	196.0	201.9	3.62
3	800	20	10	181.7	187.1	3.14	208.4	214.7	3.17	210.9	217.2	3.56
4	800	40	20	185.1	190.6	3.12	211.3	217.6	3.15	190.7	196.4	3.54
5	1000	20	10	185.4	190.9	2.97	191	196.7	3.26	213.0	219.4	3.54
6	1000	40	20	186.5	192.0	3.03	193.3	199.1	3.21	214.7	221.2	3.58
7	1000	20	10	200.1	206.1	2.86	207.6	213.8	3.31	185.8	191.3	3.52
8	1000	40	20	188.5	194.1	3.08	209.4	215.7	3.56	191.0	196.8	3.48
9	1200	20	10	150.5	155.0	3.43	212.6	218.9	3.12	204.0	210.1	3.64
10	1200	40	20	158.2	162.9	3.28	205.1	211.3	3.19	199.3	205.3	3.66
11	1200	20	10	141.3	145.5	3.12	201.6	207.7	3.26	183.2	188.7	3.68
12	1200	40	20	149.3	153.7	2.77	199.4	205.4	3.27	192.1	197.8	3.71

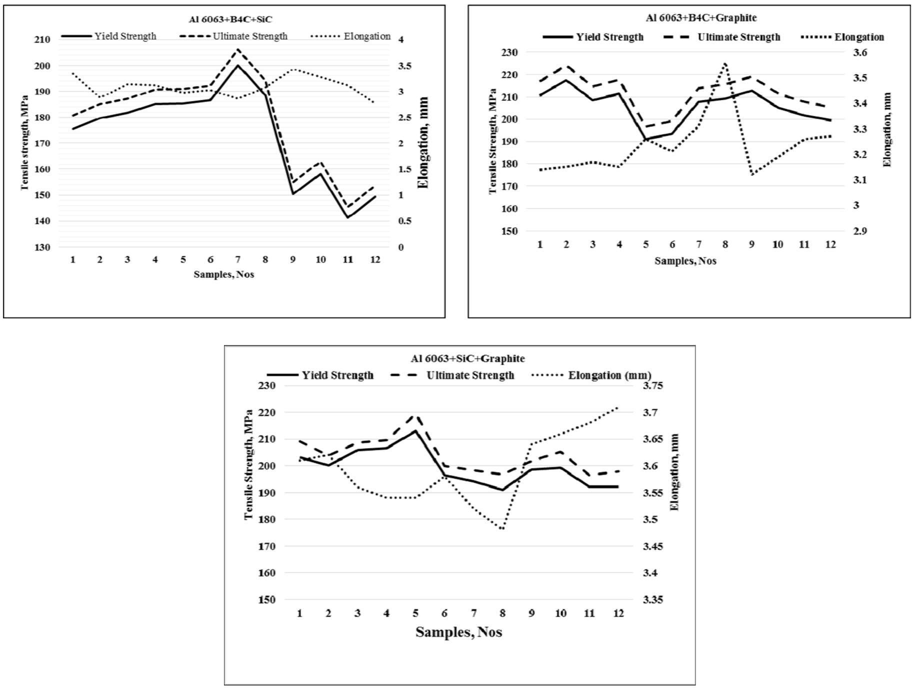

Fig. 6. Tensile behaviour of FSW processed hybrid composites.

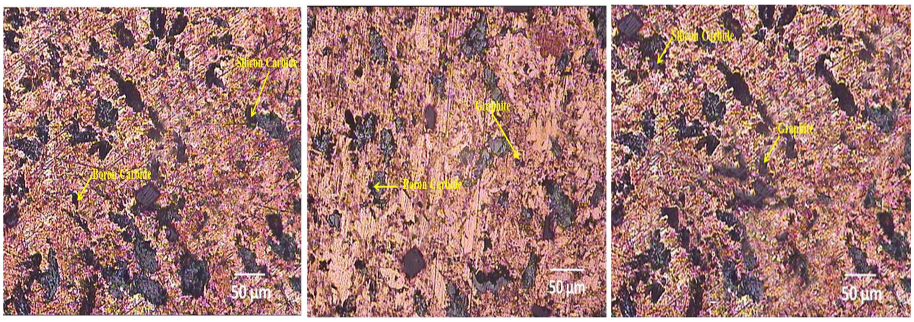

Fig. 7. SEM micrographs of hybrid composites.

of process parameters on tensile behaviour of hybrid particle reinforced composites. A 20 mm/min and 40 mm/min welding speed was observed, the defect free joints was produced when the welding speed is slower than critical value. From microstructure analysis it is observed that the surface of hybrid composites behaves crystalline nature or defect free while 20 mm/min welding speed. From Table 4, it is concluded that the welding speed influences the performance of hybrid composites significantly. Moreover the effective employability of hybrid composites correlated from all FSW process parameters of tool rotation speed, axial load and welding speed. In this process parameter analysis all three parameters are such a way that influenced gradually based on its magnitudes and it was clearly studied. Fig. 6 show that the maximum FSW join efficiency was achieved at maximum tool rotation speed of 1200 rpm approximately for all boron carbide added composites (set 1 and set 3), because of its hardness. On the other hand, the SiC+Graphite explode better tensile behaviour at the moderate tool rotation speed of 1000 rpm. In part of axial load the minimum value of 10 kN exhibits optimistic tensile behaviour for all three sets of composites, since 10 kN of axial load reforms joint without recast of hybrid composites. At last on comparatively with tool rotation speed and axial load the optimized value of welding speed was 20 mm/min was concluded for all three sets of hybrid composites.

Finally, it is concluded that only stir casted aluminium hybrid composites possess lower mechanical and physical properties. Adding of particulate gives improved properties than base matrix Al 6063, but exhibits minimum properties as compared with friction stir welded hybrid composites. From this elaborate study firstly, various combination particle influences a lot in terms of all properties to all three sets of hybrid composites. Secondly, the FSW process evidently exposes the effect of process parameters on hybrid composites in terms of physical and mechanical property.

Microstructure and fractography analysis

The microstructures of hybrid composites (set 1, set 2 and set 3) shown in Fig. 7, showing the particle

Fig. 8. Fractured surfaces of hybrid composites.

dispersion inside the composites after FSW process. The dispersion of B_4C+SiC, B_4C+Gr and SiC+Gr in friction stirred zone evidently are shown. Fig. 8 shows the fractured surfaces of the three sets of composites samples respectively. It reveals that there are differences in the morphology on fractured surfaces. More number of trail experiments were performed up to the neck formation in particular FSW zone. The neck formation while tensile test in the friction surface welded zone takes in to account for calculation of mechanical properties. From fractured surfaces of FSW processed composites, it is observed that the fracture toughness of hybrid particle reinforced composites was good, there the elongation of FSW zone was maximum comparatively the fracture occurred in other than FSW zones.

Conclusions

Al 6063 matrix composites have been successfully fabricated by the stir casting route and friction stir welding process. The particles SiC, B_4C and Graphite exhibit better wettability and interfacial bonding together with that of Al 6063 matrix. The hardness of composites has increased for all three sets of composites specimen, in particular the hardness value is high for B_4C reinforced composites (set 1 and set 2 specimen). The presence of hard B_4C particles prevents the dislocation of atoms inside the composites, resulting higher hardness compared with other set 2 composites as well as base alloy.

The yield strength and ultimate tensile strength of stir cast composites exhibit also higher than the base alloy. Also the particle dispersions inside the composites were evidently exposed using optical microscope study.

The maximum FSW joint efficiency was achieved at maximum tool rotation speed of 1000 rpm for all sets of hybrid composites, on the other hand the axial load of 10 kN and welding speed 20 mm/min exhibit optimistic tensile behaviour for all three sets of composites. As compared to base alloy Al 6063, FSW processed hybrid composite shows improved physical and mechanical properties.

References

1. J. Hashim, L. Looney, M.S.J. Hashmi, Journal of Materials Processing Technology 92-93 (1999) 1-7.
2. W. Xu, J. Liu, G. Luan, C. Dong, Materials and Design 30 (2009) 1886-1893.
3. Y.G. Kim, H. Fujii, T. Tsumura, T. Komazaki, K. Nakata, Materials Letters 60 (2006) 3830-3837.
4. P.M.G.P. Moreira, M.A.V. de Figueiredo, P.M.S.T. de Castro, Theoretical and Applied Fracture Mechanics 48 (2007) 169-177.
5. S.J. Vijay, N. Murugan, Materials and Design 31 (2010) 3585-3589.
6. K.J. Al-Fadhalah, A.I. Almazrouee, A.S. Aloraier, Materials and Design 53 (2014) 550-560.
7. P.M.G.P. Moreira, M.F. de Oliveira, P.M.S.T. de Castro, Journal of Materials Processing Technology 207 (2008) 283-292.
8. A. Baradeswaran, A.E. Perumal, Composites: Part B 54 (2013) 146-152.
9. S.A. Sajjadi, H.R. Ezatpour, M. Torabi Parizi, Materials and Design 34 (2012) 106-111.
10. T. Ozben, E. Kilickap, O. Cakır, Journal of Materials Processing Technology 198 (2008) 220-225.
11. M. Rashada, F. Pana, A. Tanga, M. Asif, Natural Science: Materials International 24 (2014) 101-108.
12. A. Baradeswaran , S.C. Vettivel , A. Elaya Perumal , N. Selvakumar, R. Franklin, Materials and Design 63 (2014) 620-632.
13. C. Muthazhagan1, A. G. Babu, G.B. Bhaskar, K. Rajkumar, Advanced Materials Research 845 (2014) 398-402.
14. A. Kisasoz, K.A. Guler, A. Karaaslan, Trans. Nonferrous Met. Soc. China 22(2012) 1563-1567.
15. U. Soy, A. Demir and F. Findik, Industrial Lubrication and Tribology 63[5] (2011) 387- 393.
16. A. Baradeswaran, A.E. Perumal, Composites: Part B 56 (2014) 464-471.

An investigation of material removal rate and surface roughness of squeeze casted A413 alloy on WEDM by multi response optimization using RSM

Article *in* Journal of Alloys and Compounds · May 2016

DOI: 10.1016/j.jallcom.2016.05.292

4 authors, including:

Soundararajan .R
Sri Krishna College of Engineering and Technology

Arthanari Ramesh
Sri Krishna College of Technology

Mohanraj N
Sri Krishna College of Technology

Journal of Alloys and Compounds 685 (2016) 533–545

Contents lists available at ScienceDirect

Journal of Alloys and Compounds

journal homepage: http://www.elsevier.com/locate/jalcom

An investigation of material removal rate and surface roughness of squeeze casted A413 alloy on WEDM by multi response optimization using RSM

R. Soundararajan [a,*], A. Ramesh [b], N. Mohanraj [b], N. Parthasarathi [a]

[a] Department of Mechanical Engineering, Sri Krishna College of Engineering & Technology, Coimbatore, India
[b] Department of Mechanical Engineering, Sri Krishna College of Technology, Coimbatore, India

ARTICLE INFO

Article history:
Received 14 May 2016
Accepted 25 May 2016
Available online 29 May 2016

Keywords:
Squeeze cast A413 alloy
WEDM
Parameter optimization
Response surface method (RSM)

ABSTRACT

The machinability study on newly fabricated A413 alloy produced by squeeze casting route under optimal condition through wire electrical discharge machining process are also investigated as final one of the present work. The experiments were systematically carried out by adapting central composite rotatable design approach of response surface methodology to investigate the effect of wire electrical discharge machining parameters such as pulse on time, pulse off time and peak current on material removal rate and surface roughness. Analysis of variance was also carried out to check the significance of the models. The mathematical models were developed to predict the results which are within the limits of agreeable average error for material removal rate and surface roughness through additivity test. Desirability function approach was used to find the optimal parametric combinations for multi-objective optimization and successful machining of the castings. It has been verified by confirmatory experiment to show the efficiency of the proposed method. On the whole, it is stated that the investigation on squeeze casting and wire electrical discharge machining process parameter of A413 alloy have proved the better casting properties and machining quality. Hence, it is recommended for all industrial applications especially automobile, aerospace.

1. Introduction

The automobile industries are focusing their concentration towards light weight vehicles due to market demand and governing regulations. Weight reduction in vehicles can be achieved by new engineering design and application of lightweight materials such as aluminium alloys and magnesium alloys. Among the lightweight materials large amount of castings are made from Al–Si alloys. This alloy is one of the most popular alloy used in aerospace, automobile, marine and mining industries components due to excellent properties [1,2]. Squeeze casting is one of the modern casting techniques that respond best to the current demand. It is a combination of gravity die casting and closed die forging, in which the molten metal solidifies under pressure within the closed die cavity, positioned between the plates of a hydraulic unit. Castings produced through modern squeeze casting route offers high metal yield, nil or minimum gas or shrinkage porosity, excellent surface finish, low operating cost, zero defects and have superior properties over the conventional castings due to fast heat transfer rate [3,4]. The tensile properties and fracture toughness of squeeze cast A356 alloy were superior to those of the low pressure die cast and rheo cast alloy. It is also reported that squeeze casting accounted for 15–40% improvement of mechanical properties than gravity die casting process. The improvement in the mechanical property attributes to the refinement of the microstructure due the externally applied squeeze pressure [5,6]. Investigate the critical process parameters in squeeze casting technique was reported that the squeeze pressure and pouring temperature of 125 MPa and 700 °C, respectively, gave an excellent combination of hardness and tensile properties in Al-8% Si alloys having an aspect ratio not more than 2.5: 1 [7]. Aluminium exhibits better machinability than other metals and alloys. Machinability of most aluminium alloys is excellent for various wrought and cast alloys. There is a variation in machining characteristics which may require special tooling or

* Corresponding author.
E-mail addresses: soundararajan@skcet.ac.in (R. Soundararajan), ramesha@skcet.ac.in (A. Ramesh), mohanrajnagarajan@gmail.com (N. Mohanraj), sarathi1290@gmail.com (N. Parthasarathi).

http://dx.doi.org/10.1016/j.jallcom.2016.05.292
0925-8388/

technique due to high hardness and yield strength [8].

Electrical discharge machining (EDM) is one of the most extensively used nonconventional material removal processes. Regardless of hardness its exclusive feature of using thermal energy to machine electrically conductive parts has been its distinctive advantage in the fabrication of mould, die, automotive, aerospace and surgical components. Also, EDM does not make direct contact with the electrode and the work piece eliminating mechanical stresses, chatter and vibration problems during machining [9]. Compared to die sinking electrical discharge machining; WEDM is a spark erosion process used to produce complex two and three-dimensional shapes through electrically conductive work piece. In WEDM, a wire about 0.05–0.3 mm is used as an electrode and deionised water as a dielectric. A nozzle is employed to inject the dielectric in the machining area in wire EDM [10]. To study the effect of wire EDM parameters on aluminium alloy because of its growing applications in various fields. The influence of WEDM parameters on surface roughness (SR) and metal removal rate (MRR) is the conflict with each other, therefore obtaining a good surface finish and high MRR is difficult to achieve simultaneously. In WEDM is on different materials but on an observation it is found that all those materials possess a high modulus of rigidity and having the properties of low thermal conductivity and high melting point. The materials like aluminium alloys possess the above-stated properties and hence it is employed for the machining process [11]. Surface finish and dimensional accuracy plays a vital role in process planning of WEDM for machining lamellar gamma titanium aluminide in multi-pass cutting operation, i.e., first cut and trim cuts. The trim cut which includes semi − finished and finished stages; the processes are conducted to change the wire offset parameter after the first cut. It leads to achieve desired geometrical precision [12]. Ti6Al4V for the machining of WEDM process with brass wire and zinc coated brass wire. While machining formation of a thick oxide layer is identified due to phase transformation. With a lower value of time between two pulses, a considerable reduction in the formation of oxides can be obtained. In order to get uniform surface characteristics, the coated wires are preferred over the uncoated wires [13]. Machined four different materials like aluminium, brass, alloy steel and cemented carbide alloy. The experiment results concluded that constant pulse energy per discharge will produce same surface roughness but unique surface morphology and different metal removal rate for short and long pulses. In addition, short pulse duration with high peak value produces clear craters on the work piece which can generate better surface roughness. It is also found that reversed polarity machining with the appropriate pulse energy can improve the machined surface roughness [14].

The potential factors that affect the WEDM performance into five major categories viz, the different properties of the work piece material and die-electric fluid, machining characteristics, adjustable machining parameters, and component geometry. In addition, they employed the design of experiments (DOE) techniques to study and optimize the possible effects of variables during process design and development and validate the experiment results using noise to signal ratio analysis [15]. Machining characteristic of Aluminium Matrix Composite (A413-9% B_4C) by Micro-Wire Electric Discharge Machining (Micro-WEDM) process using zinc coated copper wire and tool as RSM with central composite design (CCD). The response surface optimization based on desirability analysis is an ideal technique for finding the optimal machining condition of the micro-WEDM process. The optimum various input parameters are voltage 80 V, capacitance 0.01 μF, and feed rate 15 μm/s on machining, optimum output performance of material removal rate (MRR) 0.259943 mm^3/min, Kerf width (kW) 87 μm, and surface roughness (SR) 0.97 μm were investigated [16]. Effect of parameters such as current, pulse on time and reinforcement percentage on Wire electric discharge machining (WEDM) of Al2024 reinforced with SiC on MRR and SR. Response surface methodology (RSM) technique has been applied to optimize the machining parameters for minimum surface roughness and maximum MRR peak current. The optimum value for process parameters are peak current of 3A, pulse on time of 3 μs and reinforcement of 2% for the response of MRR of 1.6478 mm^3/min and SR of 3.1 μm. From the result, SR and MRR are increased with the increase in peak current and pulse on time, whereas Surface roughness increases with increase in wt.% reinforcement and Material removal rate is decreased with the increase in wt.% reinforcement [17]. To machine Al 6063/ZrSiO4(p) (5%) metal matrix composite by WEDM to investigate the influence of process parameters such as pulse on time, pulse off time, peak current and servo voltage on cutting rate. A Box-Behnken design approach of RSM is used to plan and analyze the experiments. Significant process parameters are obtained by ANOVA and F-test. From the result, it is concluded that cutting rate increases by increasing pulse on time and peak current whereas cutting rate decreases by increase in pulse off time and servo voltage. Also, the optimum value for process parameters is pulse on time of 120 μs, pulse off time of 51 μs, peak current of 169vA, Servo Voltage of 53 V for the response of MRR 5.9877 mm^3/min [18]. At this high temperature during WEDM process, the amount of heat transfer increases which results in more material removal and leaving surface with large craters and cracks, which leads to some changes in surface roughness and microspores because of castings prepared by convention route [19].

Most of the researchers fabricated various aluminium alloy casting through gravity die casting and pressure die casting route and machined by WEDM process. Conventionally casted materials have micro-pores and nominal UTS and the WEDM process parameters gives path way to accelerate large craters and cracks on the surface while machining of castings. The applied squeeze pressure accelerate the ultimate tensile strength and pore free fine grain dendritic structure which eliminates surface cracks of the work piece during machining. Thus the present work is summarized as, to fabricate pour free fine grain aluminium alloy castings (A413) through squeeze casting technique, the alter the mechanical properties such as hardness and UTS due to the effect of the squeeze pressure, die preheating temperature and melt temperature respectively. The high strength aluminium alloy castings find its application in various engineering field components, so that WEDM process is chosen as an account for machining the pour free high strength castings. The optimal process parameter ranges are subjected to study the effect of machinability of squeeze casted samples using CCRD. Further, RSM models have been developed to map the interactions, and their models were compared with the experimental interactions. Also multi objective optimization of process variables was carried out using desirability function analyzing in RSM technique. The developed A413 squeeze casted sample are experimentally analyzed and optimized has not been reported in the scientific community.

2. Fabrication of A413 aluminium alloy castings

Fabrication of A413 aluminium alloy castings was processed by squeeze casting method under optimal parametric condition. The A413 alloy ingots of 1 kg were melted at 725 °C in the crucible. The crucible was covered with a flux in order to minimize the oxidation of molten metal, and the melt was degassed by adding degasser. Then the molten metal is poured in to the preheated die 225 °C through preheated pathway. The melt is permitted to solidify in the mould under the applied squeeze pressure of 140 MPa. There were 4 recast samples prepared in which 2 samples were used for mechanical testing as per the same ASTM standard procedures. The hardness, ultimate tensile strength and yield strength of the castings were found and noted as 95 BHN, 305 MPa and 176 MPa. The prepared two samples which are taken for WEDM machining is shown in Fig. 1.

3. WEDM experimental setup

3.1. Pilot experiments in WEDM process

The pilot experiments were carried out using ELEKTRA SPRINTCUT 734 wire cut machine which is shown in Fig. 2. During the experimental work, the following parameters are kept constant at a fixed value; Zinc coated brass wire of 0.25 mm diameter, demineralized water is used as a dielectric medium (Conductivity of dielectric 20 mho), wire feed (2 units), wire tension (4 units), servo voltage (20), flushing pressure (1 unit) (15 kg/cm^2), servo feed (2100 unit), peak voltage: 2 unit (110 V DC). A piece of rectangular cross section is cut from a cylindrical cross section of squeeze casted A413 alloy of 15 mm thickness and it is taken as a work piece. The selection of influencing parameters was done through pilot experiments in first pass by using one factor at a time approach. Pulse on time (T_{on}), (105–131), Pulse off time (T_{off}), (40–63), Peak Current, (IP) (70–230) are varied and remaining parameters are kept constant during pilot experimentation for first cut and the various responses are measured. The effects of the input parameters are studied on MRR and SR.

3.2. Selection of process parameters and their factor levels

Based on the pilot experiments the following levels of most significant influencing process parameters are selected for the present work. Pulse on time (T_{on}), Pulse off time (T_{off}) and Peak Current (IP) are found to influence metal removal rate and surface roughness and they are varied to perform the experiments. The following WEDM parameters and their range/values are selected for the machining investigation by using one factor at a time approach. Table 1 show the most influencing parameter working ranges and its levels would be selected for experimental design methodology using response surface methodology. Table 2 shows the range of machine units and actual units of the WEDM process parameters. Figs. 3 and 4 shows the machined specimens of A413 alloy.

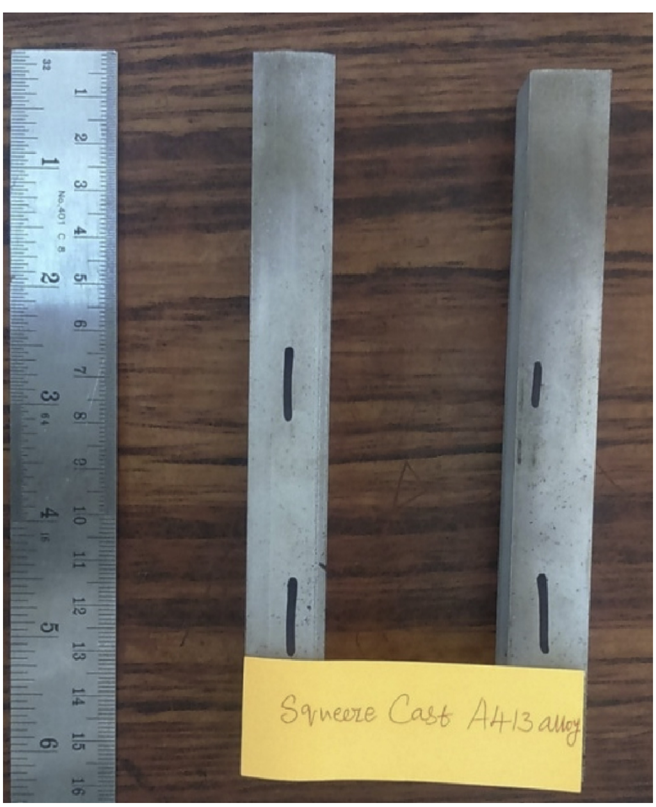

Fig. 1. A413 Alloy work piece for WEDM.

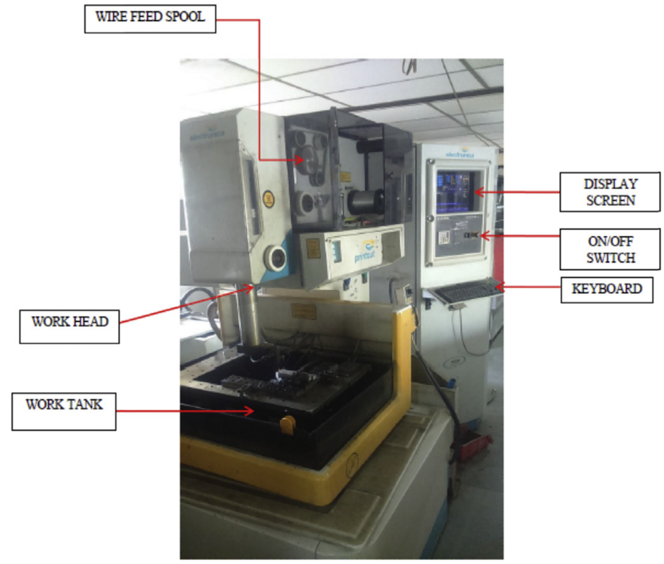

Fig. 2. Pictorial view for WEDM machine tool.

3.3. Design of WEDM experiments using response surface methodology

The response surface methodology is one of the most effective statistical methods to develop and analyze the interactive and quadratic effects between the variables. It is well known and widely used methodology to develop quantitative models in manufacturing and machining application. The experimentally measured responses in the present investigation are considered for modeling and analysis using RSM. In general, most of the experimental data fit to quadratic models, and the general second order polynomial response is described.

In order to study the effect of wire electrical discharge machining process parameters of A413 alloy, a second order polynomial response can be fitted in to the following Equation (1).

$$Y = b0 + b1 \times 1 + b2 \times 2 + b3 \times 3 + b11 \times 12 + b23 \times 22 + b33 \times 32 + b12 \times 1 \times 2 + b13 \times 1 \times 3 + b23 \times 2 \times 3 \quad (1)$$

Where Y is the response and x_1, x_2 and x_3 are the quantitative variables. Similarly b_1, b_2 and b_3 represent the linear effects of x_1, x_2 and x_3 respectively, b_{11}, b_{22} and b_{33} represent the quadratic effects of x_1, x_2 and x_3 respectively, b_{12}, b_{13} and b_{23} represent linear-by-linear interaction between x_1& x_2, x_1& x_3, x_2& x_3 respectively.

The co efficient of response surface has been estimated by using the proposed scheme of the box and hunter in the central composite design. This model fit the second order response surface very accurately. The replication was eliminated for finding the error terms, and the mean square error was estimated by replicating the centre points.

In the present work, twenty experiments were designed based on full factorial central composite rotatable design (CCRD) by using

Table 1
Machining parameters used in the experiments for A413 work piece.

Parameter	Symbol	Unit	Low level (−1)	Middle level (0)	High level (+1)
Pulse on time	T_{on}	μs	109	115	121
Pulse off time	T_{off}	μs	47	53	59
Peak Current	IP	Amps	160	180	200

response surface method in design expert software and the input parameters like pulse on time, pulse off time and peak current are varied to ascertain their effects on the responses.

A three-factor, three-level central composite design was used to determine the optimal factors of MRR and SR of the WEDM process of A413 alloy. The design variables were pulse on time (T_{on}), pulse off time (T_{off}), and peak current (IP), and their levels were coded −1, 0, and +1. The MRR and SR were selected as response variables. The factorial fraction of central composite design (CCD) is a full factorial design with all the combinations of the factors at two levels (high +1 and low −1) and composed of the eight star points, six central points (coded level 0), and six axial points (+1.68179, −1.68179). Twenty different experimental combinations were chosen at random according to CCD in RSM. The experimental study was carried out based on the CCD given in Table 3.

Table 2
Process parameters, symbols, and their ranges for machining A413 work piece.

Parameter	Symbol	Unit	Range (Machine units)	Range (Actual units)
Pulse on time	T_{on}	μs	109–121	0.55–1.15
Pulse off time	T_{off}	μs	47–59	20–44
Peak Current	IP	Amps	160–200	160–200

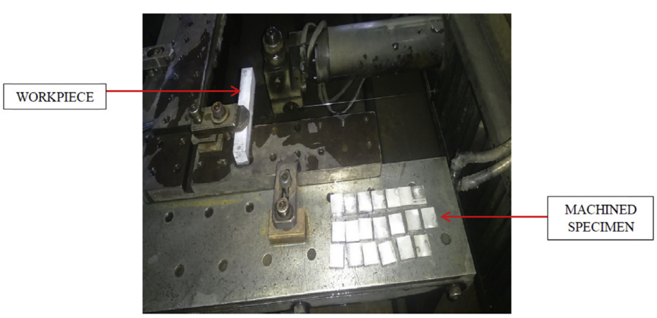

Fig. 3. Work material mounted on WEDM machine.

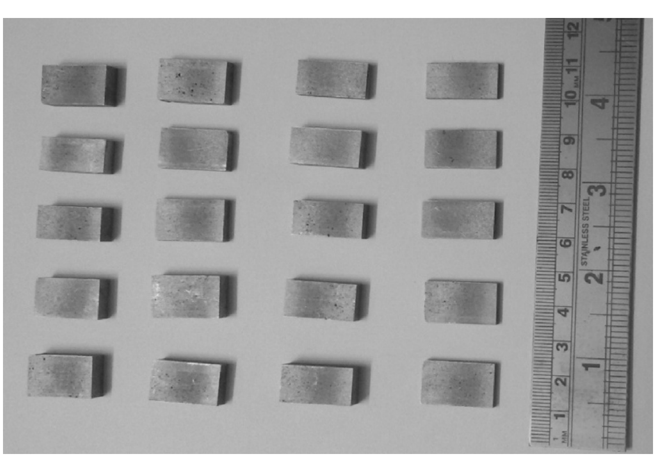

Fig. 4. Machined A413 specimens from WEDM experiments.

4. Measurement of experimental responses

The discussions regarding to the measurement of WEDM experimental process parameters like metal removal rate (MRR), Surface Roughness (SR) are given below.

4.1. Measuring of interactions for work materials

The material removal rate is calculated with the help of Equation (2) and the help of values of cutting speed which are directly displayed in the computer monitor attached to machine as shown in Fig. 5. Values are noted after a distance of 3 mm from the initiation of cut to ensure that readings are noted only when the cutting velocity is stabilized.

Kerf width measurements were made at a distance of 6 mm from the Ra cuttings and the kerf width is measured using Mitutoyo's optical microscope. To have a better average of kerf width in each cut, it has been measured at three different places. The schematic view of kerf width during machining is shown in Fig. 6.

$$\text{Material Removal Rate (MRR)} = \text{cutting speed} * \text{kerf Width} * \text{Height}(\text{mm}^3/\text{min}) \quad (2)$$

4.2. Measurement of surface roughness for work materials

Roughness is a quantity of the texture of a surface. It is measured by the vertical deviations of a normal surface from the ideal arrangement. If the deviation is large, the surface is rough and if it is small, the surface is smooth. The symbol used for indicating general Surface Roughness (SR) is Ra. It determines average roughness by comparing all the peaks and valleys to the mean line. Cut off length is the length that the stylus is dragged across the surface; a larger cut-off length will give a better average value. A shorter cut-off length gives a less precise result over a shorter stretch of surface.

Table 3
Design of experiments using CCRD in RSM for machining A413 work piece.

Std	Run	Block	A:T_{on} μs	B:T_{off} μs	C:IP Amps
20	1	Block 1	0.85	32.00	180.00
12	2	Block 1	0.85	52.00	180.00
10	3	Block 1	1.35	32.00	180.00
9	4	Block 1	0.35	32.00	180.00
15	5	Block 1	0.85	32.00	180.00
11	6	Block 1	0.85	12.00	180.00
17	7	Block 1	0.85	32.00	180.00
8	8	Block 1	1.15	44.00	200.00
16	9	Block 1	0.85	32.00	180.00
13	10	Block 1	0.85	32.00	150.00
3	11	Block 1	0.55	44.00	160.00
4	12	Block 1	1.15	44.00	160.00
7	13	Block 1	0.55	44.00	200.00
2	14	Block 1	1.15	20.00	160.00
1	15	Block 1	0.55	20.00	160.00
19	16	Block 1	0.85	32.00	180.00
5	17	Block 1	0.55	20.00	200.00
14	18	Block 1	0.85	32.00	210.00
6	19	Block 1	1.15	20.00	200.00
18	20	Block 1	0.85	32.00	180.00

Fig. 5. Set up for Cutting rate observation.

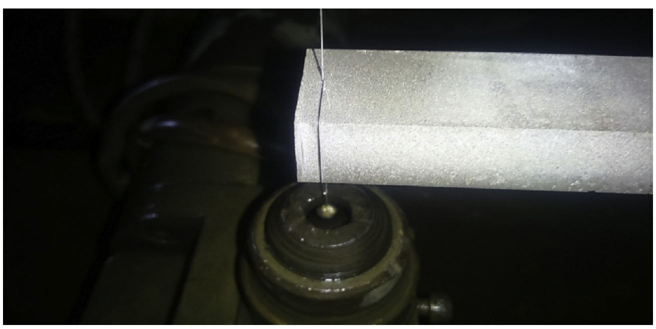

Fig. 6. Pictorial view of kerf width.

Surface roughness measurements in μm were repeated for three times for cut off length of 4 mm and measured using Mitutoyo's surftest, portable surface roughness tester equipment shown in Fig. 7 and the average value was considered as SR value for the analysis purpose (see Fig. 8).

In this investigation, totally twenty experiments were conducted and the response for A413 alloy were presented below.

5. Results and discussions

5.1. RSM based design of experiments and their results for machining of A413 workpiece

The developed A413 alloy through squeeze casting route was machined with different levels of T_{on}, T_{off}, and IP as framed by DOE. For the minimum - maximum ranges of parameters, MRR seems to be 8.451–36.241 mm3/min and SR seems to be 1.39–3.16 μm. The absence of pore-free high strength A413 casting increases the kerf width during discharge of spark between the electrodes. Electrode wire cut-off is eliminated during the machining of high strength alloy, because of the absence of micro porosity in the casting due to the processing of squeeze casting technique. Designed experiments with its responses were shown in Table 4.

5.2. Effect of process parameters on responses for machining of A413 workpiece

5.2.1. Analysis of material removal rate for machining A413 workpiece

It is hard to find the optimal process parameter with maximum signal and minimum noise ratio to machine the high strength squeeze cast A413 alloy. As a result, ANOVA technique is employed. ANOVA implies that the F-value of this MRR model is 28.76 which indicate the model is significant. This "Model F-Value" occurs due to noise with a chance of only 0.01%. The model terms are significant when the values of "P > F" is less than 0.0500. In this experiment, all the input parameters and their interaction such as A, B, C and B^2 are significant model terms. The model terms are not significant when the values are greater than 0.05000. In this case, AB, AC, BC, A^2, and C^2 are not significant terms, and it can be eliminated from the models. Based on statistical analysis, "Lack of Fit F-value" of 6.53 implies the Lack of Fit is significant. There is only a 3.00% chance that this "Lack of Fit F-value" occurs due to noise. The "Predicted R-Squared" and "Adjacent R-Squared" values are 0.7439 and 0.9293 in reasonable agreement. "Adequate Precision" shows the signal to noise ratio. Adequate accuracy greater than 4 is desirable, as it measures the signal to noise ratio of 20.448. Table 8 shows the ANOVA for MRR of A413 alloy and noted that the developed model is considered to be relatively fitted with the observed values as the residuals are located along a straight line and it indicates the errors are normally distributed. In Fig. 9, it is observed that the residuals are structure less because it is scattered randomly. Therefore, the developed second-order for MRR is shown in Equation (3).

$$MRR = +46.47656 - 0.87724 * T_{on} + 0.56217 * T_{off} - 0.68667 * IP - 0.45306 * T_{on} * T_{off} + 0.16542 * T_{on} * IP - 6.61979E-003 * T_{off} * IP + 1.49634 * T_{on}^2 + 9.48433E-003 * T_{off}^2 + 2.81509E-003 * IP^2 \quad (3)$$

ANOVA indicates that among the various input process parameters considered while machining high strength squeeze cast A413 alloy, it is observed that the Ton, T_{off}, and IP are found to be significant at 95% confidence. From Table 5, it is also noted that the IP is the primary influencing factor with 30.47% contribution followed

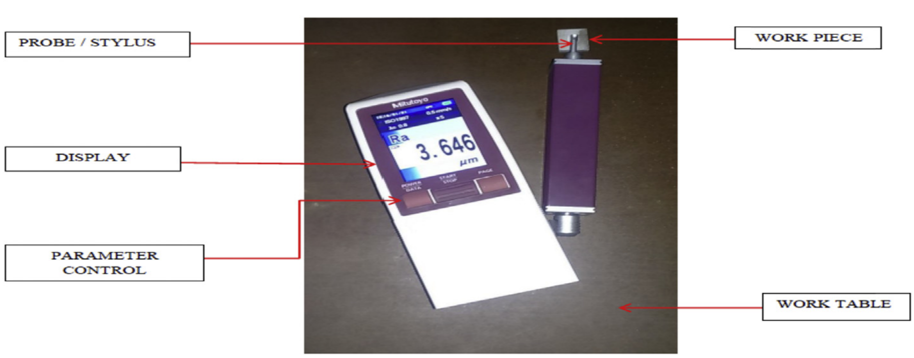

Fig. 7. Surface roughness measurement.

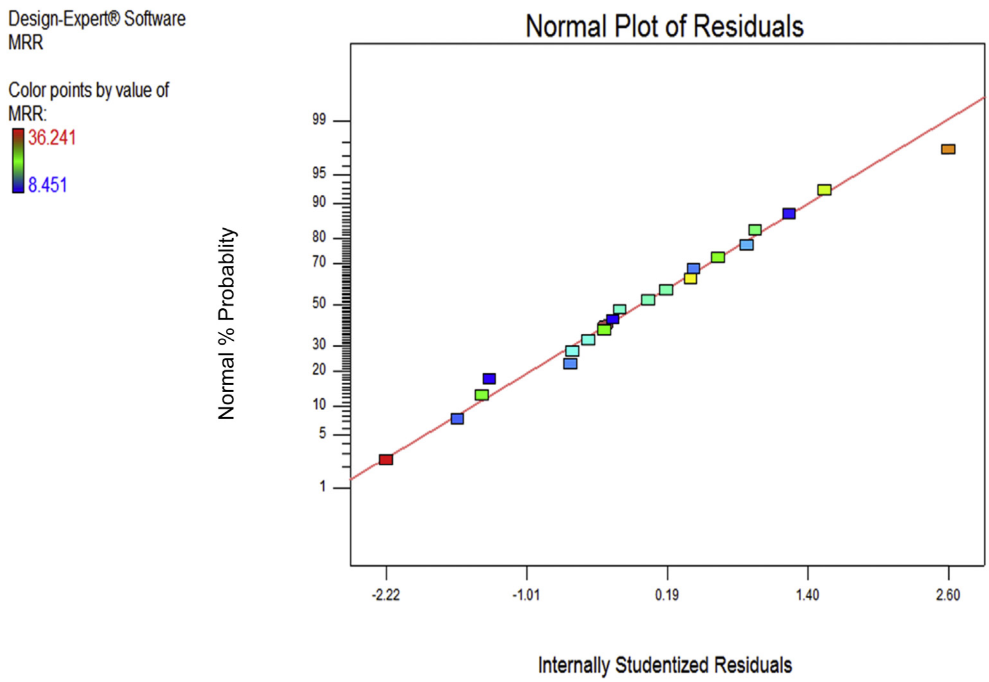

Fig. 8. Normal plot of residuals on material removal rate for A413 work piece.

by Ton and T_{off} with 30.15% and 27.90% respectively. From the response graph Fig. 10, it is observed that the MRR increases with increase in Ton and IP where as MRR decreases by increasing T_{off}. From the combined response graph Fig. 11, it is found that the MRR increases with increase in Ton and decrease in T_{off}. Fig. 12 shows that MRR increases with increase in Ton and increase in IP. Fig. 13 reveals that MRR increases with a decrease in T_{off} and increase in IP.

The material removal rate depends on the discharge energy which is based on the electrical and thermal conductivity of the work piece. It is evident from the above data that MRR increases with the rise of Ton and IP. The discharge energy produces very high temperature at the point where the spark strikes the surface of high strength squeeze cast A413 alloy. In the latter case, the large quantity of heat and energy transmitted to the work piece for melting and vaporization [20]. Also, the high-intensity spark energy produces more potent explosion results in more material melting. It is evident that increasing Ton and IP, heat energy increases as well which leads to MRR development. Due to the generation of more discharge energy, a large amount of material melts due to spark in the gap. Hence, to obtain higher MRR pulse on time should be kept as high as possible [21].

Also, it is evident from the observation that the MRR decreases due to an increase in T_{off}. This is due to the effect of less number of discharges for a specific period. Thus, larger T_{off} results in a small quantity of metal melting in the gap. Also, if the interval is too short, the ejected work piece material would not be flushed away with the flow of dielectric fluid. Therefore minimum T_{off} has to be maintained for effective machining for higher MRR [22,23].

Table 4
Design of experiments and results for machining A413 work piece.

Std	Run	Block	A: Ton µs	B: Toff µs	C: IP Amps	Cutting velocity mm/min	Kerf width mm	R1: MRR mm3/min	R2: SR µm
20	1	Block 1	0.85	32.00	180.00	2.999	0.357	16.062	2.28
12	2	Block 1	0.85	52.00	180.00	2.556	0.359	13.761	1.97
10	3	Block 1	1.35	32.00	180.00	5.10	0.365	27.924	2.72
9	4	Block 1	0.35	32.00	180.00	1.637	0.344	8.451	1.65
15	5	Block 1	0.85	32.00	180.00	3.154	0.360	17.034	2.06
11	6	Block 1	0.85	12.00	180.00	5.508	0.358	29.578	2.43
17	7	Block 1	0.85	32.00	180.00	2.958	0.356	15.796	2.19
8	8	Block 1	1.15	44.00	200.00	3.794	0.369	21.003	2.36
16	9	Block 1	0.85	32.00	180.00	3.138	0.352	16.572	2.16
13	10	Block 1	0.85	32.00	150.00	1.996	0.328	9.824	1.39
3	11	Block 1	0.55	44.00	160.00	2.270	0.3	10.217	1.63
4	12	Block 1	1.15	44.00	160.00	2.427	0.354	12.891	1.84
7	13	Block 1	0.55	44.00	200.00	2.279	0.347	11.866	1.89
2	14	Block 1	1.15	20.00	160.00	4.80	0.337	24.267	2.29
1	15	Block 1	0.55	20.00	160.00	2.722	0.308	12.576	1.76
19	16	Block 1	0.85	32.00	180.00	3.517	0.356	18.785	2.12
5	17	Block 1	0.55	20.00	200.00	4.382	0.351	23.073	1.89
14	18	Block 1	0.85	32.00	210.00	5.583	0.384	32.159	2.37
6	19	Block 1	1.15	20.00	200.00	6.425	0.376	36.241	3.16
18	20	Block 1	0.85	32.00	180.00	3.226	0.358	17.328	2.23

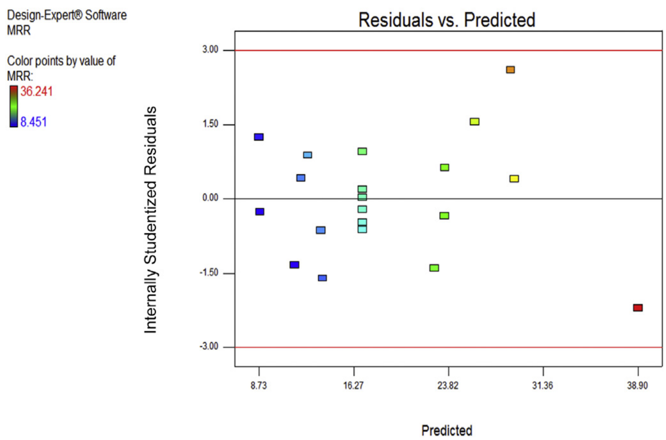

Fig. 9. Residuals Vs Predicted on material removal rate for A413 work piece.

5.2.2. *Analysis of surface roughness for machining A413 work piece*

Finding the significant process parameter with maximum signal and minimum noise ratio for machining the high strength squeeze cast alloy A413 is a challenging task. The ANOVA was conducted to test the significance of the model, individual model terms, and lack of fit. Natural log transformation was performed on the responses for ANOVA validation. Depending on the condition, model terms sometimes are significant and not significant when Prob > F value is between 0.05 and 0.1. If the "Prob > F" value is less than 0.05, it is significant, but if it exceeds 0.1, it is not significant it occurs due to noise. Values of "P > F" less than 0.0500 indicate that the model terms are significant because 95% confidence interval is considered. In this experimental case, all the input variables and their interaction A, B, C, AB, AC, C^2 are significant. Values of "P > F" greater than 0.0500 indicate model terms are not important because 95% confidence interval is considered. In this experimental case BC, A^2, and B^2 are not significant; hence these terms will not be taken into consideration for SR. lack of fit test can decide the model adequacy and compares the residual error to the pure error. As indicated, the lack of fit value 1.63 implies there is a chance of 30.20% of error occurs due to noise. The "Predicted R-Squared" and "Adjacent R-Squared" values of the model with the reasonable agreement are 0.8465 and 0.9499. Adequate precision greater than 4 is desirable, as it measures the signal to noise ratio of 25.798. From Fig. 14 it is

Table 5
ANOVA on material removal rate for machining A413 work piece.

Source	Sum of squares	DF	Mean of square	F-Value	Contribution%	P-value	Significance
Model	1126.75	9	125.19	28.76	96.28	<0.0001	[a]
A-Ton	352.87	1	352.87	81.06	30.15	<0.0001	[a]
B-Toff	326.55	1	326.55	75.01	27.90	<0.0001	[a]
C-IP	356.69	1	356.69	81.94	30.47	<0.0001	[a]
AB	21.28	1	21.28	4.89	1.81	0.0515	
AC	7.88	1	7.88	1.81	0.67	0.2082	
BC	20.19	1	20.19	4.64	1.72	0.0567	
A^2	0.26	1	0.26	0.060	0.02	0.8114	
B^2	26.88	1	26.88	6.17	2.29	0.0323	
C^2	18.27	1	18.27	4.20	1.56	0.0676	
Residual	43.53	10	4.35		3.71		
Lack of Fit	37.75	5	7.55	6.53	3.22	0.0300	
Pure Error	5.78	5	1.16		0.49		
Total	1170.28	19			100.00		

R-Squared:0.9628 Adj R-Squared:0.9293 Pred R-Squared:0.7439 Adeq Precision:20.448.
[a] Significant.

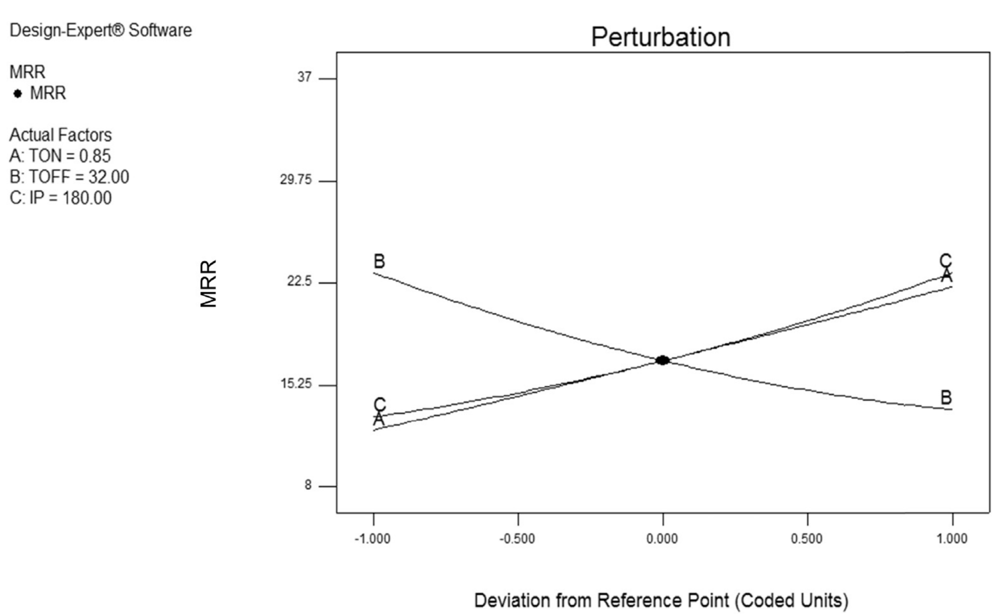

Fig. 10. Perturbation plot on material removal rate for A413 work piece.

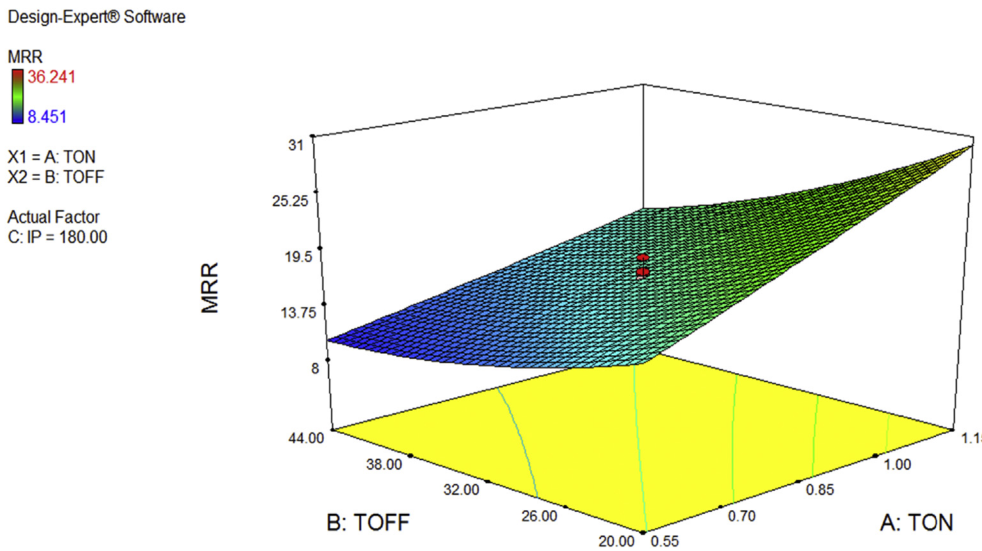

Fig. 11. Interaction plot (Ton Vs Toff) on material removal rate for A413 work piece.

observed that residuals are spread approximately in a straight line, which shows a good relation between experimental and predicted values and the variable follows the normal distribution. Hence, the developed model is considered to be fairly fitted with the observed values. From Fig. 15 it is viewed that the residuals are scattered randomly representing that they are independent. Therefore, the developed second-order for SR were presented in the Equation (4).

$$SR = -6.99235-1.61595 * T_{on} + 0.034537 * T_{off} + 0.088178 * IP - 0.038889 * T_{on} * T_{off} + 0.020833 * T_{on} * IP - 1.14583E\text{-}004 * T_{off} * IP + 0.091137 * T_{on}^2 + 9.37893E\text{-}005 * T_{off}^2 - 2.49079E\text{-}004 * IP^2 \quad (4)$$

While machining A413 alloy, among the various input process parameters, it is observed from ANOVA that the Ton, IP, and T_{off} are found to be significant at 95% confidence. From Table 6, it is also noted that the Ton is the major influencing factor with 43.79% contribution followed by IP and T_{off} with 28.1% and 11.11% respectively. From the response graph Fig. 16, it is observed that increase in Ton and IP lead to the rise in SR whereas by increasing T_{off} SR decreases. From the combined response graph in Fig. 17, it is found that the SR increases with increase in Ton and decrease in T_{off}. Fig. 18, shows that SR increases with increase in Ton and increase in IP. Fig. 19, reveals that SR increases with the decline in T_{off} and increase in IP.

From the above information, it is observed that if there is an increase in Ton and IP, SR increases due to the effect of longer spark duration of high intensity, i.e., more amount of discharge energy per spark reaching the surface. This energy causes a minor part of the specimen to melt and vaporize. A fraction of molten material is flushed away by dielectric while overheated molten metal evaporates which results in the formation of larger crater producing a rough surface [16]. Also, this high discharge energy in the spark striking the surface produces deeper and wider size craters. It is evident that deep craters will provide high SR. On the other hand, lower pulse on time leads to decrease in SR value. The mechanism behind this theory is less discharge energy per spark resulting in shallow crater produced on the surface. The presence of cavities results in low SR value which is nothing but the smoother surface. Hence, to obtain a better surface finish both the pulse on time and

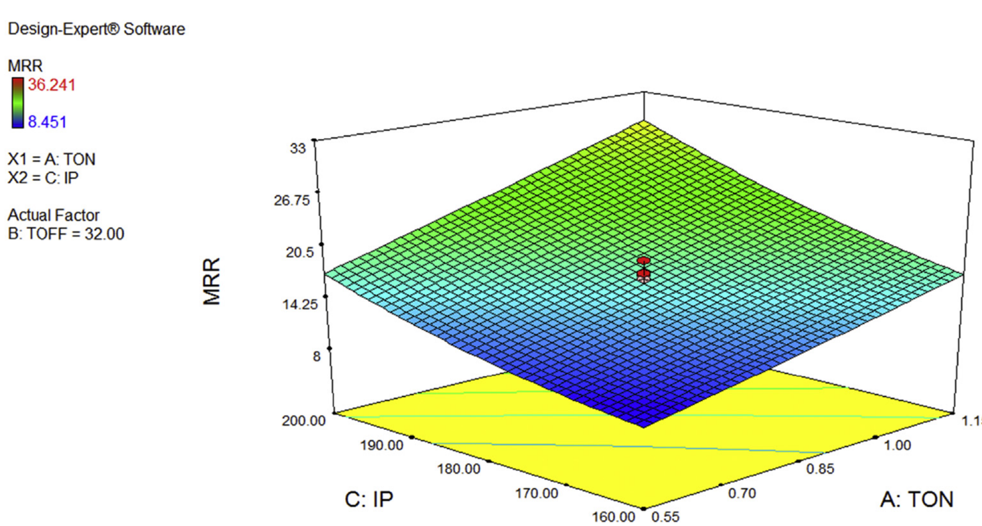

Fig. 12. Interaction plot (Ton Vs IP) on material removal rate for A413 work piece.

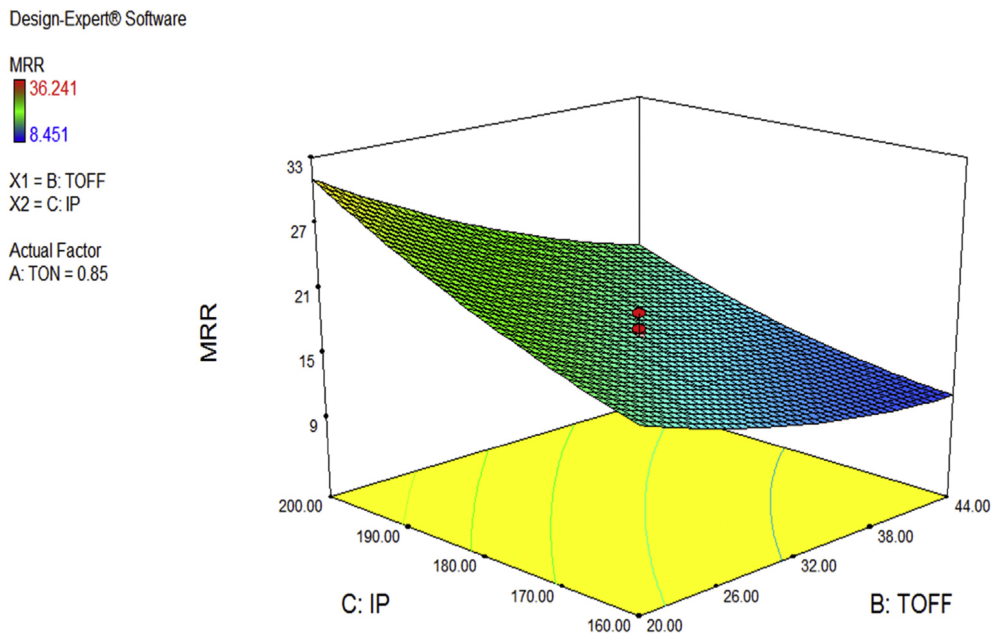

Fig. 13. Interaction plot (Toff Vs IP) on material removal rate for A413 work piece.

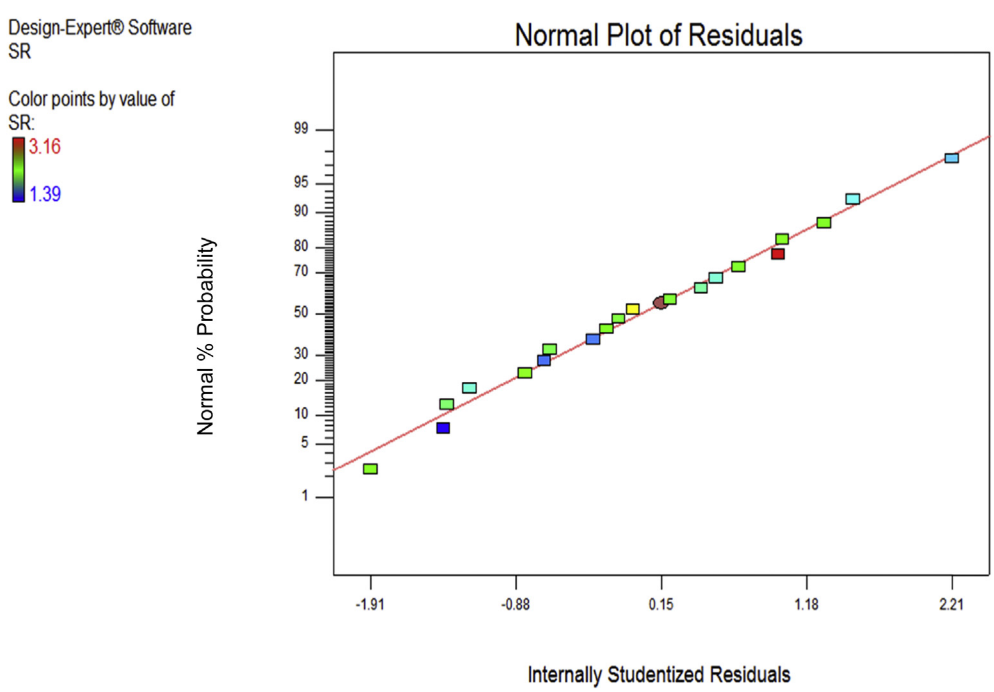

Fig. 14. Normal plots of residuals on surface roughness for A413 work piece.

peak current should be kept as minimum as possible [11].

It is also evident that if there is an increase in T_{off}, SR decreases. This trend is due to the effect of less number of discharges occurring for a particular period, resulting in a small number of craters and less micro-damage on the surface. Thus, the SR value depends on the size of the crater. As a result, surface quality is better which has low SR value. To obtain a good surface finish, T_{off} should be kept as maximum as possible [21]. Due to the absence of void formation, better surface characteristics are observed in high strength squeeze cast work piece. Thus, the irregular variation in the surface roughness is minor.

6. Additivity test of experimental vs prediction for machining A413 workpiece

Additivity test is performed for MRR and SR in all the 20 experiments to validate the mathematical model (i.e. RSM predictive model) of output response shown in the Equation (3) and Equation (4). Figs. 20 and 21 illustrate the comparison between the experiment sets and RSM prediction for material removal rate and surface roughness. It indicates that the experimental and predicted values are nearly equal 7.30% & 3.0% for MRR and SR respectively. Thus, it can be concluded that RSM model predicts accurately, and these

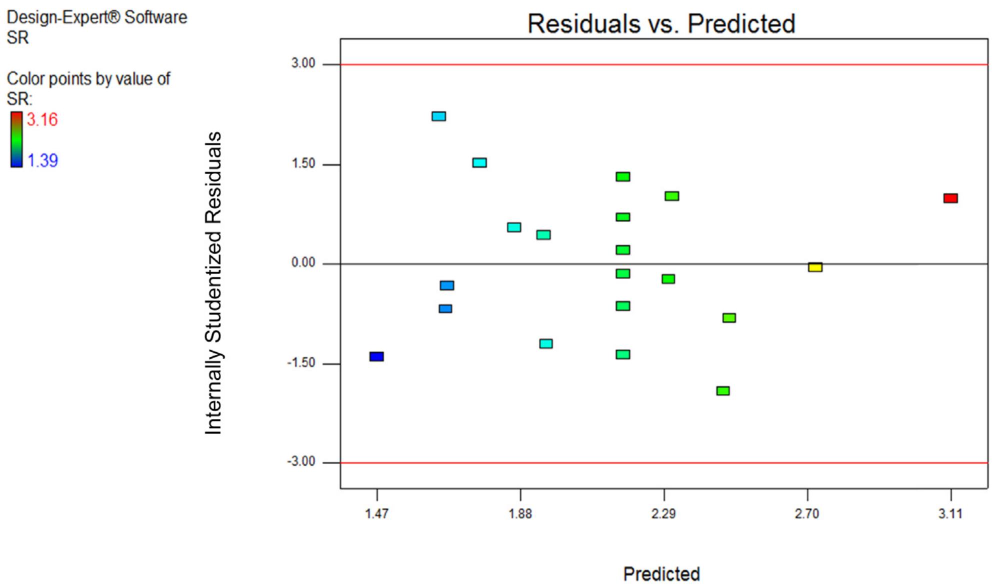

Fig. 15. Residuals Vs Predicted on surface roughness for A413 work piece.

Table 6
ANOVA on surface roughness for machining A413 work piece.

Source	Sum of squares	DF	Mean of square	F-Value	Contribution%	P-value	Significance
Model	2.98	9	0.33	40.99	97.38	<0.0001	[a]
A-Ton	1.34	1	1.34	165.79	43.79	<0.0001	[a]
B-Toff	0.34	1	0.34	41.99	11.11	0.0001	
C-IP	0.86	1	0.86	106.39	28.1	<0.0001	[a]
AB	0.16	1	0.16	19.38	5.22	0.0013	
AC	0.13	1	0.13	15.45	4.24	0.0028	
BC	6.050E-003	1	6.050E-003	0.75	0.19	0.4074	
A^2	9.696E-004	1	9.696E-004	0.12	0.031	0.7364	
B^2	2.629E-003	1	2.629E-003	0.32	0.085	0.5812	
C^2	0.14	1	0.14	17.69	4.57	0.0018	
Residual	0.081	10	8.089E-003		2.64		
Lack of Fit	0.050	5	0.010	1.63	1.63	0.3020	
Pure Error	0.031	5	6.147E-003		1.01		
Total	3.06	19					

R-Squared:0.9736 Adj R-Squared:0.9499 Pred R-Squared:0.8465 Adeq Precision:25.798.
[a] Significant.

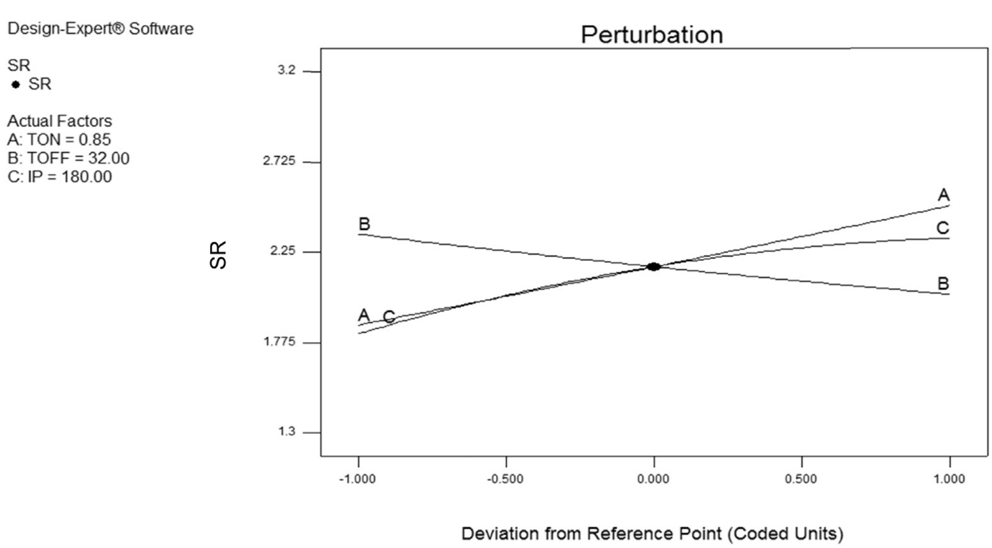

Fig. 16. Perturbation plot on surface roughness for A413 work piece.

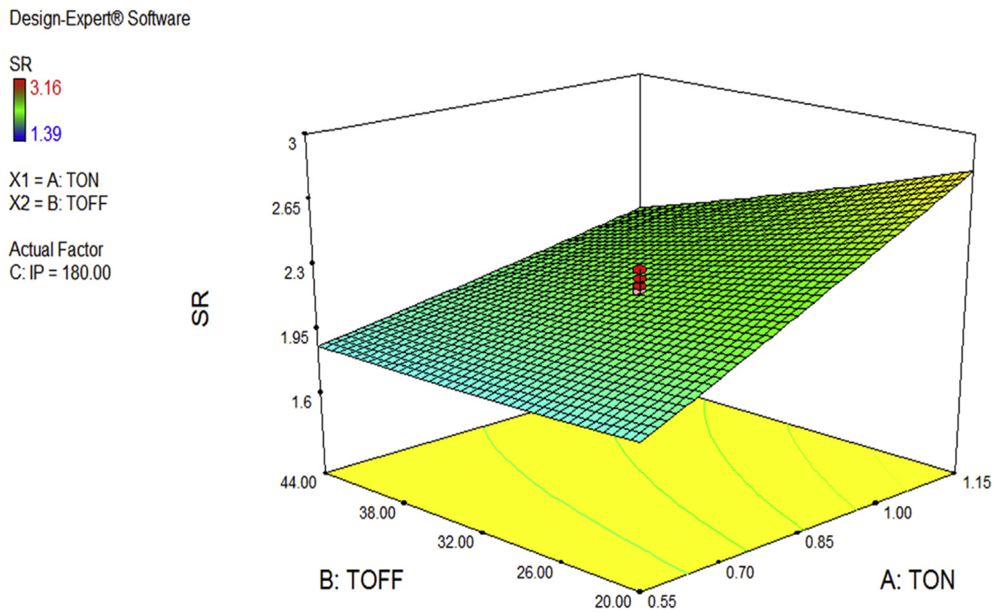

Fig. 17. Interaction plot (Ton vs Toff) on surface roughness for A413 work piece.

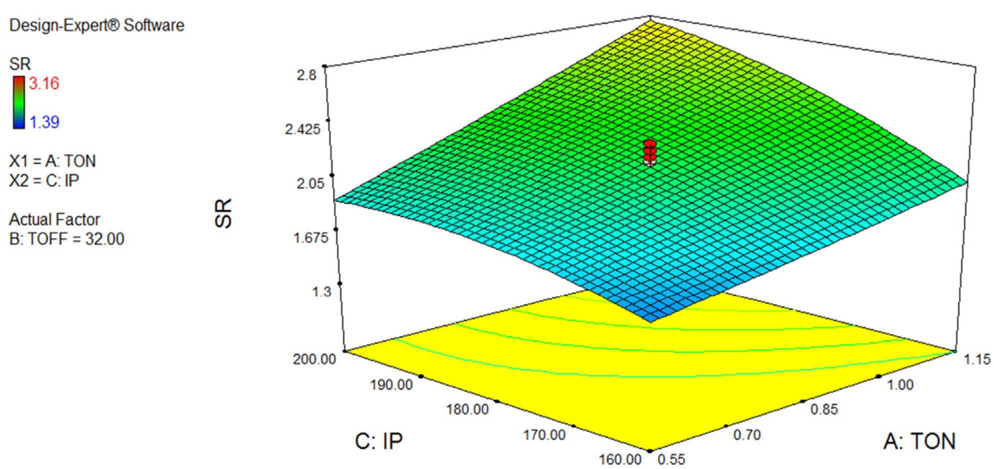

Fig. 18. Interaction plot (Ton vs IP) on surface roughness for A413 work piece.

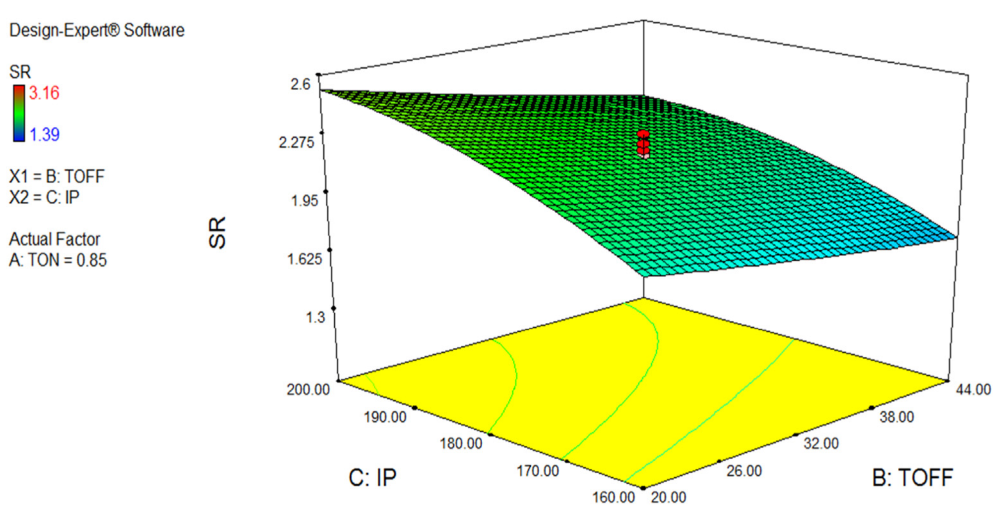

Fig. 19. Interaction plot (Toff Vs IP) on surface roughness for A413 work piece.

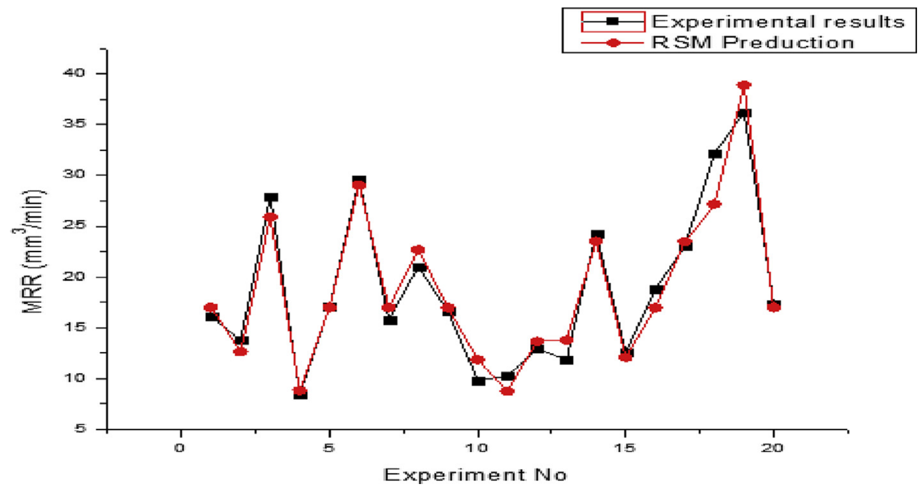

Fig. 20. Experiment sets Vs RSM prediction on material removal rate for A413 work piece.

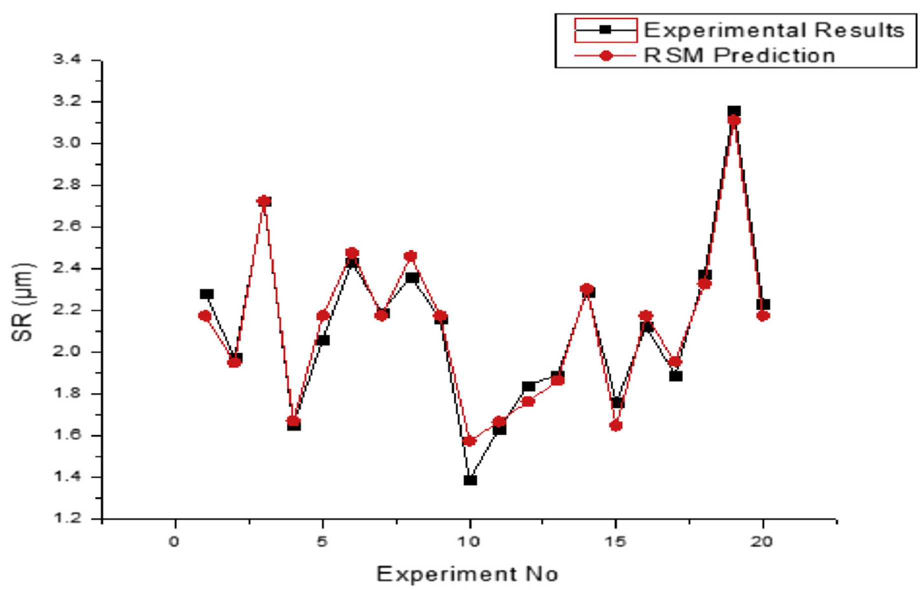

Fig. 21. Experiment sets vs RSM prediction on surface roughness for A413 work piece.

models can be used for advance prediction for the purpose of time and cost reduction.

7. Multi-objective optimization using desirability approach for machining A413 workpiece

This method makes use of a target function, D(X), called the desirability function. It is used to reflect the desirable ranges for each response (di) varying from zero to one. The objective simultaneous function is a geometric mean of all transformed responses and is shown by Equation (5).

$$D = (d1 \times d2\ x \ldots dn)\ \hat{}\ 1/n \tag{5}$$

In the Equation (5), n is the number of responses to the measure. The overall function becomes zero if any of the responses or factors falls outside their desirability range. For simultaneous optimization, every response must have a low and high value assigned to each goal. On the worksheet, the “Goal” field for responses must be one of five choices: “none”, “maximum”, “minimum”, “target”, or “in range”. If there is no goal, the response will not be used for the optimization. Goals can be set for any number responses, factors and components provided. At least one response is included in the

Table 7
Multi-response optimization of WEDM process parameter for machining A413 workspace.

Performance measures/responses	Input factor			Output response		Desirability
	Ton (µs)	Toff (µs)	IP (Amps)	MRR (mm3/min)	SR (µm)	
Maximum MRR	1.03	20.00	200	35.760	2.875	0.837
Equal MRR & SR	1.15	20.00	160	23.515	2.302	0.716
Minimum SR	0.89	20	160	18.519	2.015	0.732

Table 8
Results of confirmation test for machining A413 work piece.

S.No	Input factor			Output response experimental		Output response predicted		% Error	
	Ton (μs)	Toff (μs)	IP (Amps)	MRR (mm3/min)	SR (μm)	MRR (mm3/min)	SR (μm)	MRR	SR
1	1.03	20.00	200	35.760	2.875	35.732	2.873	0.1	0.08
2	1.15	20.00	160	23.515	2.302	23.516	2.302	0.01	0.01
3	0.89	20	160	18.519	2.015	18.425	2.010	0.5	0.26

goal set. In the desirability objective function D(X), each response can be assigned an importance about the other responses. Importance (ri) varies from the least important (+) a value of 1, to the most important (+++++) a value of 5. If all the importance values are the same, the simultaneous objective function reduces to the normal form of desirability.

In this investigation Multi-response optimization for the WEDM of A413 is obtained using desirability function approach. Different criteria such as weights and importance are changed for three different performance measures. For maximum MRR value of 5 (+++++) importance are given for MRR and value of 1 (+) importance is given for SR. For equal MRR and SR, the value of 3 (+++) importance is given for both MRR and SR. For minimum SR, a value of 1 (+) importance is given for MRR and value of 5 (+++++) importance is given for SR. The optimal results are listed in Table 7.

7.1. Confirmation test for machining A413 work piece

Confirmation tests were performed to confirm the results of multi-response optimization during WEDM of A413. Table 8 shows the error percentage between optimal and experimental values for each response.

8. Conclusions

The machining of fabricated squeeze cast A413 alloy was investigated. Based on this experimental study, the following conclusions were made:

- The A413 alloy was successfully fabricated through squeeze casting route, the specimen with a higher hardness of 95 BHN and ultimate tensile strength of 305 MPa was machined effectively by WEDM process. It can be utilized for automobile applications.
- It was observed from ANOVA for machining parameters such as T_{on}, $T_{off,}$ IP and their interactions are the significant parameters for MRR and SR based on percentage contribution.
- Through additivity test, the predicted results from the mathematical model are within the limits of agreeable error with respect to the experimental results. The average error percentage in RSM prediction is around 7.30% & 3.0% for MRR and SR respectively.
- In addition to that the formulated multi-constrained optimum parametric combination for maximum MRR of 35.760 mm^3/min are T_{on} (1.03 μs), T_{off} (20 μs) and IP (200 Amps) respectively. Equal MRR and SR of 23.515 mm^3/min and 2.302 μm are obtained by setting T_{on}, T_{off} and IP to 1.15 μs, 20 μs and 160 Amps and minimum SR of 2.015 μm are obtained by setting T_{on}, T_{off} and IP to 0.89 μs, 20 μs and 160 Amps respectively. These results are confirmed by the confirmation run and it's found to be in good agreement.

References

[1] John R. Brown, Foseco Non-ferrous Foundryman's Handbook, eleventh ed., Butterworth Heinemann, 1994.
[2] George E. Totten, D. Scott Mackenzie, Hand Book of Aluminium, Volume 1 Physical Metallurgy and Processes, Marcel Dekker Inc, 2003.
[3] J.R. Franklin, A.A. Das, Squeeze casting—a review of the status, Br. Foundrym. 77 (3) (1984) 150–158.
[4] T.M. Yue, G.A. Chadwick, Principles and applications of squeeze casting, Metals Mater. 5 (1) (1989) 6–12.
[5] Kyuhong Lee, Yong Nam Kwon, Sunghak Lee, Effects of eutectic silicon particles on tensile properties and fracture toughness of A356 aluminum alloys fabricated by low-pressure-casting, casting-forging, and squeeze-casting processes, J. Alloys Compd. 461 (1–2) (2008) 532–541.
[6] E.S. Kim, K.H. Lee, Y.H. Moon, A feasibility study of the partial squeeze and vacuum die casting process, J. Mater. Process. Technol. 105 (1) (2000) 42–48.
[7] A. Raji, R.H. Khan, Effects of pouring temperature and squeeze pressure on Al 8% Si alloy squeeze cast parts, AU J. Technol. 9 (4) (2006) 229–237.
[8] Ed Joseph, R. Davis, Aluminum and Aluminum Alloys, ASM International, 1993.
[9] G.F. Benedict, Electrical Discharge Machining (EDM), in: Non-traditional Manufacturing Processes, Marcel Dekker, Inc, New York & Basel, 1987, pp. 225–235.
[10] Friedhelm Altpeter, Roberto Perez, Relevant topics in wire electrical discharge machining control, J. Mater. Process. Technol. 149 (1) (2004) 147–151.
[11] Pujari Srinivasa Rao, Koona Ramji, Beela Satyanarayana, Experimental investigation and optimization of wire EDM parameters for surface roughness, MRR and white layer in machining of aluminium alloy, Procedia Mater. Sci. 5 (2014) 2197–2206.
[12] S. Sarkar, M. Sekh, S. Mitra, B. Bhattacharyya, Modelling and optimization of wire electrical discharge machining of Gamma-TiAl in trim cutting operation, J. Mater. Process. Technol. 205 (1) (2008) 376–387.
[13] Shajan Kuriakose, M.S. Shunmugam, Multi-objective optimization of wire-electro discharge machining process by non-dominated sorting algorithm, J. Mater. Process. Technol. 170 (1) (2005) 133–141.
[14] Fuzhu Han, Jun Jiang, Dingwen Yu, Influence of machining parameters on surface roughness in finish cut of WEDM, Int. J. Adv. Manuf. Technol. 34 (5–6) (2007) 538–546.
[15] R. Konda, K.P. Rajurkar, R.R. Bishu, A. Guha, M. Parson, Design of experiments to study and optimize process performance, Int. J. Qual. Reliab. Manag. 16 (1) (1999) 56–71.
[16] Palani Sivaprakasam, P. Hariharan, S. Gowri, Optimization of micro-WEDM process of aluminum matrix composite (A413-B4C); A response surface approach, Mater. Manuf. Process. 28 (12) (2013) 1340–1347.
[17] Ashish Srivastava, Amit Rai Dixit, Sandeep Tiwari, Experimental investigation of wire EDM process parameters on aluminium metal matrix composite Al2024/SiC, Int. J. Adv. Res. Innovation 2 (2) (2014) 511–515.
[18] A. Sharma, M.P. Garg, K.K. Goyal, Prediction of optimal conditions for WEDM of Al 6063/ZrSiO4p MMC, Procedia Mater. Sci. 6 (2014) 1024–1033.
[19] Prediction of optimal conditions for WEDM of Al 6063/$ZrSiO_4$ MMC, Procedia Mater. Sci. 6 (2014) 1024–1033.
[20] Ergun Ekici, Ali Riza Motorcu, Abdil Kus, Evaluation of surface roughness and material removal rate in the wire electrical discharge machining of Al/B4C composites via the Taguchi method, J. Compos. Mater. (2015) 1–12.
[21] Shyam Lal, Sudhir Kumar, Z.A. Khan, A.N. Siddiquee, Multi –response optimization of wire electrical discharge machining process parameters for Al7075/SiC/Al2O3 hybrid composite using taguchi-based grey relational analysis, J. Eng. Manuf. 229 (2) (2015) 229–237.
[22] D. Sathishkumar, M. Kanthababu, V. Vajjiravelu, R. Anburaj, N. Thirumalai Sundarrajan, H. Arul, Investigation of wire electrical discharge machining characteristics of Al6063/SiCp composites, Int. J. Adv. Manuf. Technol. 56 (9–12) (2011) 975–986.
[23] A. Pramanik, A.K. Basak, M.N. Islam, G. Littlefair, Electrical discharge machining of 6061 aluminium alloy 2015, Trans. Nonferrous Metals Soc. China 25 (2015) 2866–2874.

Digest Journal of Nanomaterials and Biostructures Vol. 11, No. 3, July - September 2016, p. 845 - 852

THE EFFECT OF PARTICLE HYBRIDIZATION ON MICRO STRUCTURE ANALYSIS AND MECHANICAL BEHAVIOR OF METAL MATRIX COMPOSITES: AN EXPERIMENTAL APPROACH

T. PRIDHAR[a*], R. A. SANKARAN[b], K. RAVIKUMAR[c]. C. BOOPATHI[a]
[a]*Department of Mechanical Engineering, Sri Krishna College of Technology, Coimbatore, India*
[b]*Department of Mechanical Engineering, Salem College of Engineering and Technology, Salem, India*
[c]*Department of Mechanical Engineering, Dr.NGP Institute of Technology,Coimbatore, India*

Mechanical and physical performance of alumina and boron carbide particulate filled reinforcement with Al7075 matrix prepared by stir casting techniques were investigated experimentally. The composite comprises of the base matrix Al7075 with various concentration of two particle reinforcements named alumina (Al_2O_3) and boron carbide (B_4C). In that one of the particle reinforcement alumina has various altitude of 2,4,6,8 and 10 wt% and other one boron carbide has 5 wt% kept as constant for all specimens. The specimens were prepared by stir casting techniques to preserve the perfect dispersion of particulate reinforcement in final fabricated composites.The influence of alumina and boron carbide particulate in final composites were analyzed by examining the mechanical properties such as tensile behavior and hardness of composites. To study the micro structure and dispersion of particle reinforcements, the alumina and boron carbide particulate dispersion was evidently exposed by scanning electronmicroscopy (SEM) techniques and XRD techniques. The result shows addition of particulates directly increases the hardness and density of composites. In the same way result exposes mechanical behavior of tensile property also increased with addition of filler reinforcements.

(Received June 11 , 2016; Accepted August 9, 2016)

Keywords: Al 7075, Alumina, Boron carbide, Mechanical properties, Stir casting, Micro structure

1. Introduction

Metal Matrix Composites (MMC) has acknowledged increasing attention at present era researchers, because of their favorable mechanical and physical properties over monolithic metals. In that aluminium matrix composite plays a vital role in all over automobile and aerospace applications. The challenges and opportunities of aluminium matrix composites are viable for further processing in various applications [1]. The MMC briefly summarized for continuous fiber, discontinuous fiber and particle reinforced fiber for a different automobile, military, aerospace and sports applications [2].The suitability of MMC and their technical issues like material design and development methodologies, characterization and control of interfacial properties are clearly studied for developing second generation of MMC [3]. Various attempts has been made to review the different combination of reinforcing materials used in the processing of hybrid aluminium matrix composites and how it affects the mechanical, corrosion and wear performance of the materials [4,5]. The reinforcement of short fiber and particle in aluminium matrix composites has made strong interfacial bonding so that the wear properties and fracture toughness were influenced in positive manner [6].The most commonly used reinforcements are Sic, B_4C, Al_2O_3, WC,

*Corresponding author: preeth_t@rediffmail.com

graphite, fly ash, mica, talc, coconut shell . Hybrid metal matrix composites are current generation composites where more than one reinforcement of different shape and size are used to attain improved properties [7, 9].

In general, manufacture of composites are classified into two broad categories namely solid phase and liquid phase fabrication methods. From all the processing routes, liquid metallurgy method is the most sought due to its several advantages such as cost-effective, mass production, near net shaped components can be produced. It is found that the stir cast method offers better matrix particle binding due to stirring action of particles into the melts. In part of that the stir casting techniques was evaluated for silicon carbide aluminium matrix MMC [8]. It was reported that by controlling the processing variables such as holding temperature, stirring speed, size of the impeller and the amount of reinforcement, it is possible to manufacture a composite by stir casting with a broad range of mechanical properties. The researchers revealed that uniform distribution of reinforcements was observed in the stir cast composites [10-13]. The addition of Particulates like silicon carbide, boron carbide, aluminium oxide to aluminum alloy significantly improves the density, micro hardness, thermal stability, tensile strength, and wear of the base alloy. In the same way increase of particulates decreases the impact toughness of the composites. In addition to that the microstructural analysis has employed to evince the existence of particle reinforcements and its influences in results. The SEM micrograph noticeably depicts the uniform distribution of reinforcements and also elucidate the homogeneity of cast composites[14-16].

Moreover this present work makes an attempt to analyse the influence of alumina and boron carbide particulate in base Al7075 matrix composites by examining the mechanical properties like tensile behavior and hardness of composites. The reinforcement used was alumina and boron carbide with different volume of fractions. Micro structure and dispersion of particle reinforcements is evidently exposed by scanning electron microscopy (SEM), the XRD techniques was used to ensure the presence of chemical compositions of base matrix and particle reinforcements.

2. Material and methods

Materials

The metal matrix chosen for the current investigation is AL7075 which was purchased from Perfect metal works, Bangalore. The chemical composition for the alloy is show in table 1. alumina and boron carbide particulates are used to fabricate the composite with an average particle size of 37 microns which were supplied by Speed fam Chennai.

Table 1. Chemical Composition of Al 7075 in weight percentage

Chemical Composition	Si	Fe	Cu	Mn	Mg
% of comp	0.4	0.5	1.6	0.3	2.5
Chemical Composition	Cr	Zn	Ti	Al	-
% of comp	0.15	5.5	0.2	Bal	-

Material fabrication:

In the present study, the base matrix Al 7075 was reinforced with 2,4,6,8 and 10 wt% AL_2O_3 and 5% of B_4C about average particle size of 37 μm. The actual chemical composition of Al 7075 alloy is given in table 1. In order to increase the wettability magnesium of 2.52% [9] in weight was added during production of the hybrid composites

Preparation of hybrid composites

A liquid metallurgy route has been adopted to prepare the hybrid composites. In this technique, the calculated amount of AL7075 was melted in an open electrical resistance furnace at a temperature of about 700°c. The temperature of the furnace was maintained at an accuracy of ±50°c using a digital thermo couple. Degassing process was carried out to force out all the absorbed gases and to reduce the porosity. The ceramic particles are preheated in a muffle furnace to around 1000°C for 2 hours for oxidizing the surfaces. To obtain homogeneous distribution of reinforcement in the composites proper stirring is mandatory. The base metal was stirred with the assistance of a mechanical stirrer with a speed of about 525 rpm to form a fine vortex for 10 minutes. Magnesium of about 2.52 wt % was also added to enhance the wettability property of the composites. The pre heated reinforcements and magnesium were added at a constant feed rate into vortex formed in the melt. For the proper mixage of the reinforcement the Stirring was continued for about 10min even after the completion of reinforcement addition. The stir casting setup is shown in Fig. 1

Fig.1Stir Casting Setup

The melt with reinforcement particles was poured into a cylindrical permanent metallic mold with a diameter of 15 mm and 120 mm length. The manufactured composite was allowed to solidify in atmospheric air and was taken out from the mould after solidification. The same procedure was used to manufacture with different weight percentage (2, 4, 6, 8 and 10 wt. %) of alumina and 5 wt % of boron carbide powder. For the comparison study purpose, unreinforced aluminium alloy was also cast under similar cast conditions

Density measurement

Density measurements were carried out on the base alloy and particulate reinforced samples using the Archimedes principle. Mass of the specimen was determined by measuring the weight of the specimen using an electronic weighing machine having accuracy up to 0.001 mg. The density was measured by weighing the composites in air and in another liquid of known density. According to Archimedes principle the density can be measured using the Eqn.1

$$\rho_{mmc} = \frac{m}{m - m_1} \rho_w \tag{1}$$

Where

m is the mass of the cast composite in air
m_1 is the mass of the same composite sample in distilled water
ρ_w is the density of the distilled water (998 kg/m^3 at 20°c)

Hardness test

The hardness tests were carried out to find the effect reinforcements in the base alloy. A Brinell hardness tester (AKB-3000(M)) was employed to determine the values as per ASTM E10-07 standards. A load of 500 kg was applied on the specimen with a 10mm steel ball indenter for 30 seconds at room temperature. An optical microscope was deployed to measure the indentation diameter. The hardness was calculated using the Eqn.2.The hardness was measured at five different places of the specimen and mean value was calculated

$$BHN = \frac{2P}{\pi D(D - \sqrt{(D^2 - d^2)})} \tag{2}$$

Where

P is the applied force in N
D is the diameter of indenter in mm
d is the diameter of indentation mm

Tensile test:

The Aluminium alloy and the particulate reinforced composites were machined and subjected to micro tensile test as per the ASTM E8 standard shown in Fig. 2.

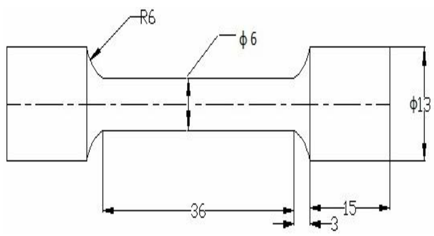

Fig.2Tensile specimen size

A universal testing machine loaded with 20kN was used to conduct the experiment. The test was repeated thrice for each melt. The mean values obtained were considered to calculate the tensile strength of the composites.

Micro structural Analysis

The microstructure of the hybrid composites was examined using a scanning electron microscope (JSM-6360). The specimens for microstructure test were polished metallographically. The Polished surface of the specimen was then etched with 10% of NaOH Solution and examined for the uniformity in distribution of reinforcements in aluminium hybrid composites. The XRD technique was used to evidently ensure the presence of base matrix and its particle reinforcement dispersion.

3.Result and discussions

Microstrucutrual characterization

An analysis for the distribution of alumina and boron carbide particles reinforced with aluminium matrix composites was done after completion of fabrication. It is visibly shown that the dispersion of the boron carbide and alumina reinforcements and particles are embedded inside the base aluminium matrix. The Fig.3 shows the SEM micrograph of the hybrid composites, as it can be seen that distribution of the alumina and boron carbide median size of the particles in the aluminum matrix are uniformly distributed over the fabricated composites.

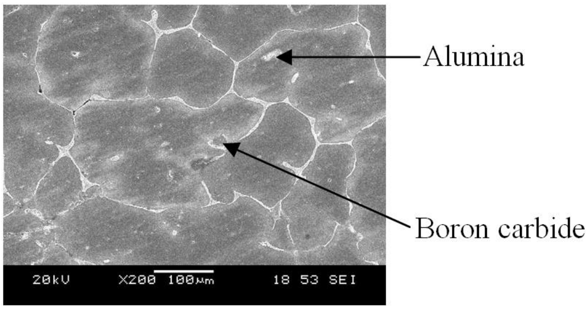

Fig 3 SEM image of hybrid composite

In general the strength and stiffness of the composites based on their reinforcement inter locking with base matrix of the composites. However, the testing of chemical composition is also one of the guaranteed techniques to ensure the homogeneous dispersion of reinforcements and matrix. For that the XRD techniques was carried to show cast the various chemical composition present in composites, Fig.4 shows the presence of aluminium, boron carbide and alumina.

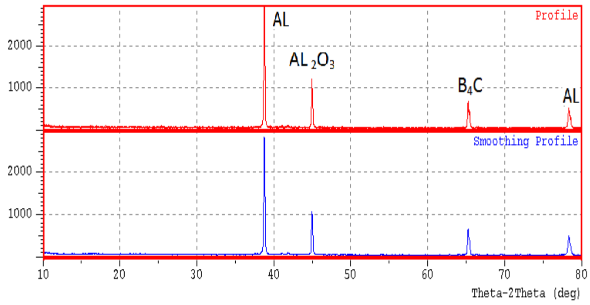

Fig 4. XRD Analysis of the hybrid composites

In that the dispersion of reinforcements plays vital role to decide the strength and stiffness of the composites. The Fig.3 SEM micrograph provides a clear schematic view about the perfect dispersion of reinforcements.

Density Measurements

The density of composites was influenced by the addition volume fraction of reinforcement particles. The theoretical and experimental density value of fabricated composites are shown in table 2.The comparison of theoretical and experimental density obtained by Archimedes principle is shown in Fig 5. From the results it is evident that the density of hybrid composites is higher than the base material. The density increases with the addition of the reinforcements.

Table 2 Theoretical and Experimental density of composites

Sample.No.	Samples	Theoretical Density(g/cc)	Experimental density(g/cc)
01	Base alloy	2.81	2.79
02	2% Al_2O_3 , 5% B_4C	2.82	2.81
03	4% Al_2O_3 , 5% B_4C	2.84	2.83
04	6% Al_2O_3 , 5% B_4C	2.86	2.84
05	8% Al_2O_3 , 5% B_4C	2.88	2.86
06	10%Al_2O_3 , 5%B_4C	2.91	2.88

The figure 5 shows the theoretical and experimental density of various samples. It is clear that the density of composites increased by increasing the volume fraction of reinforcements, also it can be concluded that the reinforcement particles not melted with base aluminium matrix.

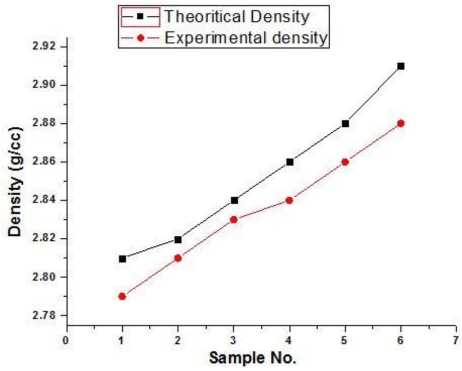

Fig. 5 Theoretical and Experimental density values of composites

Hardness Measurements

The hardness of the fabricated composites was influenced by the variation of particle reinforcements. From the Brinell hardness test it was evident that the hardness of the composite is greater than that of its cast matrix alloy. Due to the increase of ceramic phase in the hybrid composites the hardness value increases linearly with the increase in volume fraction of particle reinforcements. The addition of alumina and boron carbide particulates in matrix has improved the hardness by acting as a barrier for the motion of dislocation of the matrix lattice. The table 3 and Fig. 6 evidently expose the improvement of hardness of fabricated composites.

Table 3 Hardness values of composites

Sample. No	Samples	Hardness value(BHN)
01	Base alloy	65
02	2% Al_2O_3 , 5% B_4C	82
03	4% Al_2O_3 , 5% B_4C	98
04	6% Al_2O_3 , 5% B_4C	112
05	8% Al_2O_3 , 5% B_4C	125
06	10% Al_2O_3 , 5% B_4C	137

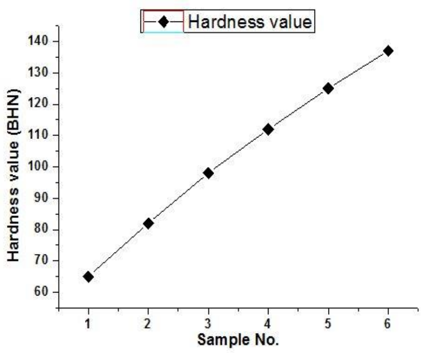

Fig. 6 Brinell values of hybrid composites

Tensile Strength

Variation in ultimate tensile strength of hybrid metal matrix composites reinforced with alumina and boron carbide of different volume of fractions is shown in table 4. The Ultimate Tensile strength was increased with an increase of alumina particulates in the composites. This may be credited to the reality that addition of Alumina and boron carbide leads to an increase in tensile strength and decrease in ductility. The particle reinforcement used in this aluminium matrix notifies that the binding ability between matrix and reinforcement highly increased with adding of particles. It was Evident from Fig7 that the tensile strength value keeps on increasing with addition of particle reinforcement.

Table 4Tensile strength values of composites

Sample. No	Samples	Tensile Strength(Mpa)
01	Base alloy	198
02	2% Al_2O_3 , 5% B_4C	230
03	4% Al_2O_3 , 5% B_4C	248
04	6% Al_2O_3 , 5% B_4C	265
05	8% Al_2O_3 , 5% B_4C	287
06	10% Al_2O_3 , 5% B_4C	305

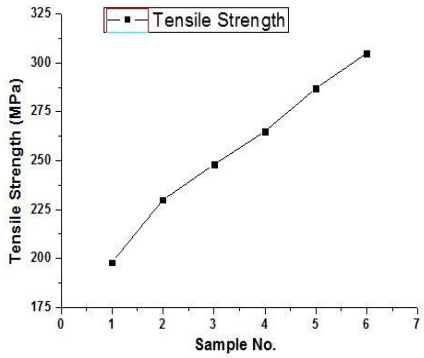

Fig. 6 Tensile strength values of hybrid composites

In this part of work increasing tensile properties of composites was increased with the particle reinforcements, it is clear that binding ability between base matrix and particle reinforcements was good in nature. Also the particle reinforcements of alumina and boron carbides are predominantly plays a vital role to transfer the stress induced in the composites.

4. Conclusions

The major conclusions of the current investigations are summarised below.

a) The liquid metallurgy route was found to be suitable method to fabricate the aluminium hybrid composites matrix composites.

b) The micro-structural studies of SEM and XRD techniques revealed the homogeneous distribution of the particulates in the hybrid composites

c) The density of the composites are found to be increased than the base alloy

d) Weight percentage of reinforcements showed a direct relation with hardness, tensile strength. Increase in addition of alumina and boron carbide restricts the deformation of the aluminium alloy, resulting in increased hardness, tensile strength

References

[1] M.K. Surappa, Sadhana, **28**, 319 (2003).
[2]J. Eliasson, Key Engineering materials Trans Tech Publications, Switzerland, **104-107**,33 (1995).
[3] D.B.Miracle, Composites Science and Technology **65**, 2526 (2005).
[4] Michael Oluwatosin Bodunrina, Journal of Material Research and technology, **4,**434 (2015).
[5] T Matsunaga, P K. Rohatgi Journal of Transactions of AFS, **104**,1097 (1996).
[6] S.J. Harris, Materials Science and Technology, **4**, 231 (1988).
[7] J. Hashim, Journal of Material processing technology,92-93,1999.
[8] Isil Kerti, Materials Letters, **62,** 1215 (2008).
[9] S. Suresha, Materials and Design, **31,** 1804 (2010).
[10] Manoj Singla, Journal of Minerals and Materials Characterization and Engineering, **8**, 455 (2009).
[11] Tamer Ozben, Journal of Materials Processing Technology **198**, 220 (2008).
[12] Krishnan Ravi Kumar, Science and Engineering of Composite Materials, **19,** 247 (2012).
[13] T.J.A Doel, Composites Part A, Applied Science and Manufacturing, **27**, 655 (1996)
[14] Y.Sahin, Journal of Materials and Design, **24**, 671 (2003).
[15] A. Baradeswaran, Composites: Part B **56**, 464 (2014).
[16] T.Rajmohan, Transactions of Nonferrous Metals Society China, **23**, 2509 (2013).